# Robot-driven Epidural Spinal Cord Stimulation Compared with Conventional Stimulation in Adult Spinalized Rats

A Thesis

Submitted to the Faculty

of

Drexel University

by

Fu-Han Hsieh

in partial fulfillment of the

requirements for the degree

of

Doctor of Philosophy

October 2011

# DEDICATION

Dedicated to my parents.

# AKNOWLEDGEMENTS

First and foremost, I would like to express my heartfelt gratitude to my advisor, Prof. Simon Giszter, who guided me throughout my time at Drexel. With his patience and insight, he has taught me the way to approach problems. Through his guidance, I also learned to use different aspects of my data to assess the results of the experiments. I also appreciate that he provided his proficient skill in rat spinal transection for all of the animals in this study. As a mentor, he has inspired a passion for neuroengineering, and he has been most understanding and supportive when I met some difficult times during my foreign study. I am very grateful to him for all of these.

I would like to thank my co-advisor, Dr. Karen Moxon, who taught me the concept of theoretical neuroscience, and also provided critical suggestions during my study. Her research in brain-machine interface also inspired me to study biomedical engineering.

I would like to thank Dr. Michel Lemay, who gave me suggestions for deciding the type of the electrode and the form of stimulation signal. He also provided valuable suggestions generously during my research time.

I would like to express my gratitude to Dr. Todd Doehring, who always provided me with valuable discussions. He also led me to think what I have really learned from my research and what I want to teach people after my study.

I also appreciate Dr. Kenneth Barbee provided valuable discussions as my committee.

This study was sponsored by the National Institute of Health (NIH) NS44564, NIH NS54894, the Craig Neilsen Foundation, and PA Dept Health through a Tobacco settlement award.

I would like to express my gratitude to Dr.Weiguo Song. We had good experience during cooperation of epidural stimulation research. He contributed two rats in continuous epidural stimulation. He is also a nice senior, no matter in scientific research, or in personal life.

I would also like to express my gratitude to my colleagues. Arun Ramakrishnan helped me many times when I had problem in programming. Ime taught me the know-how in doing rat experiments. Taegyo Kim provided his knowledge in electrics and photography helped me solve many problems during experiments. He is also a good friend. Chinton Oza took care the rats for me when I have emergency.

Moses Nakamura provided valuable assistance for developing the firmware to control robot-driven epidural stimulation.

Mike Smeltzer helped me train the animals when I had emergency. He’s really a trustworthy person.

I would also like to thank my friends, Anderson, Tu Qiang, Taegyo, Fang-An, Leko, Lydia, Iris, Xiao-Qin, Jingjia, Osamu, Hisanori, Arun, and Min. They make me feel I’m not alone, and we had memorable times in Philadelphia.

Finally, I deeply appreciate the love and support from my parents. Without their support, I may not have enough stamina to finish this study. I also appreciate my relatives and friends supported me in different ways.

# TABLE OF CONTENTS

# LIST OF TABLES

# LIST OF ILLUSTRATIONS

# Abstract

Robot-driven Epidural Spinal Cord Stimulation Compared with Conventional Stimulation in Adult Spinalized Rats

**Author's Name: Fu-Han Hsieh**

**Supervisor's Name: Simon F. Giszter, Ph.D.**

Epidural stimulation to trigger locomotion is a promising treatment after spinal cord injury (SCI). Continuous stimulation during locomotion is the conventional method. To improve recovery, we designed and tested an innovative robot-driven epidural stimulation method, coupled with a trunk-based neurorobotic system. The system was tested in rats, and the results were compared with the results of the neurorobotic therapy combined with the conventional epidural stimulation method, and with robotic rehabilitation alone. The rats had better recovery after treatment with the robot-driven epidural stimulation than conventional stimulation or controls in our neurorobotic rehabilitation system.

# 1. Introduction

People lose lumbosacral spinal control after severe spinal cord injury (SCI). However, the capability to generate rhythmic motion is still preserved in the neural circuits in the lumbosacral spinal part. The set of neurons responsible for creating these kind of motor patterns are commonly referred to as central pattern generators (CPGs) and are found in all invertebrate and vertebrate animals [1, 2]. Although how CPGs really work is still poorly understood, the phenomenon has been documented extensively. There are also indirect data supporting the idea that spinal CPGs for locomotion exist in cats and primates (including human) [3]. Therefore, it may be possible to activate CPGs directly to generate lumbosacral motor outputs after SCI.

Triggering locomotion and balancing the body simultaneously is a major issue for rehabilitation after spinal cord injury. After completely spinalizing at a thoracic level, hind limb locomotion of adult rats can still be driven by central pattern generators (CPGs) in the isolated spinal cord circuitry. However, special measures are needed to activate the CPGs. Many methods have been developed to trigger locomotion after SCI, including: pharmacological interventions [4-6], epidural [7-15] or intraspinal electrical stimulation [16, 17], and motor training [5, 18-21], but the details about how these interventions change the spinal network after SCI and the relation between these changes and the restoration of stepping ability are still not clear. Continuous epidural stimulation has been tested as a promising method to drive CPGs and trigger hind limb locomotion in both animal and clinical studies [7-12, 20, 22-25]. Furthermore, recent

studies show that continuous epidural spinal cord stimulation has identified new aspects of how specific locomotor in rats, cats, and humans function [7, 13, 14].

Robot devices have been used widely to assist rehabilitation after SCI [26, 27]. There are different types of robot control strategies, including: assistive, challenge-based, haptic simulation, and coaching. Assistive strategies have been developed the most, and are divided into four categories: impedance-based assistance [28-30], counterbalancing assistance [31-33], EMG(Electromyography)-based assistance [34-36], and performance-based adaptation [37-39]. Impedance-based assistive robots are simple and easy to use; counterbalancing assistive robots have larger effective force range; EMG-based assistive robots can acquire the command of the desired movement directly from the neural stimuli of specific muscles, but accuracy is not easy to control; performance-based adaptation can provide online feedback/feedforward, but need more complex arrangements. In this study, we used an impedance-based neurorobotic system that provides elastic force around the mid-caudal trunk of adult spinalized rats. Parts of the rats' trunk above the lesion remain under supraspinal control after complete transection at thoracic levels. In neonatal spinalized rats, these circuits can be driven with cortical aid to support well-integrated weight-bearing whole-body locomotion [40]. Thus, the recovery process and rehabilitation should be designed not only to train the spinal circuitry; there should also be training of integration with the supraspinal systems. Since the pelvis is the main mechanical junction between the trunk and the hind limbs, we designed a pelvic orthoses to connect the rat to the robot. This assists the rehabilitation of weight support and of interaction and integration

between supraspinal and spinal systems. From former studies in our lab, we know in robot rehabilitation in this fashion long term adaptation occurred and the motor function of the rats improved significantly [19].

In order to improve the recovery, we modified our neurorobotic system to drive electric spinal epidural stimulation so as to help restore spinalized rats' hindlimb stepping motor function. We found that the rats with the robot-controlled stimulation achieved a higher degree of hindlimb weight support than others, had less lateral deviation, and achieved higher function scores earlier than those in the continuous stimulation or control groups. This robot-driven stimulation combined with trunk-based neurorobotics is a possible solution to help trigger locomotion, promote better stepping and train balancing of the body simultaneously.

# 2. Hypotheses and Specific Aims

*Hypotheses*

(1) Continuous electric epidural spinal stimulation can trigger hind limb locomotion without mechanical interference. Impedance based neurorobotic system training can assist self body weight support of animals after spinal cord injury. Therefore, *we hypothesize that using continuous stimulation combined with impedance based neurorobotic system could assist the rat to improve functional recovery and regain self body weight support through systematic training.*

(2) If we can link the stimulation with pelvic height, the stimulation can be diminished naturally after the rat completely regained self body weight support. Therefore, *we hypothesize that epidural stimulation linked with pelvic motion could be a better treatment than continuous stimulation.*

*Specific aims*

(1) *To trigger hind limb locomotion by continuous electric spinal epidural stimulation and assist body weight support restoration by impedance based neurorobotic system*: Hopefully, the combination of these two strategies can simultaneously trigger hind limb locomotion and assist self body weight support.

(2) *To improve the effects of electric spinal epidural stimulation by linking the stimulation with pelvic motion*. We believe that robot-driven epidural stimulation could be a better strategy than continuous epidural stimulation.

# 3. Background and Significance

## *3.1 Spinal Cord*

Spinal cord is part of the central nervous system (CNS). It is the major pathway the brain uses to communicate with the skin, joints, and muscles of the body. Damage to the spinal cord causes loss of sensation and muscle control. Movement can be roughly classified into three categories: reflex movement, rhythmic movement, and voluntary movement. Spinal cord integrates these three kinds of movement.

### *3.1.1 Anatomy and Function*

The spinal cord is divided into four sections, cervical, thoracic, lumbar, and sacral. Cervical level usually related to head and neck, upper limb, and upper body function; thoracic level usually related to chest function and abdominal function; lumbar level usually related to leg function; and sacral level usually related to bowel, bladder, and sexual function. Each section is comprised by several segments. In human spinal cord, there are 8 cervical segments, 12 thoracic segments, 5 lumbar segments, and 5 sacral segments. Fig. 1 shows an example of human spinal cord. Where in rat spinal cord, there are 7 cervical segments, 13 thoracic segments, 6 lumbar segments, and 4 sacral segments. Each segment has a bilateral pair of spinal nerves. Right before a spinal nerve contacts the spinal cord, it separates into dorsal root and ventral root. The Dorsal root carries sensory information to CNS, and the ventral root carries motor information to muscles and glands. The Dorsal root ganglion, a swelling part on a dorsal root, contains cell bodies of sensory neurons (see Fig. 2).

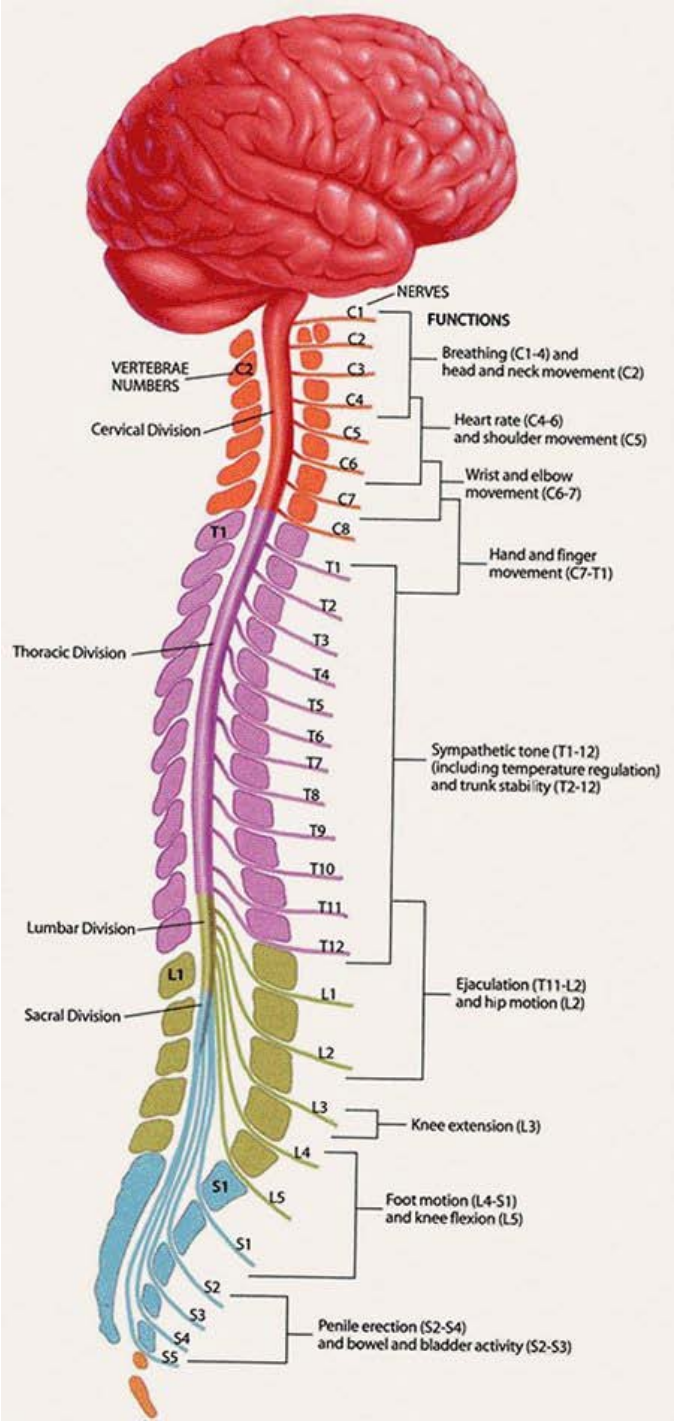


Fig. 1. Human spinal cord divisions and related functions. [reproduced from [41] with permission ]

In cross section, butterfly-shaped gray matter comprises the center part, and is surrounded by white matter. In the gray matter, dorsal horns contain sensory neurons, and are organized into two types of nuclei, one for somatic information, and one for visceral information. Ventral horns contain motor neurons, which transfer efferent signals to muscles and glands, and are organized into two types of nuclei, one for somatic motor information, and one for autonomic information. White matter transfer information to and from the brain. Ascending tracts in the white matter carry sensory information to the brain, and descending tracts in the white matter carry commands to motor neurons (see Fig. 2).

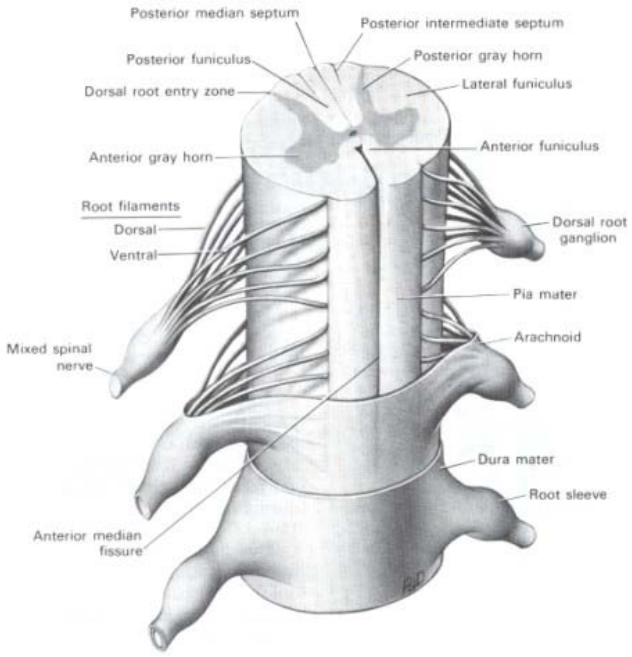


Fig. 2. Cross section view of the spinal cord. [reproduced from [42] with permission]

*3.1.2 Spinal Reflexes*

Reflexes are involuntary reactions in response to stimuli. They usually bypass the brain and the spinal cord reflex reacts nearly instantaneously, although the brain receives information about the reflexes as they occur. Reflex pathways are the neural pathways carry information between sensory receptors, muscles, and glands. Neural reflex pathways can be classified in different ways [43]:

1. By the efferent division that controls the effector
   (1) Somatic reflexes involve motor neurons and skeletal muscles.
   (2) Automatic reflexes involve autonomic neurons, such as cardiac muscles and glands.
2. By the integrating region within the CNS
   (1) Spinal reflexes integrated in the spinal cord. Triggering spinal reflexes do not require input from the brain.
   (2) Cranial reflexes are integrated in the brain.
3. By the time when the reflex develops
   (1) Innate reflexes are genetically determined, i.e. we are born with them.
   (2) Learned reflexes are acquired through experience.
4. By the number of neurons in the reflex pathway
   (1) Monosynaptic reflexes involve only two neurons: one sensory neuron and one somatic motor neuron, i.e. one afferent and one efferent.
   (2) Polysynaptic reflexes involve one or more interneurons between the afferent and the efferent. All autonomic reflexes are polysynaptic.

Autonomic reflexes often involve the internal organs of the body, and are often integrated in the brain, primarily in the areas that modulate body homeostasis, such as hypothalamus, thalamus, and brain stem. Autonomic reflexes in these areas help the body maintain heart rate, blood pressure, breathing, eating, water balance, and body temperature. Autonomic reflexes in the brain stem also control salivating, vomiting, sneezing, coughing, swallowing, and gagging. The limbic system also converts emotional stimuli into autonomic reflexes, such as urination, defecation, blushing, blanching, and piloerection. Some autonomic reflexes do not require input from the brain, such as urination and defecation. For example, bladder function can often be restored by autonomic reflexes two weeks after surgery in spinal transected rats.

Skeletal muscle reflexes contain the following components: sensory receptors, sensory neurons, the CNS, somatic motor neurons, and extrafusal muscle fibers. Sensory receptors, which are known as proprioceptors, are located in skeletal muscles, joint capsules, and ligaments. They monitor the position of our limbs and strength of effort being employed in movement. Sensory neurons carry afferent signals from proprioceptors to the CNS. The CNS integrates the afferent signals. Somatic motor neurons carry efferent signals. Alpha motor neurons are one kind of somatic motor neurons. They innervate extrafusal muscle fibers of skeletal muscle and control muscle fiber contraction. If the amplitude of the neural signal sent to alpha motor neurons is higher than action potential, alpha motor neurons will send a signal to extrafusal muscle fibers and cause contraction in extrafusal fibers.

There are three kinds of proprioceptors in the body: muscle spindles, Golgi tendon organs, and joint receptors. Sensory information from joint receptors is primarily integrated in the brain, whereas sensory information from muscle spindles and Golgi tendon organs activates muscle reflexes.

Muscle spindles are stretch receptors, and are comprised by intrafusal fibers, which are known as Ia sensory fibers. They respond to muscle stretch, and send the information to the spinal cord and brain. They are distributed among extrafusal muscle fibers. As muscles are being stretched, muscle spindles are also stretched and their sensory fibers fire more rapidly. The spinal cord receives increased afferent signals, sends increased efferent output through alpha motor neurons, and makes the muscle contract. Then the firing rate of afferent sensory neuron decreases. This mechanism prevents overstretching of the muscle, and is known as stretch reflex. For example, when a person is holding something, if the load to the hand increased, muscle and muscle spindle stretch as arm falls and generates stretch reflex to restore arm position. Gamma motor neurons receive information from CNS and innervate intrafusal fibers. They manage the stretch sensitivity of the muscle spindles to keep the spindles always active. For example, when a voluntary muscle contraction is generated, without gamma neuron, stretch on intrafusal fibers reduces and causes decreasing of firing rate of spindle sensory neurons, and the movement cannot be complete. With alpha-gamma coactivation, when alpha motor neurons are activated to contract extrafusal fibers, the gamma motor neurons are activated at the same time, and make the center of the

intrafusal fibers stretch and counteracts the release of tension on muscle spindle. In this way, the muscle spindle can remain active even during muscle contraction.

Golgi tendon organs respond to muscle tension, and are comprised by collagen fibers and sensory fibers, which are known as Ib sensory fibers. They are located at the junction of tendons and muscle fibers, and they cause a relaxation reflex. When a muscle contracts, collagen fibers are extended, pinching sensory neurons, and causing them to fire. After Golgi tendon organs being activated, they send information to activate inhibitory interneurons in the spinal cord, and the interneurons inhibit alpha motor neurons innervating the muscle, and muscle contraction decreases or ceases. This mechanism prevents excessive contraction that might injure the muscle. For example, when a person holding something on the hand, if excessive load is add to the hand, Golgi tendon will trigger relaxation reflex to protect the muscle.

### *3.1.3 Central Pattern Generator*

The central nervous system can coordinate muscles and joints to facilitate rhythmic and alternating movements, such as walking and running. To understand how the central nervous system controls this kind of automated movements has become a main challenge for modern neuroscience. In early works of neuroscience, there are mainly two hypotheses for the generation of rhythmic and alternating movements: the reflex chain model, and the central pattern generator (CPG) model (Fig.3). These two models have been debated for a long time. In the reflex chain model, a sensory neurons innervating muscle fire and excite interneurons that activate motor neurons to the antagonist muscle. In the CPG model, a central neural network generates rhythmic

patterns of activity in the motor neurons to antagonist muscles. The first direct experiments designed to figure out this question were attempts to eliminate all sensory feedback to the central nervous system. The earliest work to support the CPG hypothesis has been done by Wilson and his colleagues [44-46]. They successfully showed that using non-rhythmic stimulation to stimulate the nerve cord of a deafferented locust could generate rhythmic flight motor patterns. This kind of motion is called fictive locomotion and is an evidence to prove that CPGs can generate rhythmic output even after movement related afferent input is completely eliminated. Recently, the CPG model has been adopted widely.

A central pattern generator is a set of neuronal networks that can generate repeating rhythmic particular actions in the absence of phasic sensory input from peripheral receptors, such as walking, breathing, swimming, and flying. CPGs are located in the spinal cord, and are controlled by supraspinal levels. The classic CPG model is the 'half-center' model as termed by Brown [47, 48]. One part of this center controls flexors, and the other part controls extensors. For example, in human locomotion, as a gait initiates, supraspinal levels send a signal to activate CPGs of the hind limbs, CPGs generate rhythmic signals and delivered the information to motor neurons in flexors and extensors and generate locomotion. Some of the afferents send feedback directly to the CPGs to meet the environmental demands, and some of the afferents send feedback to supraspinal levels. As the man want to terminate the gait, supraspinal levels remove the signal series to CPGs, CPGs stop sending information to related motor neurons and coordinate muscles and joints of the lower limbs to stop locomotion.

Recently, it has been found that through treadmill training, SCI patients can regain some locomotor activity. This recovery is thought to be caused by reactivation of CPGs in the spinal cord. In early adult spinal cats' experiments, recovery level was always constrained because the cats cannot fully support themselves after complete spinal cord injury. It has been found that by applying body weight support, the recovery level after treadmill training can be improved significantly[49]. Pearson *et al.* found that after treadmill training, the pattern of cat's hind limb motion was more complex than that of untrained animals[50]. It suggested that treadmill training may induce reorganization of spinal circuitry and improved recovery of stepping ability. In this thesis, we use a novel neurorobotic system to assist body weight support as the rat walking on the treadmill. We believe that treadmill training with body weight support can help reorganize spinal circuitry in adult spinalized rats and help them regain stepping ability.

(a) (b)

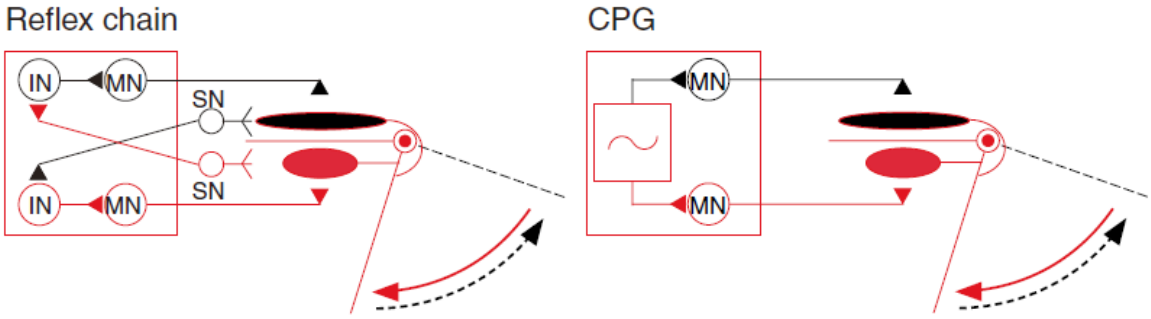


Fig. 3. Reflex chain model and CPG model. (a) Reflex chain model: sensory neurons innervating a muscle fire and excite interneurons that activate motor neurons to the antagonist muscle. (b) Central pattern generator (CPG) model: a central circuit generates rhythmic patterns of activity in the motor neurons to antagonist muscles [51].

*3.2 Locomotion*

Locomotion is the ability or action of an animal to move from one place to another, including walking, swimming, and flying. After initiation of locomotion being generated, it repeats a stereotyped movement rhythmically, and is also modified by sensory neural networks to adapt to changes in environments. Therefore, the two fundamental questions about locomotion are how these rhythmic movements are generated, and how sensory neural networks modify these patterns to fit the situation.

To study the neural control of locomotion, several methods have been developed, including spinalization, decerebration, deafferentation, immobilization, and using neonatal rats and mice. In spinalization, the spinal cord is transected at the lower thoracic level to isolate the limb control from supraspinal level. This allows investigations on the role of neural spinal networks in generating rhythmic locomotion. In decerebration, transection is made at the level of midbrain. This allows investigations of the role of the cerebellum and structures in the brain stem in controlling locomotion. In deafferentation, all the dorsal roots that innervate the limbs are transected. This was used to prove the rhythmic locomotion can still be generated even without sensory inputs from the moving limbs, which disproved the “reflex chain” model. In immobilization, muscles are paralyzed by competitive inhibitors of acetylcholine to block synaptic transmission at the neuromuscular junction. This allows intracellular and extracellular recording from neurons in the spinal cord, which are used to examine the organization and of neural pathways controlling locomotion. In the neonatal rat preparation, the spinal cord is transected between 0-5 days after the

rat was born. The spinal cord will recover to certain level after the rat grows up. This allows more detailed analysis of the locations and roles of the specific neurons involved in rhythmic movements.

After early studies in mammalian stepping, four major conclusions were found [52]:

1. Supraspinal structures are not necessary for producing the basic motor pattern for stepping.
2. The basic rhythm of stepping is produced by neural networks within the spinal cord.
3. The spinal neural network can be evoked by tonic descending signals from the brain.
4. The pattern-generating networks do not require sensory input, but are regulated by input from limb proprioceptors.

To analyze the patterns of muscle contraction, in man, the step cycle was divided into four phases: flexion (F), first extension ($E_1$), second extension ($E_2$), and third extension ($E_3$), as showed in Fig. 4.

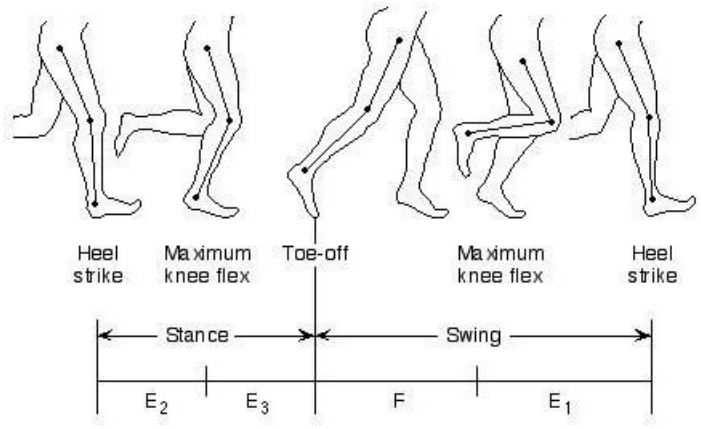


Fig. 4. Step cycle can be divided in to four phases: flexion (F), first extension ($E_1$), second extension ($E_2$), and third extension ($E_3$). [reproduced from [53] with permission]

F and $E_1$ comprise swing phase, and $E_2$ and $E_3$ comprise stance phase. In F phase, hip, knee, and ankle flex. In $E_1$, the knee and ankle begin to extend while the hip still flexes, and the leg is ready to support weight. In $E_2$, the knee and ankle flex, and the hip begin to extend. In $E_3$, the hip, knee, and ankle all extend, and provide a propulsive force to move the body forward. These four phases comprise the motor pattern of stepping.

As mentioned in 3.1.3, stepping can be generated by CPGs in the spinal neural network even in spinalized animals. However, steppings are also regulated by sensory inputs from moving limbs. Three major types of sensory information are used to modify stepping, including somatosensory input from the moving limbs, input from vestibular apparatus, and visual input. In spinalized animal, the body and limbs are isolated from supraspinal level, so only somatosensory inputs in the muscles and skin are able to provide feedback to modify body movements. In spinalized cats, it is found that the stepping rate can match the treadmill speed [54]. Therefore, it suggests that afferent input regulates the duration of the stance phase. It is also found that applying electric stimulation to sural cutaneous afferent nerve can produce higher and longer swing phase [55]. Sherrington was the first to propose that proprioceptors in muscles acting at the hip modulate locomotor patterns. He found that rapid extension at the hip joint led to contractions in the flexor muscles of spinal transected cats and dogs [56]. Hiebert *et al.* also found that stretching the detached hip flexor muscle in a walking decerebrate cat inhibited the extensor half-center and caused an earlier onset of flexor activity [57]. Muscle spindles and Golgi tendon organs are important proprioceptors

for regulating the step cycle. Electrical stimulation from these receptors prolongs the stance phase [58].

Exteroceptors in the skin also contribute greatly to modifying rhythmic locomotor patterns generated by CPGs. They detect external obstacles and adjust the stepping movements to fit the situation. Forssberg *et al.* found that this type of modification is phase dependent [59]. In spinalized cats, as the paw hit an obstacle during swing phase, flexor motor neurons were excited and extensor motor neurons were inhibited to elevate the leg to cross the obstacle. Interestingly, in stance phase, they produced an opposite mechanism: extensors were excited so that the ongoing extensor action was reinforced, which is appropriate. If the flexor motor neurons were excited, the animal may collapse.

Although basic motor patterns for stepping can be generated in spinal cord, fine tuning of stepping movements requires cooperation with the brain. Supraspinal modification of stepping can be roughly divided into three functional systems: one initiates walking and controls the speed, one responds to feedback information from the limbs and modify the motor pattern, and one guides the stepping movements based on visual input. It is found that stimulating the mesencephalic locomotor region rhythmically in decerebrated cats initiates stepping when animals are placed on a freely moving treadmill [60]. The rhythm of the locomotion generated was not related to the pattern of the stimulation, but related to its intensity. The higher the amplitude of the stimulation, the faster the stepping was generated. It suggests that a specific region in the brain stem initiates locomotion, and also control its speed by the intensity.

Recently, Mori *et al.* found that the signals that activate locomotion and control the speed are transmitted via the reticulospinal pathway [61].

Damage to the cerebellum causes ataxia. It suggests that the cerebellum is involved in the regulation of locomotion. The cerebellum receives information about stepping via two ascending pathways: dorsal and ventral spinocerebellar tracts. The cerebellum compares the signals from proprioceptors carried by the dorsal spinocerebellar tract (actual movements) with the signals from the CPGs carried by the ventral spinocerebellar tract (intended movements), calculates corrective signals, and sends to various brain stem nuclei. In this way, the cerebellum modifies the locomotor pattern as unexpected deviation happens.

Normal walking is usually visually guided walking, and motor cortex is an essential part in visuomotor coordination. Although damage to the motor cortex does not prevent animals from walking, skilled walking tasks require the coordination between motor cortex and visual area. For example, walking on a horizontal ladder requires this kind of coordination. This visuomotor coordination may also influence the regulation of locomotion.

### *3.3 Recovery of Locomotion after Spinal Cord Injury*

After spinal cord injury, many kinds of sensorimotor functions can be restored, ranging from simple spinal reflexes to more complex functions, such as locomotor function. Recovery relies on reorganization of CPGs, descending pathways, and afferents from peripheral receptors.

*3.3.1 Locomotor Recovery after Complete Spinal Transection*

After complete spinal cord transection, the spinal network is isolated from supraspinal level, all descending pathways from the brain are lost, only the spinal networks and sensory afferents are preserved to initiate and organize hindlimb (lower limb) locomotion. Therefore, reorganization of spinal networks and sensory afferents are two key roles in rehabilitation after complete spinal cord transection. Since the descending pathway from the brain is lost, triggering locomotion becomes a key issue after complete spinal cord transection. Many methods have been developed to assist locomotion generation after SCI, including pharmacological interventions [4-6], transplantation of neural progenitor cells [62, 63], bridging [64], and epidural [7-15] or intraspinal electrical stimulation [16, 17]. Pharmacological intervention using neuropharmacological agents to mimic supraspinal excitatory drive to trigger locomotion. For example, serotonin or agonists of 5-$HT_{2A}$ and 5-$HT_{1A/7}$ receptors can activate the quiescent locomotor circuitry, and can facilitate treadmill stepping with limited weight bearing in adult rats [4] and mice [6]. Neurotrophic factors can be transplanted to the injured spinal cord to promote and enhance locomotor recovery in spinal rats [62] and cats [63]. The spinal nerve exist above the injury can be disconnected and inserted into the cord caudal to injury. The inserted nerve then regenerate into the cord and synapse on neurons and forms a bridge to bypass the injury [64]. In intraspinal electrical stimulation, tonic electrical microstimulation was applied to the ventral [17]or dorsal [16] horn of the lumbosacral enlargement to trigger locomotor patterns. In epidural spinal cord stimulation, it was found that applying

electrical stimulation at the L2 or S1 spinal segment can generate locomotion in rats [7-12], cats [13-15], and humans [13]. It was also found that behavior training may reorganize the plasticity in the spinal network and improve the results of rehabilitation [5, 18-21]. Sensory afferents assist the modification of locomotor patterns, as described in section 3.2.

*3.3.2 Locomotor Recovery after Partial Spinal Lesions*

After partial spinal cord injury, damage to specific region causes specific deficits. Spared pathways originating from supraspinal and propriospinal structures play an important role in the recovery process. Damaged pathways may regenerate, or undamaged pathways may sprout, or undamaged pathways may be optimized to compensate the function lost caused by partial spinal cord injury.

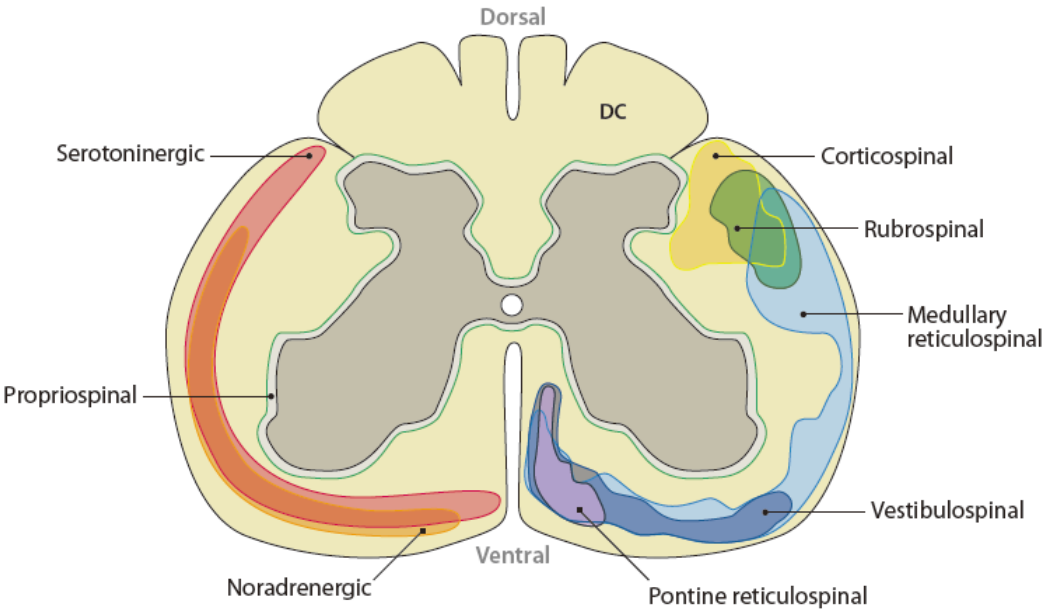


Fig. 5. Descending pathways in the spinal cord [65].

Ventral and ventrolateral lesions damage reticulospinal and vestibulospinal pathways. As mentioned in 3.2, the brain stem initiates the locomotion and sends the signal through reticulospinal pathways to CPGs in the spinal cord to generate locomotion. Damage to reticulospinal pathways may lead to problems in initiating locomotion. Vestibulospinal tracts transfer information from the vestibular labyrinth in the inner ear. Damage to this part may cause balancing and posture control problems. It is found that applying electrical stimulation to reticulospinal pathways [66] or vestibulospinal pathways [67, 68] can reset hindlimb rhythm during fictive locomotion in adult cats. It was suggested that preserving part of the ventrolateral tracts is required to evoke locomotion after SCI [69-71]. However, it was later found that cats [72-78] and monkeys [79] could walk with their hind limbs even after large bilateral lesions of ventral pathways at T13. Similarly, in human clinical record, it was found that patients with a surgical section of ventral pathways for pain relief can retain walking capability [80].

Dorsal and dorsolateral lesions cause damage to corticospinal and rubrospinal pathways, which may affect skilled walking, such as walking on a horizontal ladder [81]. It was found that applying electrical stimulation to the pyramidal tract during fictive locomotion in adult cats can reset the hindlimb rhythm, which indicates that the rhythm generating network involves corticospinal tracts [82]. Contrary, stimulation to the rubrospinal pathways did not reset the hindlimb rhythm [83]. Therefore, rubrospinal pathways may not effect the hindlimb rhythm generation as directly as corticospinal pathways. Although corticospinal pathways may influence the hindlimb

rhythm, they are not necessary in generating locomotion. It was found that lesions at the dorsal/dorsolateral part of the spinal cord produced only transient deficits in overground or treadmill locomotion [76, 84]. Propriospinal pathways surround gray matter, and interconnect various levels of the spinal cord. They also play an important role after incomplete spinal cord injury. Bareyre *et al.* found that after corticospinal tract lesions in rats, new connections in the lumbosacral section could be established through cervical propriospinal pathways [85].

Norepinephrine (NE) and serotonin (5-HT) are two important neural transmitters. Their pathways in the spinal cord also play important roles in recovery after spinal cord injury. They are synthesized in the brain stem. Norepinephrine is a kind of hormone and also a neural transmitter. It also underlies fight-or-flight responses. Approximately 80% of serotonins exist in the enterochromaffin cells in the gut to regulate intestinal movements. Others are distributed in the CNS. Lesions at the noradrenergic pathways and serotonergic pathways will lead to various kinds of dysfunction in neurotransmission. Activating or blocking NE or 5-HT receptors influences locomotion generating after SCI [86-88].

In actual situation, spinal cord injury usually causes damages to several pathways simultaneously. Two models are used to mimic partial spinal cord injury: contusion and hemisection. Contusions in experiments can be made by several kinds of impact devices. In actual life, the contusive lesion is a major form of spinal cord injury. It is usually caused by a direct impact to the vertebral column, and results in a central cavity surrounded by spared white matter. The extent of spared white matter affects

greatly to locomotor function recovery after SCI [89-92]. Spared pathways and motor training also play an important role after contusion. Singh *et al.* examined the role of spared pathways in locomotor recovery after body-weight-supported treadmill training in contused rats [93]. It was found that the contused rats without body-weight-supported treadmill training had an immediate decrease in kinematic parameters, whereas the contused rats trained with 8-week body-weight-supported treadmill training didn't show decrease in kinematic parameters immediately. Furthermore, the kinematic parameters decreased and muscle atrophy increased within two weeks if discontinue the training to the contused trained transected animals. It suggested that spared pathways can assist recovery after contusion, and continuous body-weight-supported rehabilitation is a key to retain locomotor activity. Contusions at different level also affect the extent of spinal function loss. For example, it was found that contusion at T13-L2 in adult rats caused greater loss of locomotor function compared with lesion at L3-L4, because lesion at T13-L2 could damage key elements of CPGs [94].

Hemisections damage ventral and dorsal tracts on one side of the spinal cord. After thoracic hemisection (T10-T11) in adult cats, the ipsilesional hindlimb became flaccid, requiring assistance to body weight support. Hindquarter support was recovered within two weeks, but foot dragging during swing phase persisted [95, 96]. It was also found that hemisections influenced the coordination between forelimbs and hindlimbs, and the extent of hemisection affect the extent of deficits. With small lesions, the coordination persisted [97]. Contrary, larger lesions caused the forelimbs and the

hindlimbs walked at different rhythms [98]. Hemisections also caused trouble to skilled locomotion in cats [96], monkeys [99], and rats [100]. As a short conclusion, basic hindlimb locomotion can be recovered after spinal hemisection, but several deficits persist, mostly observed on the side of the lesion.

## *3.4 Epidural Stimulation in Rats*

### *3.4.1 Historic Review*

Continuous epidural spinal cord stimulation has been applied widely to spinalized rats to stimulate CPGs in the spinal cord. Hindlimb responses were evoked, and hindlimb alternations were generated. Ichiyama *et al.* (2005) applied continuous epidural stimulation at the T12-L6 spinal segments in adult spinalized rats [8]. Rats were completely transected at T7-T9. Stimulation frequency was tested between 1-50 Hz, and stimulation intensity was tested between 1-10 V, without any pharmacological intervention. Stepping was induced in standing position, and was induced most often when the stimulation frequency was between 40-50 Hz applied at the L2 segment. A necessary condition to trigger hindlimb locomotion was also found: robust hindlimb locomotion only occurred when the rats bore at least 5% of their body weight. If the rats' paws were not contacting the treadmill belt, the hindlimb action evoked by epidural stimulation was very poor.

Gerasimenko *et al.* (2006) applied continuous epidural stimulation at the S1 spinal segment in adult spinalized rats during bipedal standing, and EMG responses in the

vastus lateralis, semitendinosus, tibialis anterior, and medial gastrocnemius muscles were recorded [7]. Spinal cord synaptic responses induced by epidural spinal cord stimulation can be found consistently in flexor and extensor muscles of the thing and shank. In addition, the EMG signal suggested that the distance from the electrodes placed at S1 and L2 to the motor pools of the hind limb muscles were approximately equal, i.e., they stimulated the same neural structures in the spinal cord. This study provides a new method to observe the responses in the hindlimb muscles triggered by epidural spinal stimulation, and also suggested that stimulation at S1 and L2 induced the responses of the same neural structures in the spinal cord.

Lavrov *et al.* (2006) applied continuous epidural spinal stimulation at the S1 spinal segment in adult spinalized rats during bipedal standing [22]. They recorded changes in spinal cord reflexes evoked by epidural spinal cord stimulation, and used them as a function to assess the level of recovery of stepping ability after spinal cord injury. A late response of the EMG signal of the hindlimb muscles coincided with the reappearance of polysynaptic reflexes in spinalized rats. This study further supported the EMG method to observe the effects of epidural spinal cord stimulation in the hindlimb muscles in rats, and suggested that restoration of polysynaptic spinal cord reflexes evoked by epidural stimulation can be a measure of functional recovery of spinal locomotor circuits after spinal cord injury.

Gerasimenko *et al.* (2007) applied continuous epidural spinal stimulation plus quipazine at the S1 and L2 segments in adult spinalized rats during bipedal standing [12]. Rats were randomly divided into 3 groups: (1) Intact rats; (2) Non-trained rats

with epidural stimulation and quipazine administration; (3) Trained rats with epidural stimulation and quipazine administration. 40 Hz epidural stimulation was applied at the S1 and L2 segments before and after quipazine administration to test the relation among epidural stimulation, quipazine administration, and the effects to the intraspinal neural circuits, and also to test the interaction between epidural stimulation and quipazine administration. Fourier transformation was used to analyze the EMG burst signals. It was found that quipazine administration can amplify the responses of epidural stimulation in both flexor and extensor, but had different spectral composition of the EMG burst signals in flexor muscle than that of epidural stimulation alone. This result suggested that quipazine administration and epidural spinal cord stimulation improved the hindlimb motor function recovery in unique, but complementary way. In addition, the rats treated with epidural stimulation plus quipazine had better plantar foot placement and weight-bearing capabilities than the rats only treated with epidural stimulation [7, 8, 22]. From the difference between group 2 and group 3 in this paper, it also suggested that motor training would affect the level of hindlimb locomotor function restoration.

Lavrov *et al.* (2008) applied continuous epidural spinal stimulation at the S1 spinal segment in adult spinalized rats during bipedal standing. Hindlimb EMG signals were recorded to examine the differences in the synaptic responses evoked by epidural stimulation at different stages of post-lesion recovery. The EMG method introduced in [7] was used to assess the effect of epidural stimulation. It is found that the monosynaptic EMG response and the long-latency EMG response induced by epidural

stimulation increased progressively, and was phase-dependent. In the first 3 weeks, only the monosynaptic responses can be observed. After the 4th week, both monosynaptic and long-latency responses can be found. With the recovery of stepping, a delay of long-latency responses was found, and was found only during extensor EMG bursts, but not during flexor EMG bursts. The changes in the long-latency responses may indicate the modulation of interneurons in the neural spinal network.

Ichiyama *et al.* (2008) applied continuous epidural spinal stimulation at the L2 spinal segment plus quipazine in adult spinalized rats during bipedal standing. Rats were separated into 2 groups: trained and untrained. Rats in trained group received epidural stimulation plus quipazine, whereas rats in the untrained group didn't. After training on the treadmill for 7 days a week for 6 weeks, the trained rats had higher and longer steps, narrower base of support at stance, and lower variability in EMG parameters then untrained rats, and the values of these parameters were found very close to those of intact animals. Their results suggested that step training reinforced the modulation of specific sensorimotor pathways, and facilitated a more selective and stable lumbosacral neural network.

Courtine *et al.* (2009) summarized the experiments that have been done by UCLA epidural stimulation group. Based on their experiments, they found that with either epidural stimulation or quipazine administration alone, the improvements in hindlimb motor function restoration were limited and took several weeks to recover. Epidural stimulation plus quipazine can induce stepping acutely in 1 week after spinal transection surgery. It was also found that epidural stimulation L2 facilitated flexion

and extended the swing phase, whereas epidural stimulation at S1 was more biased toward extension. Epidural stimulation induced functional remodeling in spinal locomotor network was found. Bearing at least 5% of body weight was found to be a necessary condition to induce hindlimb stepping. The best epidural stimulation frequency was found to be between 40-50 Hz.

We believe that epidural spinal cord stimulation can stimulate CPGs in the spinal neural network and evokes hind limb locomotion to improve the restoration of stepping capability. Furthermore, epidural spinal cord stimulation may also remodulate interneurons in neural spinal network so that enhances the recovery of hind limb motor function.

### *3.4.2 Stimulation Electrodes and Waveform*

The electrode generates an ionic flow to stimulate the biological tissue, and the ionic flow can be induced by two mechanisms: capacitive and faradic. The capacitive mechanism induces the ionic flow by a multi-layer electrode. There will be no chemical reaction in the tissue, but the charge density will be limited around 20 $\mu C/cm_2$ [101]. If charge density exceeds this range, dielectric may breakdown and faradic reaction may occur. The faradic mechanisms involve electron transfer between the tissue and the electrode, and cause either oxidation or reduction. Faradic charge injection can be reversible or irreversible. Reversible faradic processes will not produce new chemical compounds in the tissue and can be reversed by passing an

opposite current. For example, faradic charge injection in noble metals, such as platinum:

$$Pt + H_2O \Longleftrightarrow PtO + 2H^+ + 2e^-$$

Irreversible faradic processes will change chemical compounds in the tissue and cannot be reversible because some of the products will go into the surrounding fluid. For example, the electrode may react with the chloride ions in the tissue and cause electrode corrosion:

$$Pt + 4Cl^- \Longrightarrow [PtCl_4]^{2-} + 2e^-$$

The electrolysis of water is also an irreversible faradic process, which may affect the pH level of the environment:

$$2H_2O + 2e^- \Longrightarrow H_2 + 2OH^-$$

$$2H_2O \Longrightarrow O_2 + 4H^+ + 4e^-$$

All of these are not good for the charge injection, because they change the chemical compounds of the tissue fluid, alter the acidity of the surrounding, and may generate biologically toxic compositions. To avoid these situations, the reversible charge injection limits of the electrode should be estimated. In this limit, the charge can be injected in either the anodic or cathodic direction with reversible processes. The main factors deciding the reversible charge injection limits are the material of the electrode, the size, the shape, and the stimulation wave form. Teflon is a widely used coating for neural stimulation electrode because of its suitable dielectric and material properties, biocompatibility, and stability in microfabrication processes. Stainless steel has high stability and biocompatibility, which also makes it a suitable material for stimulation

electrodes. Hence, Teflon coated stainless steel wire seems to be durable for epidural stimulation for 6 weeks. Biphasic wave form will be used because a train of monophasic pulses will deliver DC signals to the tissue and cause water electrolysis, electrode damage, and tissue impairment. We believe that the Teflon coated stainless wire and the biphasic waveform can provide appropriate reversible charge injection limits to the stimulation site and achieve stable epidural stimulation in our experiments.

### *3.5 Robotic Assistive Rehabilitation after Neurologic Injury*

Robotic devices have been used widely as a motor functional rehabilitation therapy after neurologic injury, such as stroke and spinal cord injury. Many kinds of strategies have been developed, including assistive, challenge-based, haptic simulation, and coaching. Assistive robotic controllers use external, physical assistance to aid users to perform intended movements [28-39]. Challenge-based controllers make tasks more challenging, function as opposed to the assistive controllers [102-108]. Haptic simulation provides a virtual environment for the user to practice activities of daily living [109, 110]. Instead of contacting the user directly, coaching robots try to find the best way to exercise for the user, and help the user exercise effectively and correctly [111].

Assistive control strategies are the most developed field, and can be divided into four subcategories: impedance-based assistive controllers [28-30], counterbalance-

based assistive controllers [31-33], EMG-based assistive controllers [34-36], and performance-based adaptive controllers [37-39]. Because providing too much assistance sometimes may make people pay less effort during motor training, the best policy is to provide “assistance-as-needed”. Therefore, the concept of impedance-based assistive robotic control is that the robot will not interfere if the user moves along a desired trajectory, and if the user deviates from the desired trajectory, a force will be generated by a properly designed mechanical impedance to guide the user back to the desired trajectory, such as creating a virtual wall/channel to constrain the user moving along the desired trajectory by applying an elastic force field to the user.

Counterbalance-based assistive controllers provide force to counterbalance the weight of the limbs to assist users in reaching [33] or walking [31]. Using swimming pool in rehabilitation is a variant of counterbalancing assistance, where buoyancy counterbalances the gravity acts on the limbs.

The concept of EMG-based controllers is quite straightforward. In unimpaired person, the brain gives a command, transforms into electric neural signals, and transfers to objective muscles to perform desired movements. These electric neural signals can be captured by EMG recording. EMG-based controllers record EMG signals of the weakened limb and provide external force to drive the limb to perform desired movement. The deficiency of EMG-based controller is that sensitivity and precision are not stable. For example, when the user has extra sweat on the skin may cause extra noises to the EMG signals, and the EMG recording signals should be calibrated. Depends on different personal physical characteristics, EMG recording

parameters may also be calibrated from person to person. Some devices combined with EEG (Electroencephalography) recording to make the movement decision more precisely. For example, Dr. Sankai developed a EMG-based Robot Suit HAL (Hybrid Assistive Limb) exoskeleton robotic suit can help voluntary control of the weakened limbs, and the latest version also records EEG signals to compensate errors from EMG recording [35].

Performance-based adaptive controllers provide online adaptation of the control parameters. The parameters (time, force, stiffness, etc.) of the assistive unit will adjust with the performance change of the user to make the training fit better to the user and be more effective. This "patient-cooperative training" strategy has been used to rehabilitate in the Lokomat [39] and MIT-MANUS [112]. The concept of performance-based adaptive control strategies can be expressed as a function as follows,

$$P_{i+1} = fP_i + ge_i \quad (1)$$

Where $P_i$ is the control parameter that is adapted (for example, robot assisting force, robot stiffness, movement time, impedance, etc.), i refers to the ith movement, e is the performance error, f is a forgetting factor, and g is the gain factor of the error. The reason to include a forgetting term is to deal with the problem of participant slacking in response to assistance. If the participant pays good effort to the exercise, f can be set as 1. For example, MIT-MANUS used this setting [112].

*3.6 Trunk Based Neurorobotic System for Rats*

Recently, primarily ankle and knee based robots have been used to assist rehabilitation after spinal cord injury in rat model [8, 10, 12, 113-115]. Under this setup, the robot holds the rats in a vertical standing position, and the rats' haunches walk bipedally on the treadmill. This setup may not be appropriate. After spinal cord injury at the thoracic level, part of the trunk is still under supraspinal control [40, 116-118]. Excluding the trunk and trunk-limb interactions could constrain recovery. A trunk-based neurorobotic rehabilitation system developed by Giszter and Udoekwere allows implementing a new therapeutic approach of trunk sensory motor training [19, 117, 119]. Under this setup, the rats walk quadrupedally, which fits natural condition, and the contribution of the trunk to rehabilitation is not ignored.

In adult spinalized rats, Udoekwere *et al.* used this impedance-control based neurorobotic system, PHANTOM robot (developed by SensAble Technologies, Inc.), to apply a 3-dimensional elastic field to the pelvis of the rat as the animal walking on the treadmill to assist body balancing and body weight support [19]. A novel pelvic orthosis was used to connect the rat's pelvis to the robot arm. Pelvic height of the normal rat was set as the elastic center. Pelvic height of the spinal transected animal is always lower than that of the normal rat, so the elastic field will generate an upward force to assist body weight support of the rat. The more the rat relies on the robot arm for body weight support, the stronger the elastic force is generated. Therefore, the variation of this upward force can be used as a measure of recovery of self body weight support. The ideal situation is that self-body-weight-support of the spinalized

rat can be restored gradually during training, so that the pelvic height of the spinalized rat can approach the elastic center gradually, and reach the elastic center after self-body-weight-support completely recovered, i.e., the elastic force act on the rat's pelvis will be diminished naturally after the rat completely regain self body weight support. In the study, long term adaptation occurred, and the motor function of the rats improved significantly.

Giszter *et al.* used the same robot device to explore the mechanisms of coordinated hindlimb weight support in rats spinally transected as neonates (ST rats), and compared with normal rats [117]. ST rats with over 60% self body weight support (N = 8) and normal rats (N = 12) were trained to pass a runway with 3-dimentional force/torque sensor. Total ground reaction forces, forelimb and hindlimb contributions, and the variation of the center of pressure were recorded. The patterns to generate propulsive and decelerative force were found different between these two groups. In normal rats, forelimbs and hindlimbs acted synergistically, where in ST rats forelimbs and hindlimbs acted opposingly. On average, hindlimbs of normal rats usually bore about 80% of the vertical load carried by forelimbs, where in ST rats hindlimbs bore about 60% of the vertical load carried by forelimbs. The motion of center of pressure of the normal rats moved as a straight line as the animal crossing the runway, and lateral deviation of the center of pressure was small (<1 cm). In ST rats, the motion of center of pressure was zig-zagged and the lateral deviation of the center of pressure (~2 cm) was significantly larger than that of normal rats. This suggests that normal rats

have better walking stability and precision than ST rats, and lateral deviation can be a measure to assess walking stability and precision.

In this study, we used the same neurorobotic system (PHANTOM robot) to assist body weight support of the rat, and we believe this neurorobotic system can provide an appropriate environment to assist the rats to regain self body weight support and achieve better body balancing. The same method used by Udoekwere *et al.* [19] to analyze the variation of self body weight support was applied to assess the recovery of self body weight support of the rats in this experiment. The extent of lateral deviation and the distance of the rat's pelvis deviated from the elastic center of each group were collected by the neurorobotic system and were used to assess walking stability and precision.

# 4. Methods and Materials

60 normal Sprague-Dawley rats (250-350 g) were used in the experiment, and were spinalized at vertebral level T9/T10. First 10 of them were used to test the electrode and pelvic orthoses implantation, the best site to stimulate, and the best epidural stimulation parameters. The other 50 rats were implanted with an epidural stimulation electrode under the arch of vertebral level L2, and these were separated into 3 groups: control group, conventional stimulation group, and robot-driven stimulation group. However, animal care for completely transected rats is a difficult task. They lose various functions below the transection site, which may cause self-biting, bladder infections, and many other problems, leading to death or forced euthanasia. Only 20 rats completed the full training process, and met our criteria for inclusion in the study, 6 rats in the control group (no stimulation), 6 rats in the conventional stimulation group, and 8 rats in the robot-driven epidural stimulation group. All of the rats were trained on a treadmill with the PHANTOM neurorobotic system after complete spinal transection. The robot arm detected the position of the rat's pelvis and sent feedback to the system PC to decide the strength of the force and the timing to stimulate. The interaction forces of the rats with the robot and the pelvic position were collected by the robot system software. The vertical force data were used to assess recovery of active hindlimb weight support, and the lateral position deviation was used to assess the walking stability. All processes were video recorded. An adapted motor score (hindlimb adapted BBB, or 'AOB' for spinalized animals) was used to assess

kinematic recovery [120]. A joint marker tracking software, MaxTRAQ, was also used to assist analyzing kinematic data. Stimulation events were collected by Digidata, a data acquisition device developed by Molecular Devices, LLC. At the end of the experiments, rats were perfused with 4% formaldehyde, and the spinal cords were preserved for histology. Nissl-myelin stain and 5HT immunohistochemical stain for serotonins were used to confirm the spinal transection.

### *4.1 Surgery*

All surgical procedures were under aseptic conditions, and in compliance with IACUC recommendations. Rats were anesthetized by a ketamine cocktail (KXA) [ketamine hydrochloride (50 mg/Kg), xylazine (5 mg/Kg), acepromazine (0.75 mg/Kg)] (1 ml/kg), and maintained at a deep level of anesthesia by supplemental doses of KXA (0.38 ml/kg) per hour.

#### *4.1.1 Transection and Epidural Stimulation Electrode Implantation*

A mid-dorsal skin incision was made from T8 to L2. The fascia and muscles were removed at the appropriate vertebral levels. A partial laminectomy was performed at T9~T11, and the spinal cord was completely transected by iridectomy scissors and vacuum extracting. Gel foam was inserted into the gap created by the transection to prevent the reconnection of the spinal cord. Another laminectomy was made at the

end of L1 for inserting the electrode. A stimulation electrode was gently pushed into the L2 arch, and a ground electrode was sutured on the back muscle of the rat, as shown in Fig. 6 and Fig. 7. The opening was closed by stainless steel wound clips after surgery.

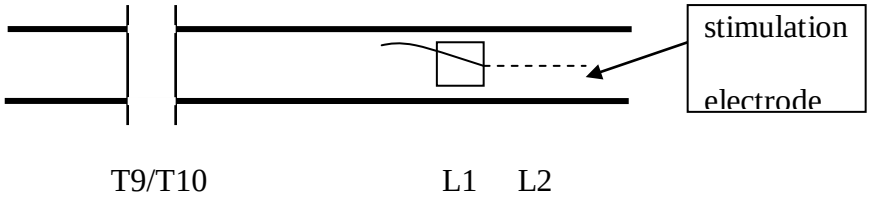


Fig. 6. Transection site and the location of epidural stimulation electrode.

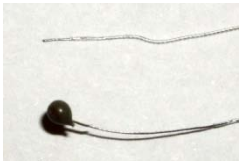


Fig. 7. The electrode for electric spinal epidural stimulation.

*4.1.2 Pelvic Implant Surgery and Wire Organizing*

A pelvic orthosis was implanted for robot attachment as described in [19] [see Fig. 8(A)]. After electrode implantation, wires were passed subcutaneously to the back, and were soldered to a connector mounted on the pelvic orthosis [see Fig. 8(B)]. The connector can be connected to a stimulator to receive epidural spinal stimulation.

(**A)** (B)

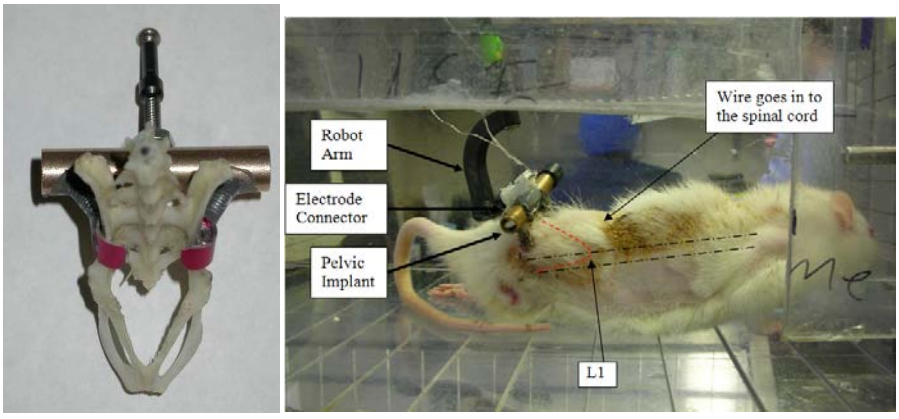


Fig. 8. Pelvic orthoses and the arrangement of the electrode and the wire. (A) Pelvic orthoses and (B) how the electrode connects to the system.

*4.1.3 Post Surgical Care*

All animals received 1.0 ml/kg of 0.05 mg/ml buprenorphine subcutaneously, every 12 hours, for 48 hours after surgery (totally 4 doses). 0.2 ml/kg Baytril were given to the animals subcutaneously every 24 hours to prevent infection caused by spinal transection. 10 ml Lactated Ringer's solution were given to all of the animals daily to maintain enough water in the animals' body for proper metabolism and to prevent crystallization in the bladder. Wound clips were removed 1 week after surgery. The rat' s bladder was checked twice a day. If the bladder was full, we pressed the bladder gently to help the urine come out. Rats' teeth were trimmed twice a week to prevent the rats from chewing themselves and the wires. If crystals were found around the rat's urinary area, we bathed the animal daily with Zymox shampoo and sprayed the urinary area with Zymox spray.

## *4.2 Neurorobotic System and Epidural Stimulation*

### *4.2.1 Neurorobotic System*

A PHANTOM Premium 1.0 device developed by SensAble Technologies, Inc. was used to assist weight support to the rats, as in Fig. 9. There were 2 parts in PHANTOM robot, one part had 4 force sensors, and the other part was the robot arm. In this study, only the robot arm was used, and only the robot data were collected and extracted. The robot arm can apply an elastic force field to the rat to assist weight support during training. The elastic field equation used was:

$$F = k\,(\ell - \ell_C) \tag{2}$$

F = force applied by the robot arm; k = stiffness of the elastic field; $\ell_C$ = the desired center of the elastic field; $\ell$ = the current point of the pelvic junction. In our experiments, k is always set at 1 robot unit, which is 33.86 N/m, for x (backward/forward), y (lateral), and z (vertical) direction to apply an isotropic elastic force field to the rats. After setting the desired stiffness and the desired center point of the elastic field, the pelvic junction is constrained around the center of the elastic field, so that the rat can be pelvis could be held weight-supported by the robot arm. In the first week, the pelvic height of a spinalized rat was usually 1000 robot unit, which is 1 inch, lower than the elastic center. Substitutes into eq.(2), weight support provided by the robot arm, F = 33.86 × 1 × 2.54 ÷ 100 = 0.86 N = 87.76 gw. At the beginning of the training, the average weight of the rats was 275 g. Hence, at the start point of the training, robot arm provided about 30% weight support of the rat weight. The more the rat regained self-weight-support, the less the robot arm provided the support. Ideally,

as the rats completely regain self weight support and approach the robot field equilibrium, the robot assistance will be naturally diminished, i.e. as $\ell = \ell_c$ ,$F = k \cdot 0 = 0$.

(A) (B)

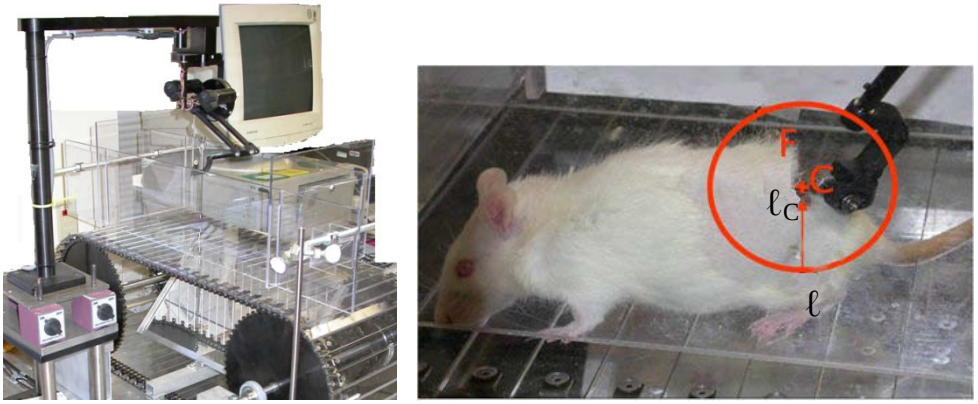


Fig. 9. Neurorobotic system. (A) PHANTOM Premium 1.0 device integrated with our treadmill. The robot arm, connect to a control center, which is under the treadmill, and connect to a card interface to the ISA port of the PC. We can use a specific operating system for PHANTOM®, which is also developed by SensAble Technologies, to set the parameters of the robot arm. We can also collect feedback data from the robot arm by this OS. (B) Robot arm applies an elastic field to the rat to assist weight support.

*4.2.2 Epidural Stimulation*

10 Sprague-Dawley (SD) rats were used to practice the implant procedure of the electrodes and the pelvic orthoses, to determine the best site in the spinal cord to trigger hindlimb stepping by epidural stimulation, and to test the best epidural stimulation parameters for our animals. Electrodes were tested at vertebral T13, L1, L2, and L3. It was found that the area between vertebral level L1 and L2 was the best site to trigger hindlimb stepping for our rats. The range we used to test optimal stimulation parameters was based on the studies of a group in UCLA Brain Research Institute doing epidural spinal cord stimulation research [7, 8, 10-14, 20, 22, 24, 25]. Frequency of stimulation was tested between 30-60 Hz, and it was found that the best stimulation frequency for our animals is 40 Hz. Stimulation amplitude was tested between 0-10 V. It was found that the optimum stimulation voltage may relate to the physiological state of the rat and was differed from rats to rats. For most rats, hindlimb stepping could be triggered by stimuli between 0.5-3 V. We found that 200 μs pulse duration could trigger hindlimb stepping properly for all of the animals, so we didn't test different pulse durations. Our parameters for this preliminary testing thus confirmed the prior published data of the UCLA group, except our optimum stimulus strength was lower.

For conventional epidural stimulation, parameter settings thus utilized those from previous works by the UCLA group [7, 8, 10-12, 20, 22]. Frequency was set to be 40Hz (inter pulse period (IPP) set to be 25 ms), pulse duration was set to be 200 μs, and amplitude was set between 0.5-3 V. The signal series stimulation series then operated through the whole training process, for 15 minutes.

Initially, 2 rats were used to test triggering epidural stimulation manually. The operator observed the stepping of the rats, tried to find the best specific step phase to trigger epidural stimulation to facilitate hindlimb stepping, and triggered epidural stimulation at that specific step phase manually. However, identifying the best step phase to trigger epidural stimulation is based on the subjective observation by the operator, so that the experiment may not be easy to reproduce. In addition, fatigue of the leg muscles of the operator caused by hitting the pad switch to trigger epidural stimulation repeatedly also influenced the timing to trigger stimulation! Because of these uncertain factors, this test was terminated. Subsequently, we instead tried to use systematic feedback from the robot to trigger epidural stimulation.

A piece of robot control code firmware, rcp_epi_stimulus.dll, was developed to control robot-driven epidural stimulation (see Appendix). The code was based on rcp_stimulus.dll, which is a piece of firmware code developed by Giszter to control robot-driven stimulation by a PHANTOM robot (SensAble Technology Inc.).

For robot-driven epidural stimulation, the same maximum inter-pulse period, pulse duration, and amplitude as the conventional stimulation group were used. The only difference was that the robot arm was used to detect the rat's pelvic position, and the robot software thereby decided the timing of stimulation. The controlling file was created by Visual Studio in .dll format. When the robot booted up, the operating system loaded the dll file automatically.

Algorithm for epidural stimulation:

1. Robot arm encodes record the height of the rat's pelvis and this is sent back to the program.

2. If the height < the center point of the elastic field, and interpulse period < 25ms, send a biphasic electric pulse to the spinal cord. (This limits stimulus frequency to < 40Hz)

3. Go to 1.

The program monitored the rat's pelvis height every 1 ms. If the pelvis was lower than the elastic center and IPP>25ms, a 200 μs 0.5-3V pulse was delivered. At the early stage of rehabilitation, the pelvis of the rat was often under the elastic center, because of the absence of self weight support. In this case, the stimulation was nearly a continuous series of 40 Hz, and nearly identical to the conventional stimulation group. After the rat more fully recovered however, the stimulation would be diminished naturally in parallel with the force.

As an aside, I would like to note I explored other approaches beside those that form the bulk of this thesis. Ventral-tegmental area (VTA) stimulation was tested to integrate with robot-driven stimulation to develop an appropriate environment for cortical and spinal plasticizing, and further enhance the optimum effect for motor function restoration. Since "pleasure centers" have been found in the rats, the investigation of brain reward circuitry has been intensively explored [121]. Numerous examples showed that electrical stimulation of reward circuitry contributed to reinforcement of learning mechanism in rats. Dopamine levels were elevated after electrical stimulation, and motivation of specific skills, such as lever-pressing, can be

enhanced [122]. Therefore, combining electrical stimulation of reward circuitry with rehabilitation process in SCI treatment can likely incubate an optimal environment for plasticizing of spinal circuitry and reinforce motor function restoration. 20 extra intact SD rats were used to test the practicability of VTA stimulation under our neurorobotic system. 10 rats received VTA stimulation as a reward, while others didn't. Stimulation parameters were based on Bao's VTA stimulation research (pulse duration = 100 μs, burst width = 1ms, frequency = 100 Hz, amplitude = 200 μA, biphasic pulse) [123]. The algorithm we explored was as follows:

1. Robot arm records the height of the rat's pelvis and send back to the program.
2. If the height > the center point of the elastic field, send a train of 5 biphasic electric pulse to the VTA of the rat, counter+1.
3. Go to 1.

The idea is: if the rat can walk higher than the elastic center (make pelvic position higher than elastic center), then the system activates VTA to give a reward to the rat.

However, after statistical tests, we found no significant difference between control rats and VTA rats. As a result, VTA stimulation was not combined with the robot-driven epidural stimulation here. Our current hypothesis regarding this negative result is that it could be that the thickness of the stainless steel electrodes we used to test VTA stimulation (shank diameter 1 mm) could be too thick so that the size of the area being stimulated was too wide, which activated a less specific area less intensely. Two years after these early tests, a colleague in our lab used the same electrode for cortical mapping and found that stimulation applying to the motor cortex with the probe types

we employed could not generate either forelimb or hindlimb movement, whereas forelimb biceps extraction could be generated consistently by using a thinner stainless steel electrode (shank diameter 125 μm). The detail processes of cortical mapping were described in [40, 124]. Accordingly, revisiting the addition of VTA stimulation in a system such as ours may have value.

Table I. Parameter settings of robot-driven epidural stimulation

| **Pulse Duration** | **Inter Pulse Period** | **Amplitude** |
|---|---|---|
| 200μs | 25ms | 0.5-3 V |

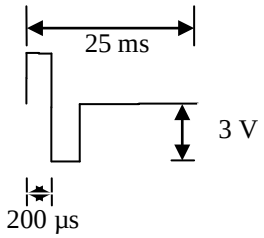


Fig. 10. One signal wave of electric epidural stimulation.

## *4.3 Data Collection and Analysis*

### *4.3.1 Overview*

Animals were trained on the treadmill with the PHANTOM neurorobotic system one week after spinal transection surgery, for 15 minutes per trial, 5 days a week, for 5 – 7 weeks. Treadmill speed was set as 12 cm/s (see Table II). Treadmill was cleaned by diluted MB-10 detergent between animals. All processes were video recorded. The interaction forces of the rats with the robot and the pelvic position were collected by the robot system software. The vertical force data were used to assess recovery of active hindlimb weight support, and the lateral pelvis position deviations were used to assess the walking stability. Data analysis including: (1) Functional scoring: An adapted motor score (hindlimb adapted BBB, or 'AOB' for spinalized animals) used to assess kinematic recovery (see Table III) [120]. (2) Self weight support examination: Z-force data from PHANTOM robot were used as a measure of functional restoration of self weight support. (3) Walking balance examination: Y-position data from PHANTOM robot were used as a measure of the lateral stability and precision of the rats' walking. (4) Kinematic data analyzing: an image tracking program, MaxTRAQ **(**Innovision Systems, Inc.**),** was used to track the kinematic changing through training**.** (5) Stimulation event analyzing: A data acquisition and analyzing device, Digidata (Molecular Devices, LLC), was used to collect the stimulation events of robot-driven epidural stimulation. The collected signals were recorded by Axoscope, an operating interface developed by the same company. The recorded events were then compared with the step cycle, and the event frequency variation with step phase was calculated.

Table II. Training settings

| Treadmill speed | Training duration | Whole treatment duration |
|---|---|---|
| 12 cm/s | 15 min per trial,<br>5 days per week | 5-7 weeks |

Table III. Adapted BBB scoring [120]

| Motor performance Level Score | Movement type | | | | |
|---|---|---|---|---|---|
| | Movement | R–L alternation | Amplitude | Body wieght support | Plantar foot placement |
| Level 1 | | | | | |
| 0 | No | – | – | – | – |
| 1 | Weak limbs jerks | – | – | – | – |
| Level 2 (Rhythmic movements/dorsal foot placement) | | | | | |
| 2 | Yes | No | Weak | – | – |
| 3 | Yes | No | Large | – | – |
| 4 | Yes | Occasional | Weak | – | – |
| 5 | Yes | Occasional | Large | – | – |
| 6 | Yes | Frequent | Weak | – | – |
| 7 | Yes | Frequent | Large | – | – |
| 8 | Yes | Consistent | Weak | – | – |
| 9 | Yes | Consistent | Large | – | – |
| Level 3 (Large alternating movements/dorsal foot placement/occasional body weight support) | | | | | |
| 10 | Yes | Yes | Large | Occasional | – |
| Level 4 (Plantar foot placement) | | | | | |
| 11 | Yes | Occasional | Large | No | Occasional |
| 12 | Yes | Frequent | Large | No | Occasional |
| 13 | Yes | Frequent | Large | Occasional | Occasional |
| 14 | Yes | Consistent | Large | No | Occasional |
| 15 | Yes | Consistent | Large | Occasional | Occasional |
| 16 | Yes | Frequent | Large | Frequent | Frequent |
| 17 | Yes | Frequent | Large | Frequent | Consistent |
| 18 | Yes | Frequent | Large | Consistent | Frequent |
| 19 | Yes | Frequent | Large | Consistent | Consistent |
| 20 | Yes | Consistent | Large | Consistent | Occasional |
| 21 | Yes | Consistent | Large | Consistent | Frequent |
| 22 | Yes | Consistent | Large | Consistent | Consistent |

*4.3.2 AOB Scoring*

AOB scoring is an adapted scoring method for spinalized animals which is developed by M. Antri and his colleagues [120]. The original BBB scoring is a scoring method to scale the recovery level for incomplete spinal cord injury. However, in BBB scoring, there are some parameters related to forelimb motion, which may not be an issue in animals transected at thoracic level. Thus, they modulated the BBB scoring method to an adapted scoring of hind limb movement recovery, which is AOB scoring. This score evaluated hindlimb joint motion, range of motion, rhythmicity, alternation, apparent weight support and plantar placement on a numerical scale.

*4.3.3 Robot Data*

The original robot output file contained 3-dimensional force and torque data for each sensor, 3-dimensional force, position, orientation, and velocity data. In this study, only robot data were collected and extracted. Z-force data were used as a measure of self body weight support recover, and Y-position data were used as a measure of the walking lateral stability and precision of the rats. The size of the data that could be recorded was constrained by the memory of the robot computer. When we started the study, the memory of the robot computer can only record data for 2 minutes. Today the memory device of the computer was upgraded, and the robot system was able to record data for 20 minutes. However, for data consistency, the duration for robotic data recording was 2 minutes for all of the animals. The data were recorded from 12 to 14 minute in the 15 minutes training process.

*4.3.4 Kinematic Data*

Optical makers were used to mark the joints of the animal's hindlimb, and a high-speed infrared digital camera was used to record the video. The recording frame rate was 120 frames per second. Before recording, 4 markers were attached to the pelvis, hip, ankle, and the first MTP (big toe) joints by superglue. Because the skin around the knee joint moved a lot during animal walking, it may be hard to decide the position of the knee joint precisely from the optical marker, so the position of the knee joint was calculated by trigonometric functions. Set ($x_1$, $y_1$) to be the pelvis joint, ($x_2$, $y_2$) to be the hip joint, ($x_5$, $y_5$) to be the knee joint, ($x_3$, $y_3$) to be the ankle joint, and ($x_4$, $y_4$) to be the first MTP joint, as showed in Fig. 11(A). When analyzing, the first frame was used to determine the length of thigh and shank of the animal, which were a and b in Fig. 11(B). Initial points of the pelvis joint marker, hip joint marker, ankle joint marker, and MTP joint marker were recorded as ($x_1'$, $y_1'$), ($x_2'$, $y_2'$), ($x_3'$, $y_3'$), and ($x_4'$, $y_4'$). The position of the knee joint in the first frame was observed carefully and recorded as ($x_5'$, $y_5'$). Thus,

$$a = \sqrt{(x_2' - x_5')^2 + (y_2' - y_5')^2} \tag{3}$$

$$b = \sqrt{(x_3' - x_5')^2 + (y_3' - y_5')^2} \tag{4}$$

Since a and b are the length of thigh and shank of the animal, they won't change during the experiment. For the following period, with ($x_1$, $y_1$), ($x_2$, $y_2$), ($x_3$, $y_3$), ($x_4$, $y_4$), a, and b known, ($x_5$, $y_5$) can be calculated.

$$x_5 = x_3 + b\cos(\beta - \alpha) = x_3 + b(\cos\beta\cos\alpha + \sin\beta\sin\alpha) \tag{5}$$

$$y_5 = y_3 + b\sin(\beta - \alpha) = y_3 + b(\sin\beta\cos\alpha + \cos\beta\sin\alpha) \tag{6}$$

$$\cos\alpha = \frac{\vec{l}\cdot\vec{b}}{|\vec{\ell}||\vec{b}|} = \frac{[(x_2-x_3)i+(y_2-y_3)j]\cdot[(x_5-x_3)i+(y_5-y_3)j]}{\sqrt{[(x_2-x_3)^2+(y_2-y_3)^2]}\cdot\sqrt{[(x_5-x_3)^2+(y_5-y_3)^2]}} =$$

$$\frac{(x_2-x_3)(x_5-x_3)+(y_2-y_3)(y_5-y_3)}{\sqrt{[(x_2-x_3)^2+(y_2-y_3)^2]}\cdot\sqrt{[(x_5-x_3)^2+(y_5-y_3)^2]}} \quad (7)$$

$$\cos\beta = \frac{x_2-x_3}{\sqrt{[(x_2-x_3)^2+(y_2-y_3)^2]}} \quad (8)$$

Under normal physical and walking condition, $0 < \alpha < \frac{\pi}{2}$, and $0 < \beta < \pi$

$$\Rightarrow \sin\alpha > 0, \text{and } \sin\beta > 0$$

$$\Rightarrow \sin\alpha = \sqrt{1-\cos^2\alpha} = \sqrt{1-\left(\frac{(x_2-x_3)(x_5-x_3)+(y_2-y_3)(y_5-y_3)}{\sqrt{[(x_2-x_3)^2+(y_2-y_3)^2]}\cdot\sqrt{[(x_5-x_3)^2+(y_5-y_3)^2]}}\right)^2} \quad (9)$$

$$\sin\beta = \sqrt{1-\cos^2\beta} = \sqrt{1-\left(\frac{x_2-x_3}{\sqrt{[(x_2-x_3)^2+(y_2-y_3)^2]}}\right)^2} \quad (10)$$

Substitute (3)(6)(7)(8)(9) into (4)(5),

$$x_5 = x_3 + \sqrt{(x_3'-x_5')^2+(y_3'-y_5')^2}\times$$

$$\left[\frac{x_2-x_3}{\sqrt{[(x_2-x_3)^2+(y_2-y_3)^2]}}\times\frac{(x_2-x_3)(x_5-x_3)+(y_2-y_3)(y_5-y_3)}{\sqrt{[(x_2-x_3)^2+(y_2-y_3)^2]}\cdot\sqrt{[(x_5-x_3)^2+(y_5-y_3)^2]}}\right.$$

$$\left.+\sqrt{1-\left(\frac{x_2-x_3}{\sqrt{[(x_2-x_3)^2+(y_2-y_3)^2]}}\right)^2}\times\sqrt{1-\left(\frac{x_2-x_3}{\sqrt{[(x_2-x_3)^2+(y_2-y_3)^2]}}\right)^2}\right] \quad (11)$$

, and

$$y_5 = y_3 + \sqrt{(x_3'-x_5')^2+(y_3'-y_5')^2}\times$$

$$\left[\sqrt{1-\left(\frac{x_2-x_3}{\sqrt{[(x_2-x_3)^2+(y_2-y_3)^2]}}\right)^2}\times\frac{(x_2-x_3)(x_5-x_3)+(y_2-y_3)(y_5-y_3)}{\sqrt{[(x_2-x_3)^2+(y_2-y_3)^2]}\cdot\sqrt{[(x_5-x_3)^2+(y_5-y_3)^2]}}\right.$$

$$\left.+\frac{x_2-x_3}{\sqrt{[(x_2-x_3)^2+(y_2-y_3)^2]}}\times\sqrt{1-\left(\frac{(x_2-x_3)(x_5-x_3)+(y_2-y_3)(y_5-y_3)}{\sqrt{[(x_2-x_3)^2+(y_2-y_3)^2]}\cdot\sqrt{[(x_5-x_3)^2+(y_5-y_3)^2]}}\right)^2}\right] \quad (12)$$

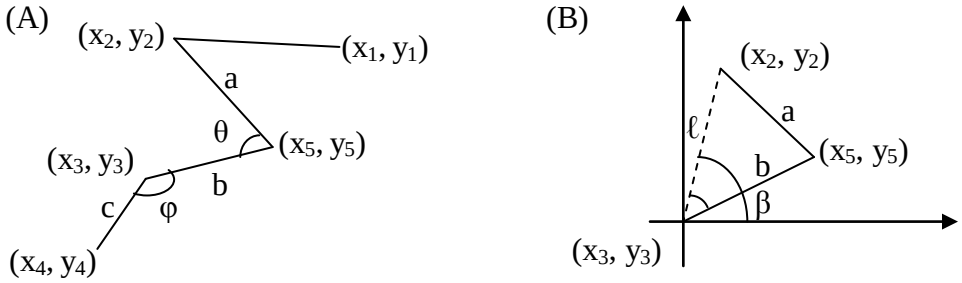


Fig. 11. Geometric settings for the hind limb joint marker calculation of the rats. (A) Whole limb. (B) Thigh and shank.

After $(x_5, y_5)$ was calculated, the angle at the knee joint ($\theta$) and at the ankle joint ($\varphi$) [see Fig. 6(a)] can also be calculated.

$$\cos\theta = \frac{\vec{a}\cdot\vec{b}}{|\vec{a}||\vec{b}|} = \frac{[(x_2-x_5)i+(y_2-y_5)j]\cdot[(x_3-x_5)i+(y_3-y_5)j]}{\sqrt{[(x_2-x_5)^2+(y_2-y_5)^2]}\cdot\sqrt{[(x_3-x_5)^2+(y_3-y_5)^2]}}$$

$$\Rightarrow \theta = \cos^{-1}\frac{(x_2-x_5)(x_3-x_5)+(y_2-y_5)(y_3-y_5)}{\sqrt{[(x_2-x_5)^2+(y_2-y_5)^2]}\cdot\sqrt{[(x_3-x_5)^2+(y_3-y_5)^2]}} \quad (13)$$

, and

$$\cos\varphi = \frac{\vec{b}\cdot\vec{c}}{|\vec{b}||\vec{c}|} = \frac{[(x_5-x_3)i+(y_5-y_3)j]\cdot[(x_4-x_3)i+(y_4-y_3)j]}{\sqrt{[(x_5-x_3)^2+(y_5-y_3)^2]}\cdot\sqrt{[(x_4-x_3)^2+(y_4-y_3)^2]}}$$

$$\Rightarrow \varphi = \cos^{-1}\frac{(x_5-x_3)(x_4-x_3)+(y_5-y_3)(y_4-y_3)}{\sqrt{[(x_5-x_3)^2+(y_5-y_3)^2]}\cdot\sqrt{[(x_4-x_3)^2+(y_4-y_3)^2]}} \quad (14)$$

After hindlimb joint marker tracking, vertical trajectory of ankle joint marker ($y_3$) was used to calculate the step cycle of the rat. By analyzing the up-down movement of $y_3$, step cycle can be obtained. Ideally, one step cycle is the period of $y_3$ goes from the baseline of the ankle joint to the highest point and drops back to the baseline, which is the period of one up-down movement in an ideal stepping pattern. However, in actual practice, I found that the up-down movement of the ankle joint marker was irregular.

For example, Fig. 12(A) shows the raw data of $y_3$ vs. time of PIETX22 at the $7^{th}$ week. Many micro up-down movements can be found in the figure. In this case, simply applying a peak counting method to count the cycle will lead to overcounting of the number of the cycles and the step cycle will be shorter than true step cycle. To eliminate the noise, the moving average filter (window size: 10) was applied to the data ($y_3$), as showed in Fig. 12(B). The signal became smoother, but was still an irregular pattern. Peak counting method was thus still not be the best to count step cycles. For example, between 1 and 2 second, there are 2 peaks. After using peak counting, it will be counted as 2 step cycles. However, it is closer to 1 step cycle in the real case. A method to count the cycle of this kind of irregular pattern was needed.

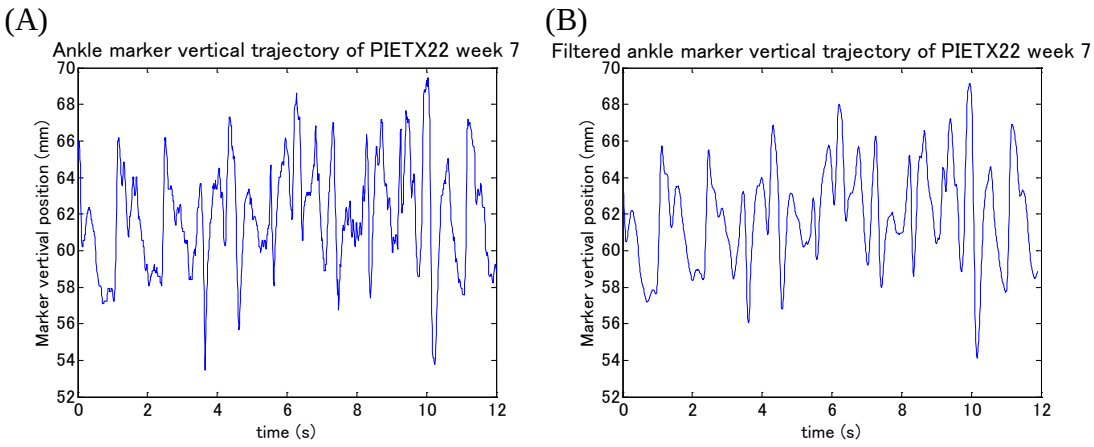


Fig.12. Ankle joint marker vertical trajectory (y3) of PIETX22 at the 7th week. (A) Raw data of ankle joint marker vertical trajectory of PIETX22 at the 7th week. (B) Ankle marker vertical trajectory of PIETX22 at the 7th week after applying moving average filter with window size 10.

Rainflow-counting algorithms are a method which can be applied to cycle counting for irregular signals. It was first developed by two Japanese engineers, Matsuishi, M. & Endo, T., to calculate the fatigue life of a structure to complex loading [125]. In 1982, Downing *et al.* modified the algorithm and created a more widely used version [126], which was then included by ASTM E 1049-85 as one of the cycle-counting algorithms [127]. It also has been introduced to analyze time-varying biological data by Jacob *et al.* [128]. The algorithm is as follows:

1) Filter the signal. Makes each point to be a local minimum or maximum.
2) Turn the sheet clockwise 90° (earliest time to the top), and imagine that the signal series as a pagoda, where the earliest time is the roof of the pagoda.
3) The peaks at the right side of the pagoda are considered as peaks, and the peaks at the left side of the pagoda are considered as valleys.
4) Each peak/valley is imagined as a source of water that "drips" down the pagoda.
5) Start raindrop from the roof.
    a) If the fall of the raindrop starts from a peak:
        i) The raindrop will stop as it reaches a more positive value (considered the right side is positive and the left side is negative) than the start point [Fig.13(A)].
        ii) The raindrop will also stop as it encounters flow from a previous path [Fig.13(B)]. If this is the case, discard the point in previous path, and connect the previous peak and the valley where the flow is terminated to form a new line [Fig.13(C)].

iii) The raindrop can fall on another roof and continue to slip according to rules i) and ii).

iv) After the drop completely stop, go down to the adjacent valley and start a new fall.

b) If the fall of the raindrop starts from a valley:

i) The raindrop will stop as it reaches a more negative value than the start point [Fig.13(D)].

ii) The raindrop will also stop as it encounters flow from a previous path [Fig.13(E)]. If this is the case, discard the point in previous path, and connect the previous valley and the peak where the flow is terminated to form a new line [Fig.13(F)].

iii) The raindrop can fall on another roof and continue to slip according to rules i) and ii).

iv) After the drop completely stop, go down to the adjacent peak and start a new fall.

6) Repeat step 5 for each peak and valley.

7) If no peak and valley can be found, stop counting.

8) Assign one half cycle to each segment. Record the amplitude and the duration of each half cycle. Pair adjacent half cycle to be one cycle and count cycle period.

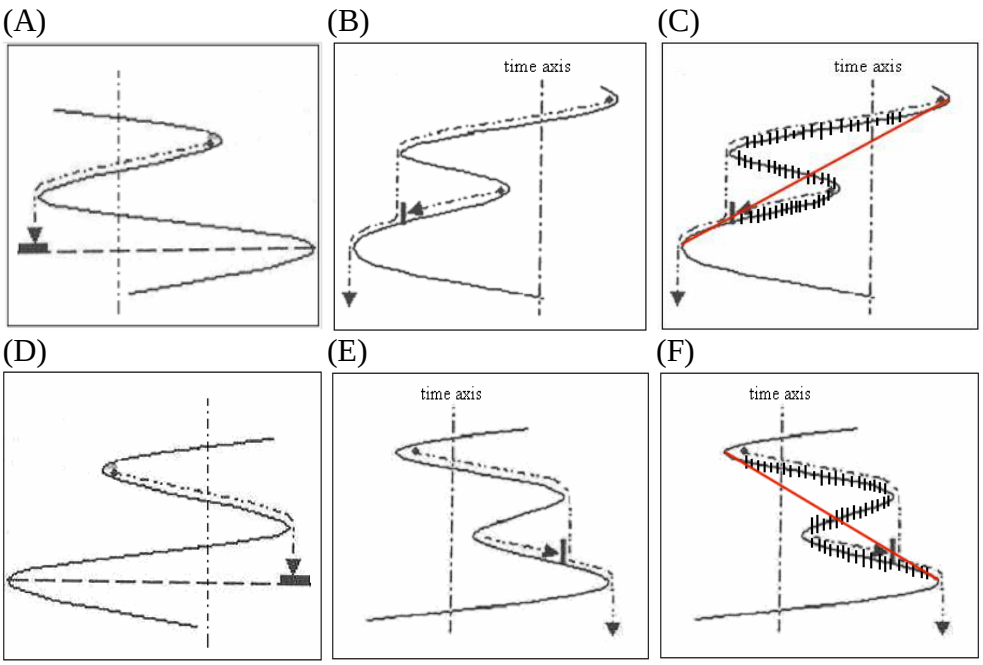


Fig. 13. Flow rules of the raindrop. (A) The raindrop start from a peak will stop as it reaches a more positive value than the start point, (B) will also stop as it encounters flow from a previous path. (C) Discard the point in previous path, and connect the source point and the valley where the flow is terminated to form a new line. (D) The raindrop start from a valley will stop as it reaches a more negative value than the start point, (E) will also stop as it encounters flow from a previous path. (F) Discard the point in previous path, and connect the source point and the peak where the flow is terminated to form a new line.

An example of using rainflow-counting method to count the cycle of the first 12 seconds of PIETX22 at the $7^{th}$ week, is shown in Fig.12(A).

1) Filter the signal. Makes each point to be a local minimum or maximum [Fig.12(B)].

2) Turn Fig.12(B) clockwise 90°, let the earliest point to be the roof of the pagoda [Fig.14(A)].

3) The raindrop starts falling from the first peak, and stops at a peak (the 3rd peak) more positive than the source [Fig.14(B)].
4) Go to the adjacent valley following and start a new raindrop. The raindrop starts falling from the first valley, and stops at a valley more negative than the new source [Fig.14(C)].
5) Go to the adjacent peak following and start a new drop. The raindrop is stopped by the path formed by 3). Discard the points in previous path and connect the first peak and the second valley to form a new line (the red line) [Fig.14(D)].
6) Go to the adjacent valley following and start a new raindrop. The raindrop stops at a valley more negative than the new source [Fig.14(E)].
7) Go to the adjacent peak following and start a new drop. The drop stops at a peak more positive than the source [Fig.14(F)].
8) Go to the adjacent valley following and start a new raindrop. The raindrop stops at a valley more negative than the new source [Fig.14(G)].
9) Go to the adjacent peak following and start a new drop. The raindrop is stopped by the path formed by 7). Discard the points in previous path and connect the third peak and the fourth valley to form a new line (the red line) [Fig.14(H)].
10) Continue these process, the final processed signal can be obtain, as showed in Fig.14(I).
11) Assign one half cycle to each segment. Record the amplitude and the duration of each half cycle. Pair adjacent half cycle to be one cycle and count cycle period.

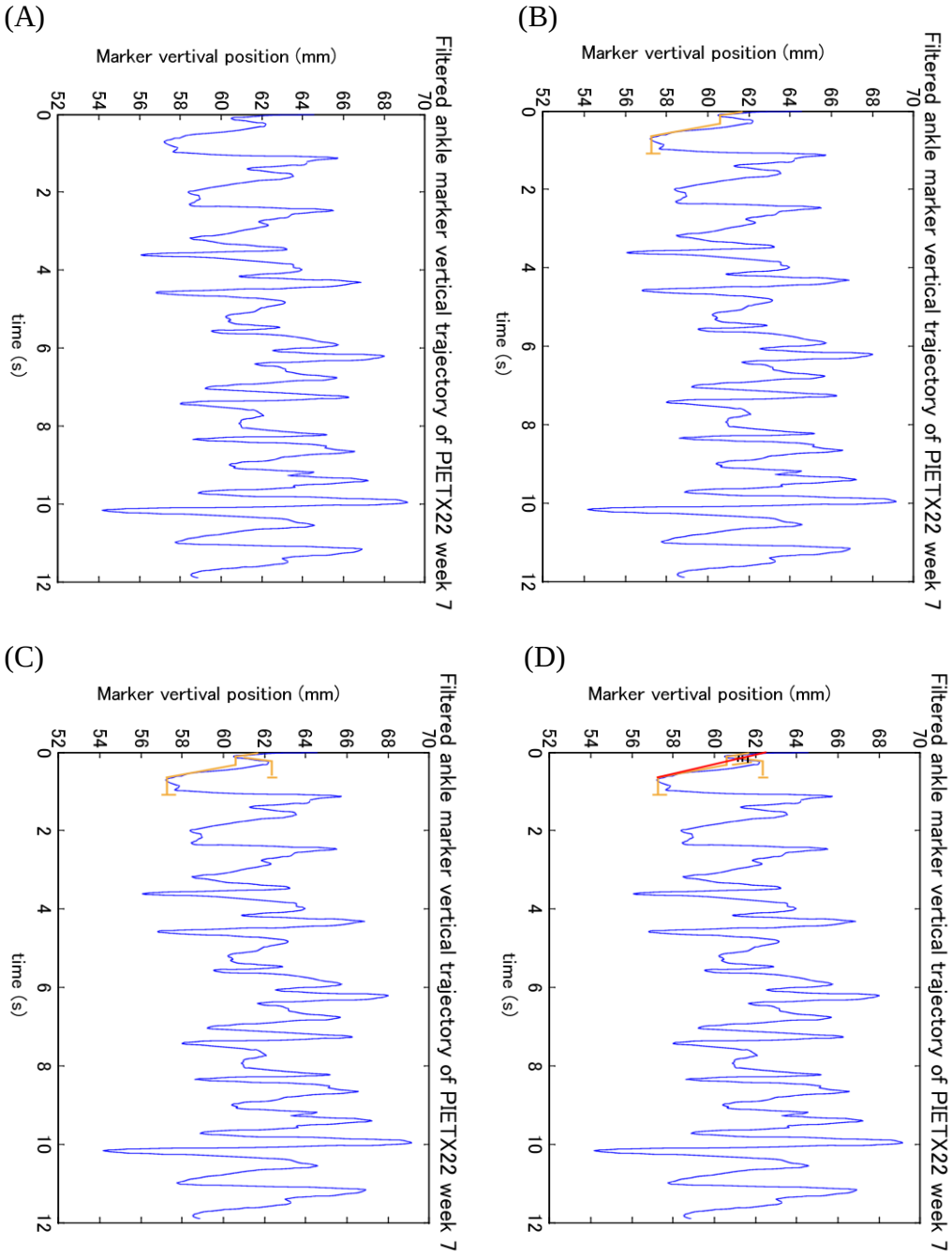
(A)
Filtered ankle marker vertical trajectory of PIETX22 week 7
Marker vertival position (mm)
time (s)
(B)
Filtered ankle marker vertical trajectory of PIETX22 week 7
Marker vertival position (mm)
time (s)
(C)
Filtered ankle marker vertical trajectory of PIETX22 week 7
Marker vertival position (mm)
time (s)
(D)
Filtered ankle marker vertical trajectory of PIETX22 week 7
Marker vertival position (mm)
time (s)

continued Fig.14

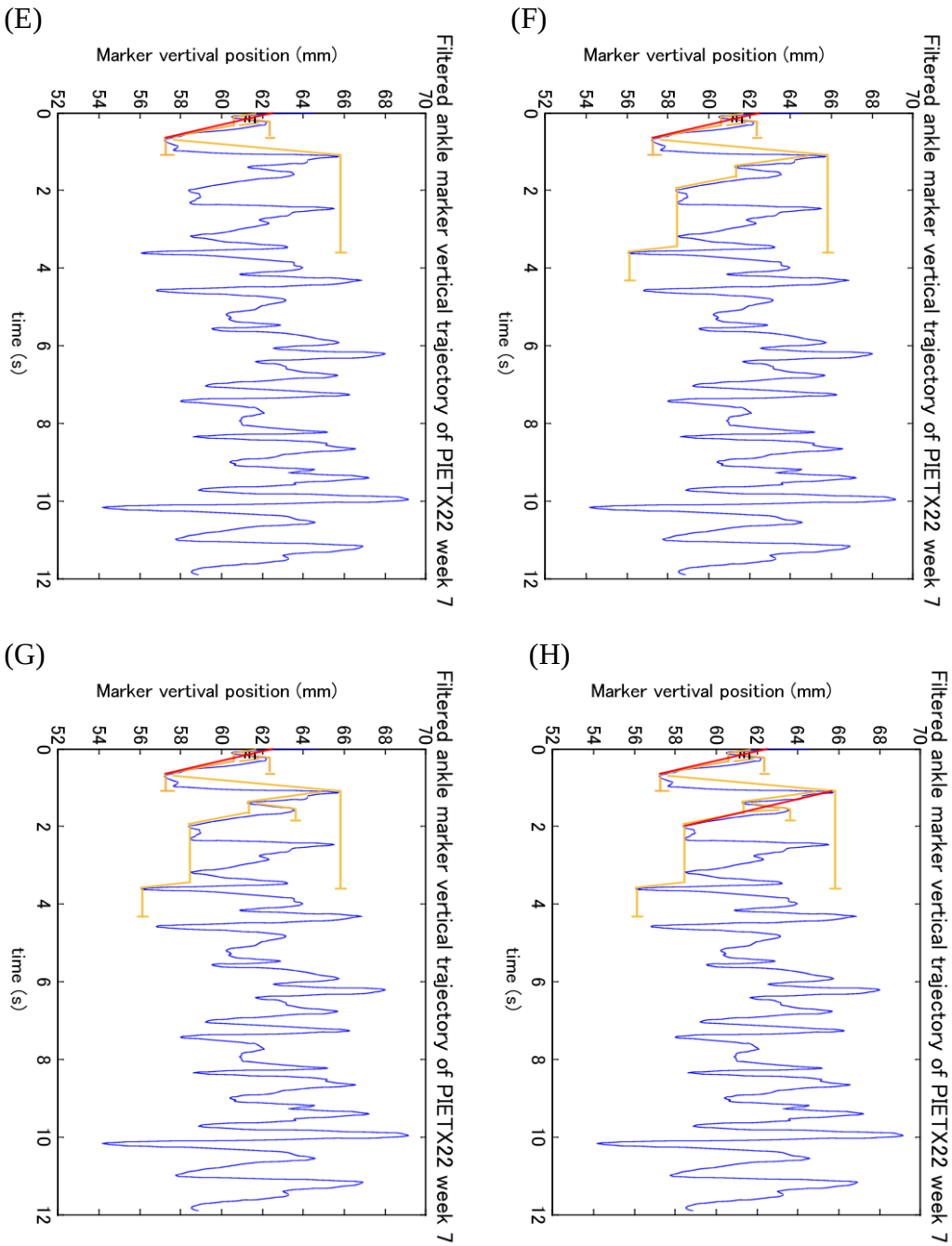

continued Fig.14

(I)

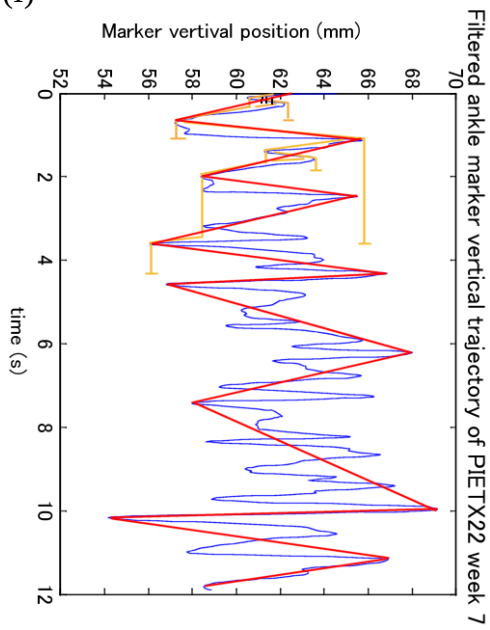


Fig. 14. An example of of using rainflow-counting method to count the cycle of the first 12 seconds of PIETX22 at the 7$^{th}$ week.

After applying rainflow-counting method, average step cycle and average step height can be obtained. Then average step length can also be calculated by calculating the variation of the ankle joint marker position in one step cycle. Horizontal variation is the step length, and vertical variation is the step height.

*4.4 Statistical Analysis*

Differences in AOB score of the last two weeks, Z-direction force of the last two weeks, Y-position, and number of stimulation events in different stepping phases to all of the groups of the last week were determined by ANOVA with groups as the factor, and were also tested by post-hoc tests. Fisher's least significant difference test (LSD) was used when the dataset had homogeneous population variances (AOB score and Z-force), whereas Games-Howell was used when the dataset had heterogeneous population variances (Y-position data and number of stimulation events in different stepping phases). We focused post-hoc tests on comparison of robot-driven and conventional stimulation. In all except one case the results of LSD and Bonferroni corrections were identical. Mann-Whitney U-test was used to determine differences in the step characteristics between the conventional stimulation group and the robot-driven stimulation group. R-square value determined the significance of the linear trend of Z-direction force.

*4.5 Histology*

After the animals completed the whole training processes, histology methods were used to examine the completeness of spinal transection. All animals were deeply anesthetized with 3mL of Euthasol and perfused intracardially with 0.9% physiological saline followed by 4% buffered paraformaldehyde to fix spinal tissue. Laminectomy was done carefully to take out the spinal cord. Placement of the epidural stimulation electrodes was also confirmed by visual inspection after laminectomy. Spinal cords

were preserved in 4% buffered paraformaldehyde for 3 days, soaked in 30% sucrose for 1 week, embedded in Thermo Scientific Shandon M-1 embedding matrix, and kept in a -75°C refrigerator. Leica CM3000 cryostat was used to do sample sectioning. Blocks containing the lesion were cut in serial, parasagittal 20 µm sections. Nissl-Myelin stain and 5HT immunohistochemical stain for serotonin with DAB (3-3' diaminobenzidine tetrahydrochloride) were used to examine the completeness of spinal transection. Typically, after Nissl-Myelin stain, we expect the absence of Nissl body and myelin at the transection site. Correspondingly, after 5HT immunohistochemical stain, we expect to see serotonin above the lesion, but no serotonergic fibers below the transection site. Fig. 13 shows an example of parasagittal sectioned lesion site of spinal cord of one of the rats in this study after Nissl-Myelin stain [Fig. 15(A)], and after 5HT stain [Fig. 15(B)]. All rats had histologically complete lesions.

(A)

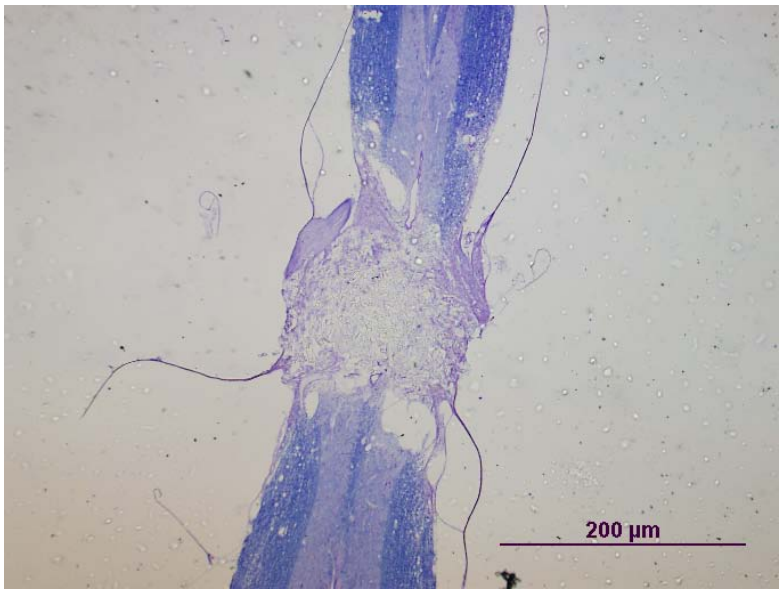


(B)

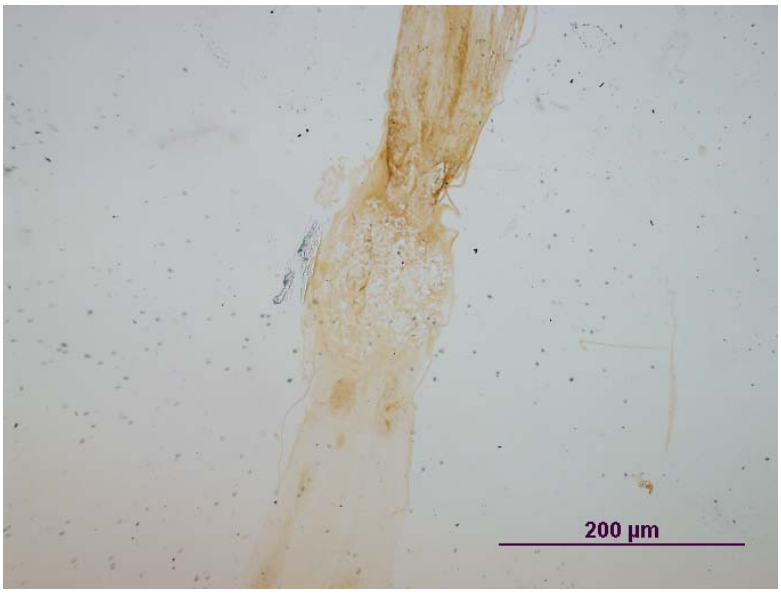


Fig. 15. Examples of histology slides. (A) Shows a sample after Nissl-Myelin staining, revealing absence of Nissl bodies and myelin. (B) Shows a sample after 5HT staining, revealing absence of serotonin below the transection site.

# 5. Results

*5.1 AOB Scores*

AOB scoring was used to assess the qualitative functional recovery of the rats after treatment. Fig. 16(A) shows average AOB scores of the control group, while 16(B) shows average AOB score of the conventional stimulation group, and 16(C) shows average AOB score of the robot-driven stimulation group. Both conventional and robot-driven epidural stimulation show significant improvements over controls. Further, in the first three weeks, there was no significant difference in AOB score among these three groups (ANOVA, $p>0.05$; post-hoc (LSD), all $p>0.05$) (see TABLE IV A). Whereas in the last two weeks, the robot driven stimulation group AOB was significantly greater than either the conventional or control group (ANOVA, $p<0.01$; LSD post-hoc test, $p<0.05$, for robot-driven and conventional as shown in TABLE IV B).

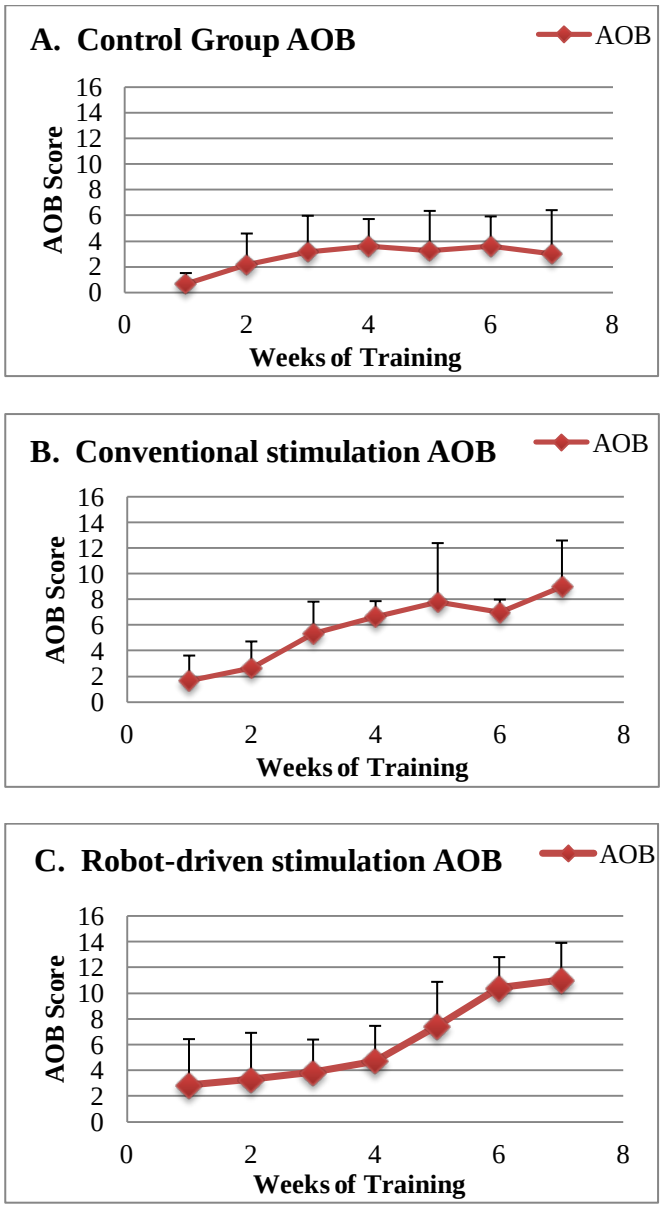


Fig. 16. Qualitative function based AOB scores: (A) Control with no stimulation but robot support. (B) Conventional continuous 40Hz epidural stimulation combined with robot support. (C) Robot driven epidural stimulation. In weeks 6 and 7 all AOB scores are significantly different (ANOVA, $p<0.001$) and robot driven is significantly greater than conventional epidural stimulation (LSD post-hoc test, $p<0.05$).

TABLE IV A.

Statistic test results of the first 3 weeks AOB score

**ANOVA**

AOB score of 3 groups

| | Sum of Squares | df | Mean Square | F | Sig. |
|---|---|---|---|---|---|
| Between Groups | 20.956 | 2 | 10.478 | 1.448 | .244 |
| Within Groups | 412.444 | 57 | 7.236 | | |
| Total | 433.400 | 59 | | | |

**Post hoc test**

AOB score of 3 groups

LSD

| (I) Experiment groups | (J) Experiment groups | Mean Difference (I-J) | Std. Error | Sig. |
|---|---|---|---|---|
| Control | Conventional | -1.22222 | .89665 | .178 |
| | Robot-driven | -1.33333 | .83874 | .117 |
| Robot-driven | Conventional | .11111 | .83874 | .895 |

TABLE IV B.

Statistic test results of the last 2 weeks AOB score

**ANOVA**

AOB score of 3 groups

| | Sum of Squares | df | Mean Square | F | Sig. |
|---|---|---|---|---|---|
| Between Groups | 338.340 | 2 | 169.170 | 24.912 | .000 |
| Within Groups | 169.767 | 25 | 6.791 | | |
| Total | 508.107 | 27 | | | |

**Post hoc test**

AOB score of 3 groups

LSD

| | | Statistics | | |
|---|---|---|---|---|
| (I) Experiment groups | (J) Experiment groups | Mean Difference (I-J) | Std. Error | Sig. |
| Conventional | Robot-driven | **-3.16667*** | 1.30295 | .023 |

## *5.2 Data from the Neurorobotic System*

### *5.2.1 Z-direction Force*

The PHANTOM robot system can detect position and velocity, and deliver force in 3-dimensions. Delivered Z-direction force was inversely proportional to self body weight support, so we could thus use it to assess the recovery of self body weight support. From Y-direction position data, which is the lateral pelvis position, we could see the scale of yaw and roll movements, and the deviation from the field center. These indicated the difference in walking stability and precision of the rats. For the control and conventional stimulation group, we found no significant trends in Z-force, so we show the average value of Z-direction force instead of a trend line. Fig. 17(A) shows average Z-direction force of the control group, Fig. 17(B) shows average Z-direction force of the conventional stimulation group, and Fig. 17(C) shows average Z-direction force trend of the robot-driven stimulation group. Statistical tests (ANOVA, $p<0.05$) showed that the Z-force data of these three groups were significantly different in week 6 and 7. Furthermore, the Z-force data of the robot-driven stimulation group was significantly different from Z-force data of the control group [$p<0.05$, post hoc test (LSD)], whereas there was no significant different between the control and the conventional stimulation group [$p>0.05$, post hoc test (LSD)] (see TABLE V).

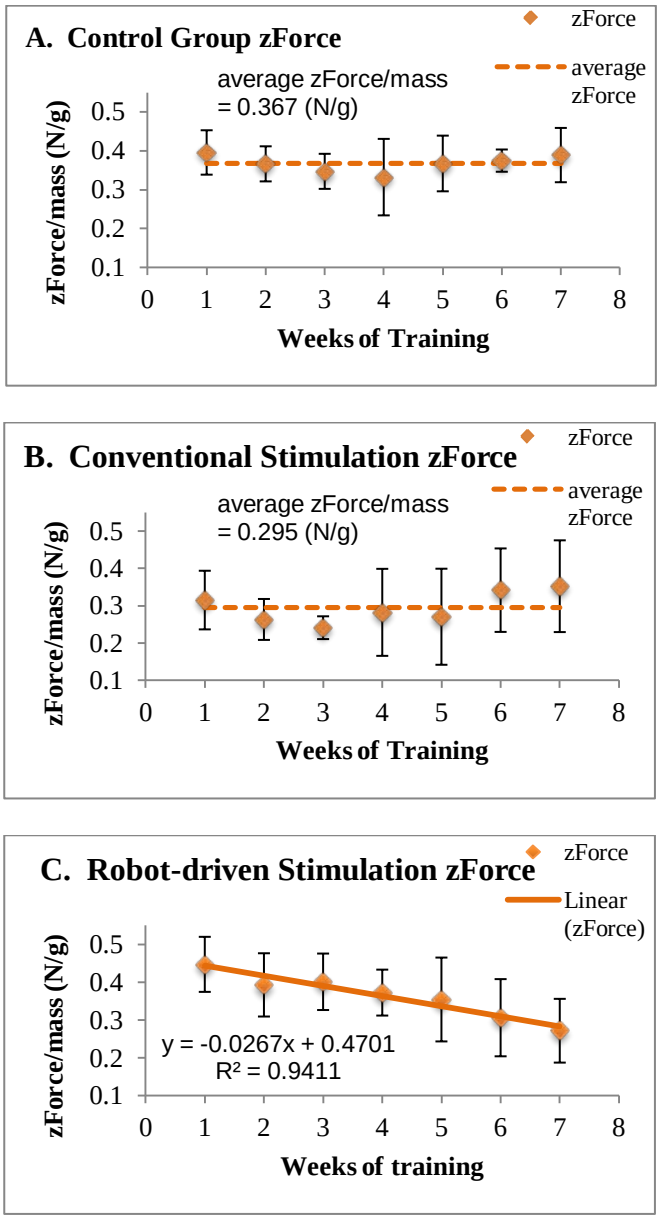


Fig. 17. Z-force weight-support contribution of robot: mean Z-force. (A) Z-direction force of the control group. (B) Z-direction force of the conventional stimulation group. (C) Z-direction force of the robot-driven stimulation group. Significant trend downward in robot contribution is seen only in (C). Mean levels in (A) and (B) differ significantly. The final mean level of Z-force is lowest in (C), using robot driven epidural spinal stimulation.

TABLE V.

Statistic test results of the last 2 weeks Z-force data

**ANOVA**

Z-force differences of 3 groups

| | Sum of Squares | df | Mean Square | F | Sig. |
|---|---|---|---|---|---|
| Between Groups | .048 | 2 | .024 | 3.521 | .045 |
| Within Groups | .170 | 25 | .007 | | |
| Total | .218 | 27 | | | |

**Post hoc test**

Z-force difference of 3 groups

LSD

| (I) Experiment groups | (J) Experiment groups | Mean Difference (I-J) | Std. Error | Sig. |
|---|---|---|---|---|
| Control | Conventional | .034261665 | .042629486 | .429 |
| | Robot-driven | .092571367* | .035346503 | .015 |
| Conventional | Robot-driven | .058309702 | .041275822 | .170 |

*. The mean difference is significant at the 0.05 level.

*5.2.2 Y-direction Position*

Y-direction position data can show lateral deviation of the pelvis of the rats from the field center, and the standard deviation of Y-direction position can show the scale of lateral movement of the animal. From the combination of the two, we can see the precision and stability of walking of the animal. Under the coordinates of our robot system, the y value is negative at the right side of the elastic center and is positive at the left side of the elastic center. When calculating average Y-position and standard deviation of the rat, the exact y value was used. However, it is observed that all of the rats in this study tend to lean on the right side of the elastic center. After calculating, the average Y-position and standard deviation of the control group, conventional stimulation group, and robot-driven stimulation group all differed. Fig. 18(A) shows average Y-position and standard deviation of the control group, Fig. 18(B) shows average Y-position and standard deviation of the conventional stimulation group, and Fig. 18(C) average Y-position and standard deviation of the robot-driven stimulation group. Statistical tests (ANOVA, $p<0.001$) showed that the Y-position data of these three groups were significantly different (see TABLE VI A). Post hoc test (LSD, $p<0.01$) showed that Y-position data of the robot-driven stimulation group and the conventional stimulation group were significantly different from data of the control group, which indicates that epidural stimulation may also helped the rat improve walking stability and precision. Furthermore, statistic test (ANOVA, $p<0.05$) of standard deviation (STD) of the Y-position data showed that the robot-driven stimulation group had significant difference with the control and the conventional

stimulation group. After post-hoc test (LSD, $p<0.05$), it was also found that the STD of robot-driven stimulation group is significantly different than that of conventional stimulation group (see TABLE VI B). It suggests that the robot-driven epidural stimulation group ultimately showing the smallest standard deviation, and the smallest systematic bias away from the field center. Thus the robot driven stimulation group used the minimal lateral assist from the robot and showed the best yaw and roll control. Y-position data varied rhythmically and can also be used to calculate step cycle. When the pelvis moves from the right to the left end, and comes back to the right end again, the period can be counted as a step cycle.

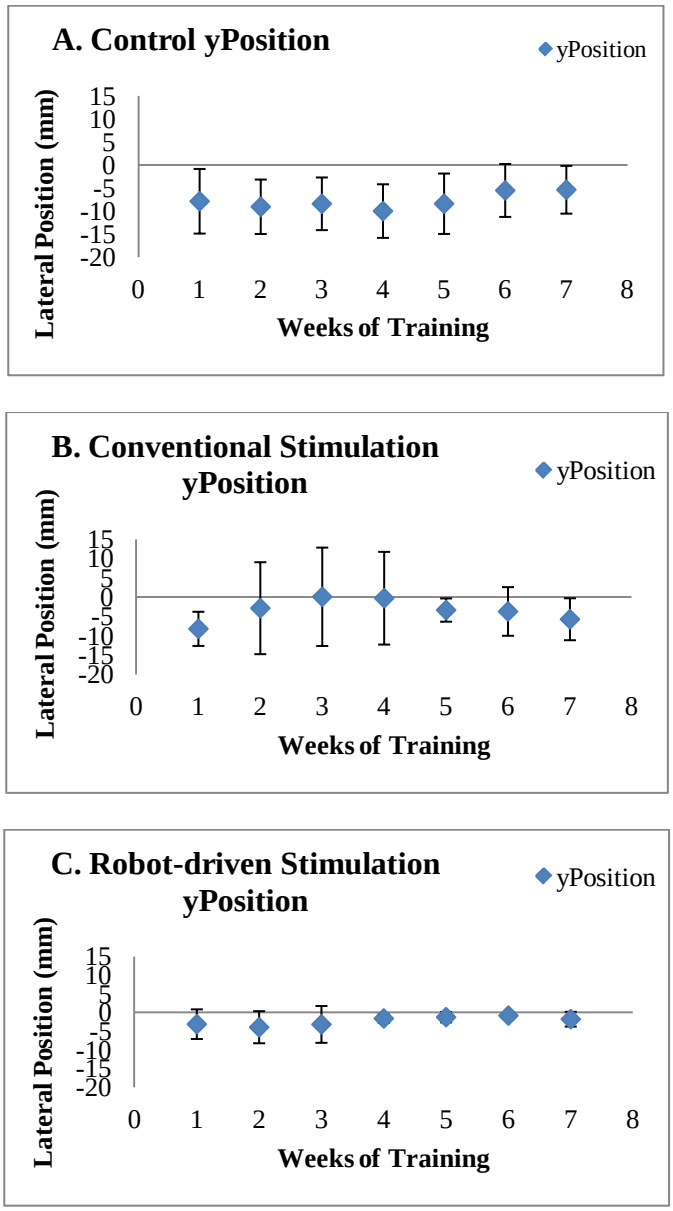


Fig. 18. Average Y-position of the rats' pelvis. (A) Average lateral position and deviation of the control group, (B) average lateral position and deviation of the conventional stimulation group, and (C) average lateral position and deviation of the robot-driven stimulation group.

# TABLE VI A.

## Y-position differences

**ANOVA**

Y-position in the 3 groups

| | Sum of Squares | df | Mean Square | F | Sig. |
|---|---|---|---|---|---|
| Between Groups | 111.042 | 2 | 55.521 | 13.295 | .000 |
| Within Groups | 75.168 | 18 | 4.176 | | |
| Total | 186.210 | 20 | | | |

**Post hoc test**

Y-position in the 3 groups

LSD

| (I) Experiment groups | (J) Experiment groups | Mean Difference (I-J) | Std. Error | Sig. |
|---|---|---|---|---|
| Control | Conventional | -4.40627132* | 1.09231002 | .001 |
| | Robot-driven | -5.24176036* | 1.09231002 | .000 |
| Conventional | Robot-driven | -.83548904 | 1.09231002 | .454 |

*. The mean difference is significant at the 0.05 level.

TABLE VI B.

Y-position Standard Deviation differences

**ANOVA**

Y-Position STD in the 3 groups

| | Sum of Squares | df | Mean Square | F | Sig. |
|---|---|---|---|---|---|
| Between Groups | 89.839 | 2 | 44.920 | 7.240 | .005 |
| Within Groups | 111.680 | 18 | 6.204 | | |
| Total | 201.519 | 20 | | | |

**Post hoc test**

Y-position STD in the 3 groups

Games-Howell

| (I) Experiment groups | (J) Experiment groups | Mean Difference (I-J) | Std. Error | Sig. |
|---|---|---|---|---|
| Conventional | Robot-driven | 5.02609039* | 1.61451526 | .040 |

*. The mean difference is significant at the 0.05 level.

## *5.3 Kinematic Data*

### *5.3.1 Hind Limb Markers Trajectory*

All of the kinematic image tracking were done by MaxTRAQ software. The software tracked markers placed on the hind limb joints of the rat and recorded the position of the markers. Link the marker points and plot them frame by frame, we can get the stick figure in several step cycles, which can show the hind limb motion. Fig. 19 (A)(C) show stick figure of a typical conventional stimulation rat, PICIN25, at the 3$^{rd}$ week and the 7$^{th}$ week, and Fig. 19(B)(D) show stick figure of a typical robot-driven stimulation rat, PIETX22, at the 3$^{rd}$ week and the 7$^{th}$ week.

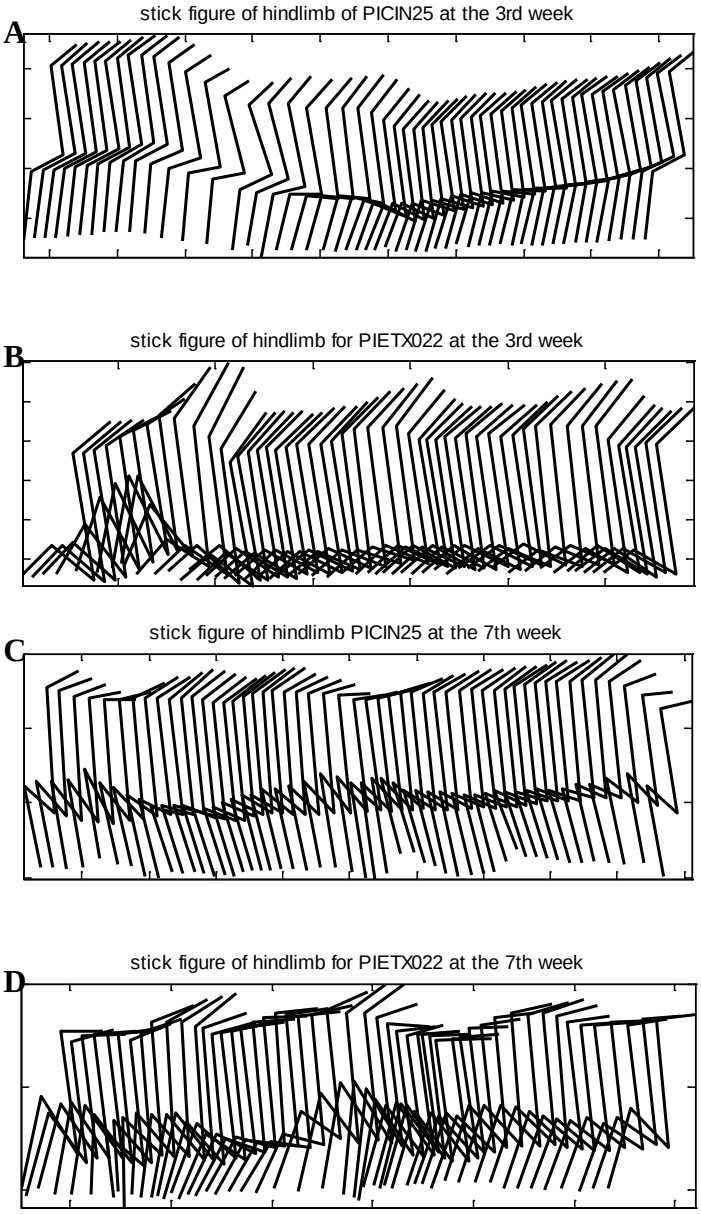


Fig. 19. Stick figure of the hind limb movement of two typical animals: PICIN25 (conventional stimulation), and PIETX22 (robot-driven stimulation) at the 3rd week and the 7th week. (a) Stick figure of PICIN25 at the 3rd week. (b) Stick figure of PIETX22 at the 3rd week. (c) Stick figure of PICIN25 at the 7th week. (d) Stick figure of PIETX22 at the 7th week. From the stick figures, PIETX22 had a larger scale of hind limb movement.

*5.3.2 Angle at the Joints*

After calculating the marker position, we then also obtained the angle at each joint in the planar view. The relation between ankle angle and knee angle of these two typical rats at the 3rd week and the 7th week are shown in Fig.20 (A) to (D).

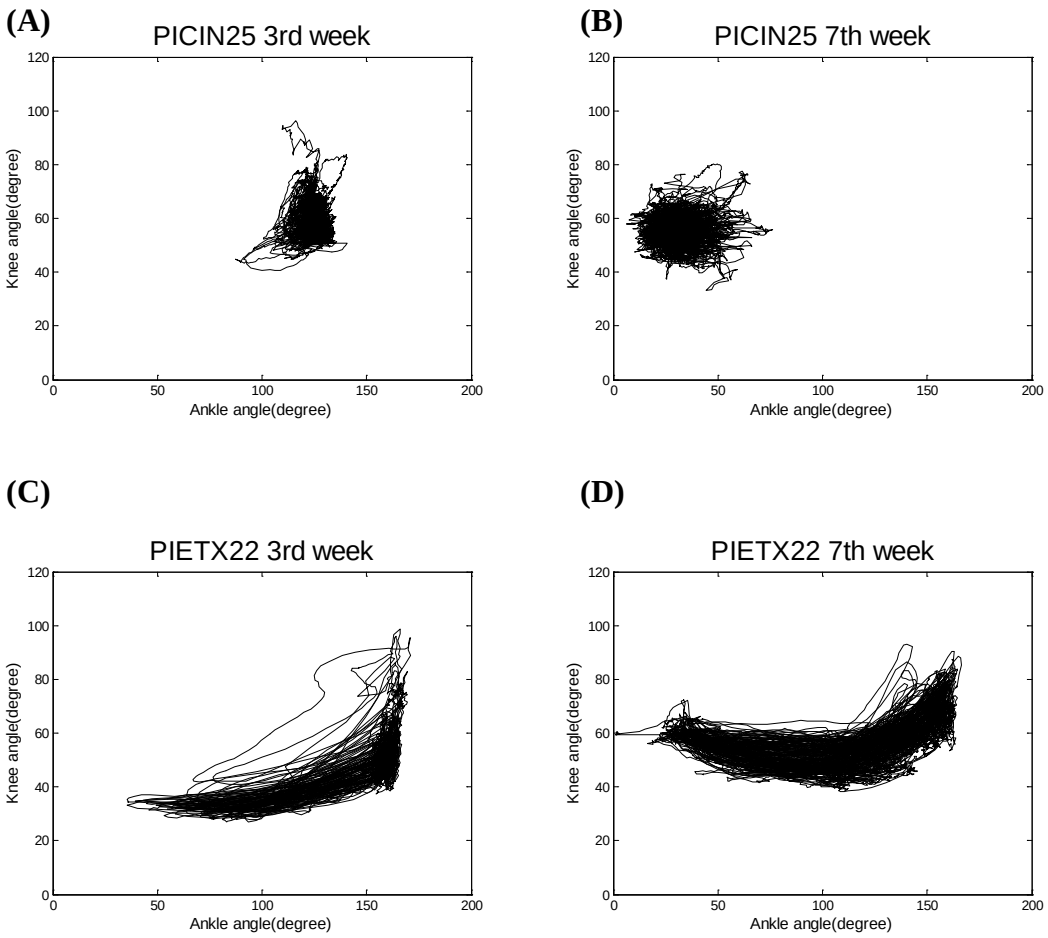


Fig. 20. Ankle angle vs. knee angle of two typical rats: one in the conventional stimulation group (PICIN25) and one in the robot-driven stimulation group (PIETX22). (A) Ankle angle to knee angle of PICIN25 at the 3rd week; (B) ankle angle to knee angle of PIETX22 at the 3rd week; (C) ankle angle to knee angle of PICIN25 at the 7th week; (D) ankle angle to knee angle of PIETX22 at the 7th week. Larger range of ankle angle of PIETX22 can be observed.

*5.3.3 Joint Marker Trajectories*

Rainflow counting algorithm [126] was used to calculate the average duration of step cycle. Based on the calculated step cycle, we plot the horizontal ankle marker trajectory and the vertical ankle marker trajectory to double check the duration of one step cycle. Fig. 21 (A) to (D) show horizontal and vertical ankle marker position of PICIN25 and PIETX22 at the 3$^{rd}$ week. It was found that the average step cycle of the conventional stimulation rat, PICIN25, at the 3$^{rd}$ week was about 0.79 s, and the average step cycle of the robot-driven stimulation rat, PIETX22, at the 3$^{rd}$ week was about 0.83 s. Fig. 22 (A) to (D) show horizontal and vertical ankle marker position of PICIN25 and PIETX22 at the 7$^{th}$ week. It was found that the average step cycle of the conventional stimulation rat, PICIN25, at the 7$^{th}$ week was about 0.69 s, and the average step cycle of the robot-driven stimulation rat, PIETX22, at the 7$^{th}$ week was about 0.96 s. The rat received robot-driven stimulation (PIETX22) had a relatively longer step cycle. The average ankle maker trajectory in one step cycle of these two typical rats were also analyzed and plotted, as shown in Fig. 23 (A) to (D), the error ellipses show standard error at each time point.

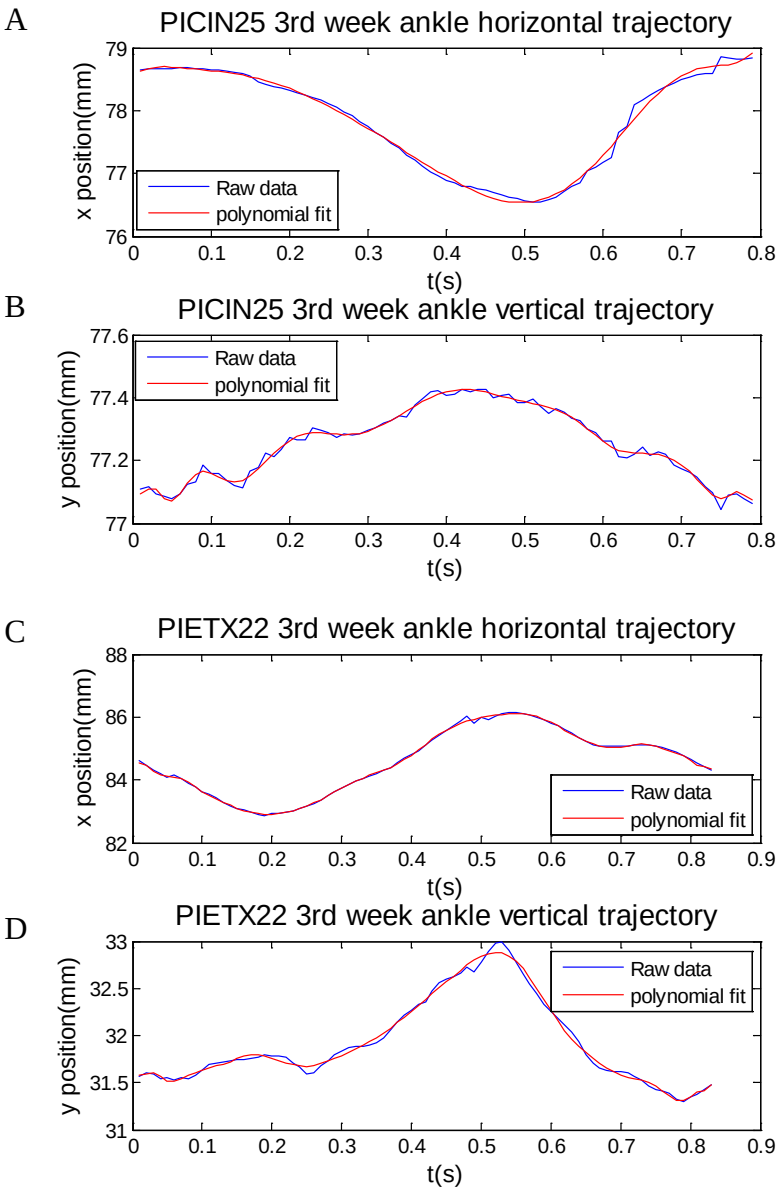


Fig. 21. Horizontal and vertical ankle marker position of two typical rats at the 3rd week. (A) The horizontal ankle marker trajectory of PICIN25 at the 3rd week. (B) The vertical ankle marker trajectory of PICIN25 at the 3rd week. (C) The horizontal ankle marker trajectory of PIETX22 at the 3rd week. (D) The vertical ankle marker trajectory of PIETX22 at the 3rd week. From the variation of x position at the ankle joint, we can find at the 3rd week, the step cycle is about 0.79 s for the conventional stimulation rat, PICIN25, and is about 0.83 s for the robot-driven stimulation rat, PIETX22.

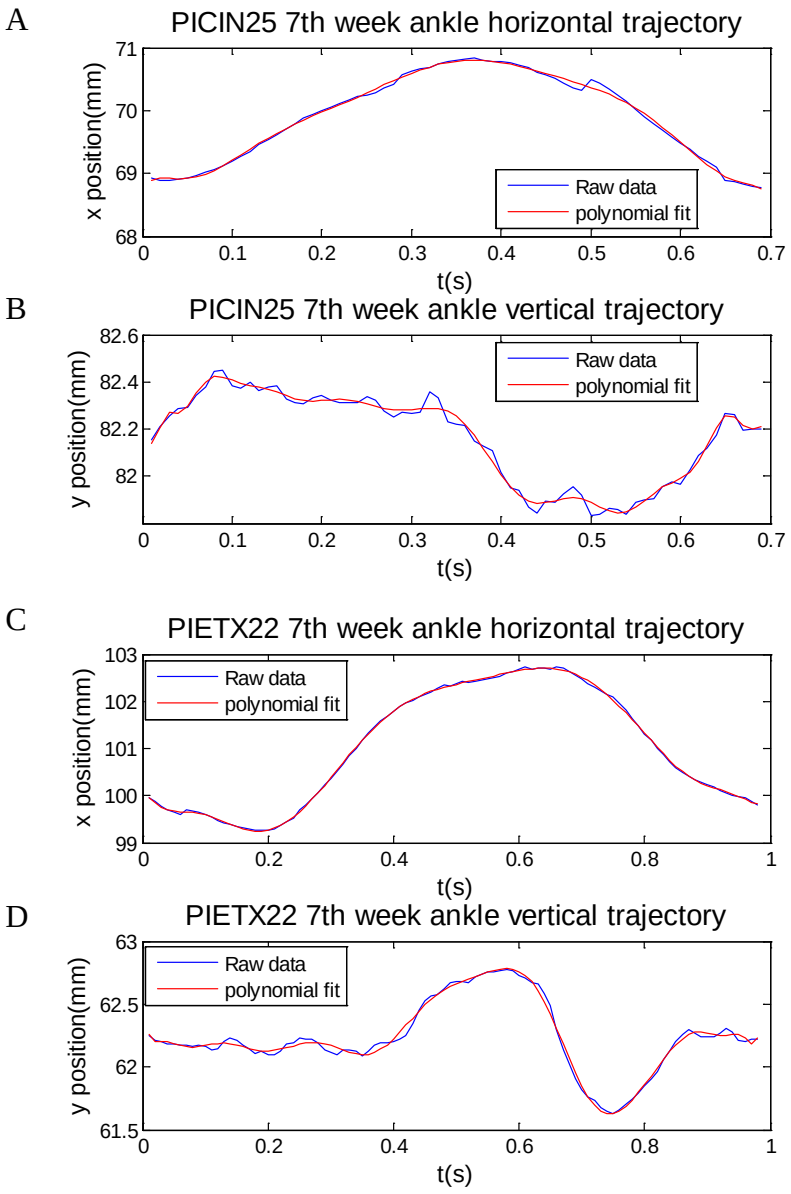


Fig. 22. Horizontal and vertical ankle marker position of two typical rats at the 7th week. (A) The horizontal ankle marker trajectory of PICIN25 at the 7$^{th}$ week. (B) The vertical ankle marker trajectory of PICIN25 at the 7$^{th}$ week. (C) The horizontal ankle marker trajectory of PIETX22 at the 7$^{th}$ week. (D) The vertical ankle marker trajectory of PIETX22 at the 7$^{th}$ week. From the variation of x position at the ankle joint, we can find at the 7$^{th}$ week, the step cycle was about 0.69 s for the conventional stimulation rat, PICIN25, and was about 0.96 s for the robot-driven stimulation rat, PIETX22.

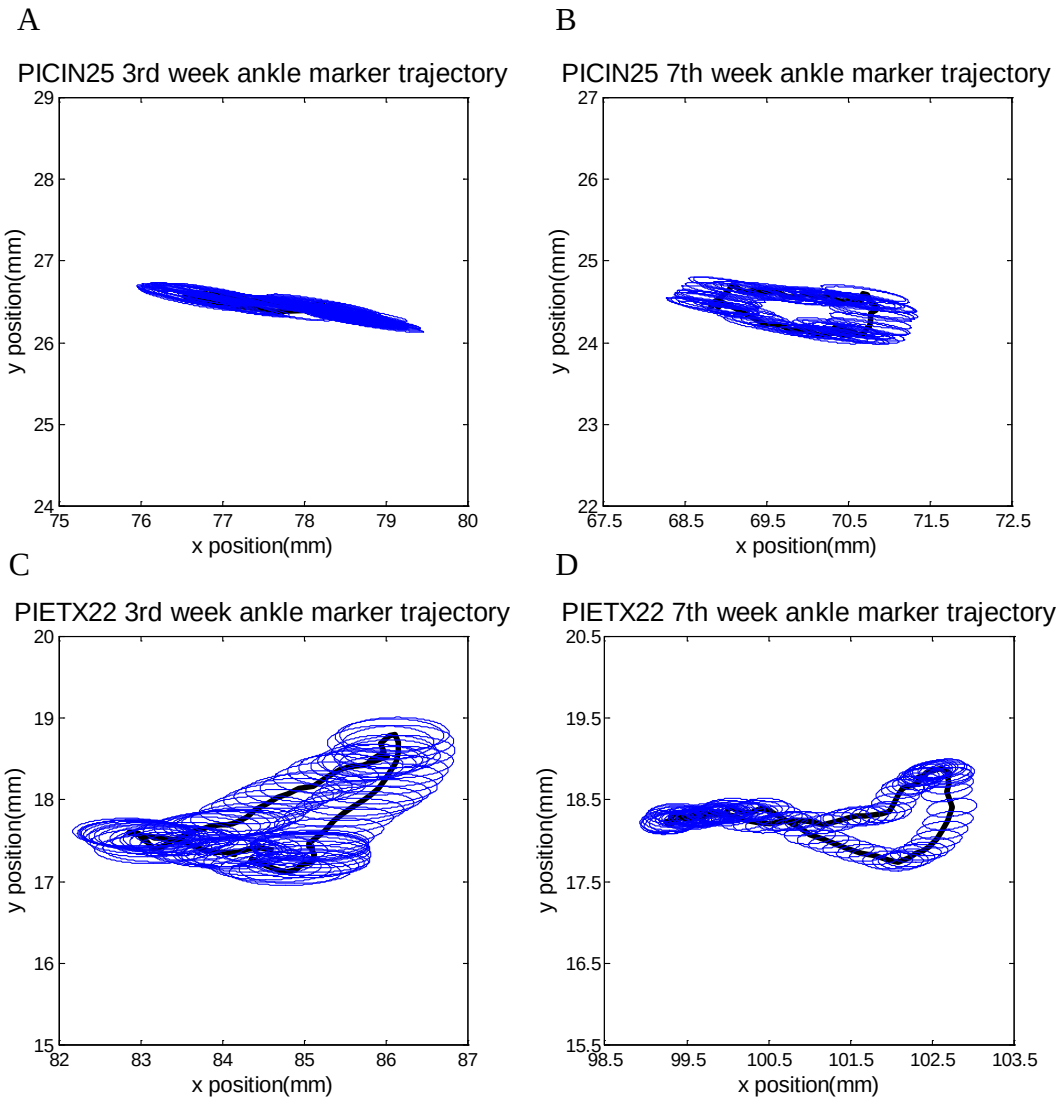


Fig. 23. Average ankle marker trajectory of two typical rats. (A) Average ankle marker trajectory of the typical conventional stimulation rat at the 3rd week, (B) average ankle marker trajectory of the typical robot-driven stimulation rat at the 3rd week, (C) average ankle marker trajectory of the typical conventional stimulation rat at the 7th week, (D) average ankle marker trajectory of the typical robot-driven stimulation rat at the 7th week. Error ellipses in each plot shows standard error at each time point.

*5.3.4 Step Cycle Parameters*

Several step cycle parameters at the 3rd week and the 7th week of the conventional stimulation group and the robot-driven stimulation group were also calculated, including: average step cycle, average swing duration, average stance duration, average step height, and average step length, as shown in Fig. 24 (A) to (E). For the control group, we did not find any step cycle at the 3rd week for most animals, so we only compare these parameters for conventional stimulation group and robot-driven stimulation group. Statistical tests (U-test, $p<0.05$) showed that the step cycles by the 7th week ($p = 0.039$), had changed in robot driven stimulation when compared to conventional. More specifically stance duration by the 3rd week ($p = 0.019$), and stance duration at the 7th week ($p = 0.039$) were both significantly different between the robot-driven stimulation group and the conventional stimulation group.

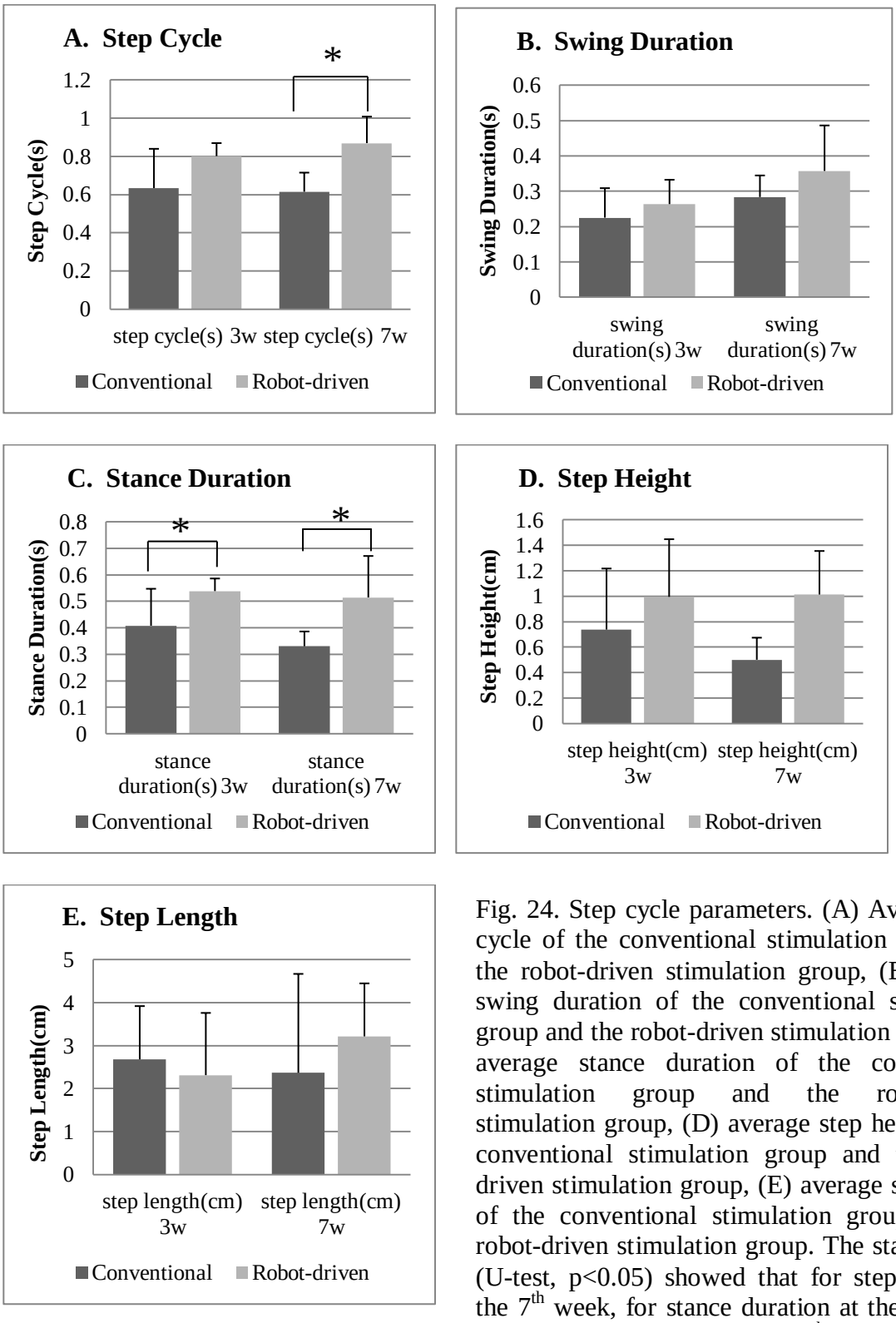


Fig. 24. Step cycle parameters. (A) Average step cycle of the conventional stimulation group and the robot-driven stimulation group, (B) average swing duration of the conventional stimulation group and the robot-driven stimulation group, (C) average stance duration of the conventional stimulation group and the robot-driven stimulation group, (D) average step height of the conventional stimulation group and the robot-driven stimulation group, (E) average step length of the conventional stimulation group and the robot-driven stimulation group. The statistic tests (U-test, $p<0.05$) showed that for step cycles of the 7$^{th}$ week, for stance duration at the 3$^{rd}$ week, and for stance duration at the 7$^{th}$ week there were significant differences between the robot-driven stimulation group and the conventional stimulation group.

TABLE VII. Step cycle parameters

| | Conventional stimulation rat 3- week | Robot-driven stimulation rat 3-week | Conventional stimulation rat 7- week | Robot-driven stimulation rat 7-week |
|---|---|---|---|---|
| Step Cycle (s) | 0.63 | 0.80 | 0.61 | 0.87 |
| Average step length (cm) | 2.68 | 2.31 | 2.37 | 3.21 |
| Average step height (cm) | 0.74 | 0.99 | 0.50 | 1.01 |
| Average swing duration (s) | 0.23 | 0.26 | 0.28 | 0.35 |
| Average stance duration (s) | 0.41 | 0.54 | 0.33 | 0.51 |

*5.3.5 Stimulation Events*

Stimulation events timing during robot-driven epidural stimulation were collected and were related to step cycles analyzed from stick figures based on hind limb joint marker tracking data. Fig.25 shows an example of the relation between stimulation signal and hindlimb movements of a rat receiving robot-driven stimulation (PIETX52). After signal processing, the total number of stimulation events was calculated, and the event frequency was determined, where event frequency = total event number /recording time. Average event frequencies of 3 sample rats in the robot-driven stimulation group, from the 1$^{st}$ week to the 7$^{th}$ week, were then calculated, as shown in Fig. 26(A). These showed significant trend. The initial onset points of continuous event trains were denoted as $T_{ON1}$, $T_{ON2}$,…etc. $T_{ON}$ interval shows the duration between one onset and the next onset of the robot-driven epidural stimulation, which measures the effective period for one burst to assist the rat walks higher than the threshold (elastic center). The termination points of the same continuous event trains were set as $T_{OFF1}$, $T_{OFF2}$,…etc. After all $T_{ON}$ and $T_{OFF}$ have been determined, burst width and pause duration of the event trains were calculated, as shown in Fig. 26(B). Burst duration shows the period of the rat walking lower than the elastic center, and pause duration shows the period that the rat is actually walking higher than the elastic center. Fig. 27(A) to (D) show the histograms of $T_{ON}$ interval, $T_{OFF}$ interval, burst width, and pause duration from a sample animal at the 7$^{th}$ week. Stepping was divided into 5 phases: 0-$\pi$/2 (phase 1), $\pi$/2-$\pi$ (phase 2), $\pi$-3$\pi$/2 (phase 3), 3$\pi$/2-2$\pi$ (phase 4), and non-stepping paused phases. Fig. 27(A) showed the interval between $T_{ON}$ and the next $T_{ON}$ was

peaked between 2-4 s, which is about 4-8 steps for a rat stepping at 2Hz. This means that the effective interval for one burst of robot-driven epidural stimulation to assist the rat is 2-4 s. After this period, the rat needs another burst to maintain the assistive effect caused by epidural stimulation. Fig. 27(B) showed the interval between $T_{OFF}$ and the next $T_{OFF}$ peaked between 2-4 s, which is consistent with the result of $T_{ON}$ interval. Fig. 27(C) showed the histogram of burst width peaked between 0-2 s, indicating the average duration of a rat walking lower than the elastic center is 0-2 s, which is 0-4 step cycles for a rat stepping at 2 Hz. Fig. 27(D) shows the histogram of pause durations, and here there were 2 peaks. One was between 0-0.2 s, the other was between 0.4-0.8 s. This indicates that pause durations were not entirely random and a pause was usually a half step cycle or occasionally longer comprising 2-3 step cycles, which means after receiving one burst of robot-driven epidural stimulation, the pelvic height of the rat can usually be raised higher than elastic center for a half step cycle, where sometimes this period could be occasionally longer comprising 2-3 step cycles. Fig. 28 shows the accumulated numbers of stimulation events in different stepping phases, by time. Statistical analysis (ANOVA, $p<0.001$) showed that the data of different stepping phases were significantly different. Furthermore, post hoc tests (Games-Howell, $p<0.05$) showed that the frequency of events in the non-stepping phase differed from all others, while during stepping behaviors the stimulation rate was modulated overall and differed among phases. In particular, the numbers of stimulation events in the step phases from $\pi/2$-$\pi$, and $3\pi/2$-$2\pi$ were significantly different (see TABLE VIII).

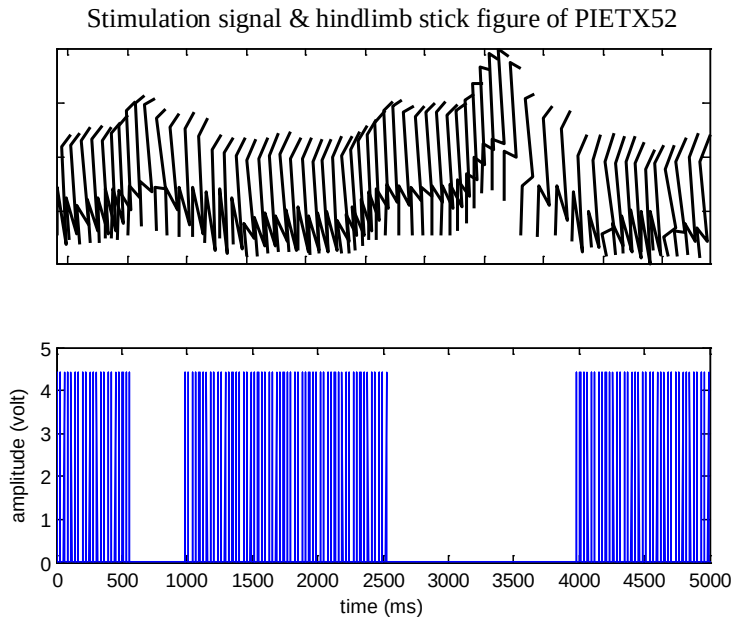


Fig. 25. An example of the relation between stimulation signal and hindlimb movements of a rat receiving robot-driven epidural stimulation (PIETX52).

(A)

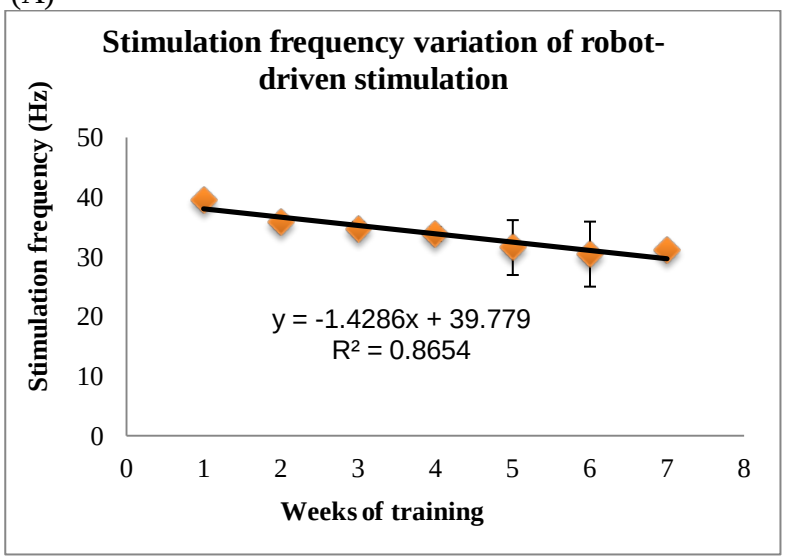


(B)

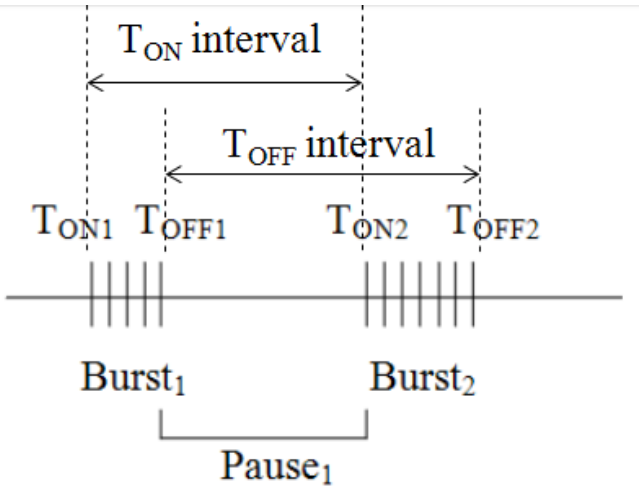


Fig. 26. Settings and frequency variation of stimulation events: (A) Stimulation event frequency variation during the whole training period. (B) Settings of stimulation event trains.

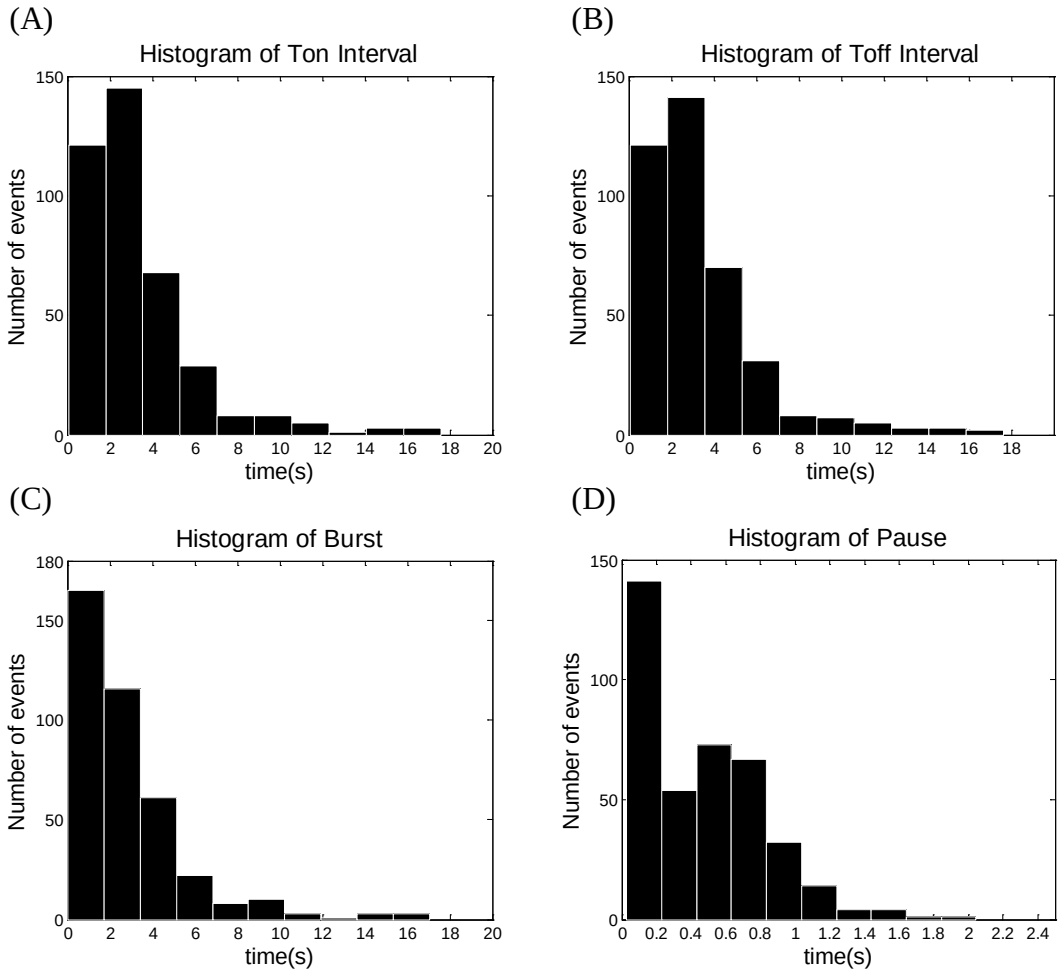


Fig. 27. Histogram of parameters of stimulation events: (A) Histogram of $T_{ON}$ interval. (B)Histogram of $T_{OFF}$ interval. (C)Histogram of burst width. (D)Histogram of pause period.

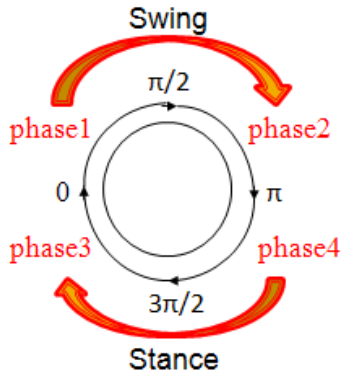


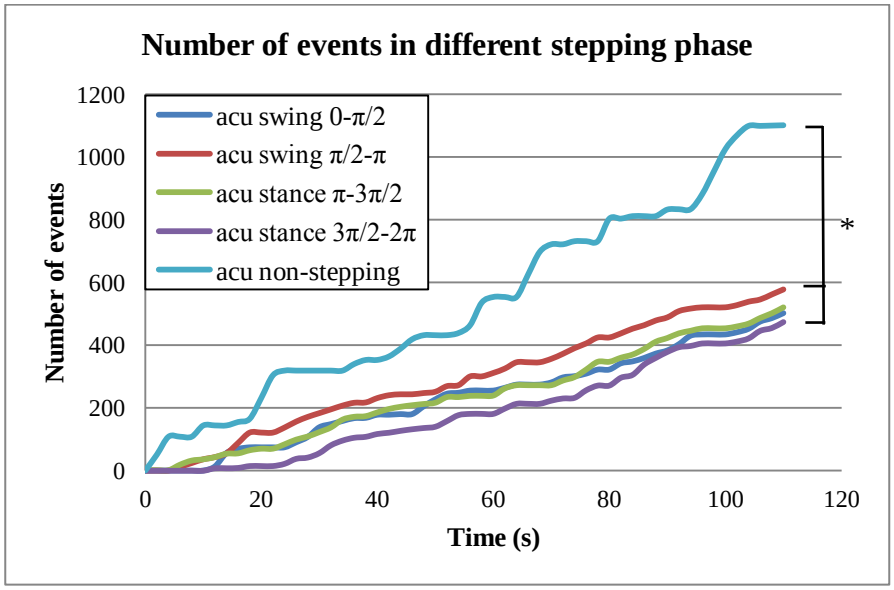


Fig. 28. Accumulation of number of stimulation events in different stepping phases, by time. The statistics (ANOVA, $p<0.001$; post-hoc (Games-Howell, phase2 to phase4, $p<0.01$;non-stepping phase to all other phases, $p<0.001$)) showed that the data of non-stepping phase, $\pi/2$-$\pi$, $3\pi/2$-$2\pi$ were significantly different.

TABLE VIII.

Distribution of stimulation events in different stepping phases

**ANOVA**

number of stimulation events

| | Sum of Squares | df | Mean Square | F | Sig. |
|---|---|---|---|---|---|
| Between Groups | 4295413.729 | 4 | 1073853.432 | 27.336 | .000 |
| Within Groups | 10803026.268 | 275 | 39283.732 | | |
| Total | 15098439.996 | 279 | | | |

**Post hoc test**

number of stimulation events

Games-Howell

| (I) Experiment groups | (J) Experiment groups | Mean Difference (I-J) | Std. Error | Sig. |
|---|---|---|---|---|
| step_cycle_phase1 | step_cycle_phase2 | -60.01786 | 30.45147 | .287 |
| | step_cycle_phase3 | -8.03571 | 28.56097 | .999 |
| | step_cycle_phase4 | 45.64286 | 28.15820 | .487 |
| step_cycle_phase2 | step_cycle_phase3 | 51.98214 | 30.92604 | .450 |
| | step_cycle_phase4 | **105.66071*** | 30.55446 | .007 |
| step_cycle_phase3 | step_cycle_phase4 | 53.67857 | 28.67075 | .338 |
| non_stepping_phase | step_cycle_phase1 | **303.67857*** | 46.38397 | .000 |
| | step_cycle_phase2 | **243.66071*** | 47.87654 | .000 |
| | step_cycle_phase3 | **295.64286*** | 46.69690 | .000 |
| | step_cycle_phase4 | **349.32143*** | 46.45165 | .000 |

***.** The mean difference is significant at the 0.05 level.

# 6. Discussion

*6.1 Robot-driven Epidural Stimulation*

To our knowledge this study is the first to explore robot-driven or motion driven epidural stimulation as a treatment paradigm for SCI. Conceivably, the robot-driven stimulation is also a form of artificial feedback or the intermittency allows dis-habituation. The framework is readily transferred to an orthosis-driven stimulation approach for subsequent off-robot function.

A 6-channel braided electrode [2cm (length) × 0.5cm (width) × 0.1 cm (thickness)] was developed to test multisite epidural stimulation, as showed in Fig. 29. The device was test with 5 animals. However, only 1 survived. All other animals died because of an immobile ileus, which also happened in the soldiers in the Lebanon war in 1982 that have acute spinal cord injuries caused by gun shot. After consulted with Dr. Lavrov, overstimulation may be one of the reasons. 30% of their rats received continuous epidural spinal cord stimulation also had the same problem. Another reason to cause the illness may be the pressure caused by inserted electrode, or the inserting process itself caused some damage to the spinal cord. However, issues arose only when stimulation was activated. Furthermore, in rat anatomy, spinal segment S1 is the section related to digestion system. Therefore, it is reasonable to infer that the inserted electrode caused extra pressure to the spinal cord and disturbed digestion function, or overstimulation to the S1 segment irritated the section controlled digestion and cause dysfunction of digestion system.

Fig. 29. 6-channel braided epidural stimulation electrode. Size of the electrode was 2cm (length) × 0.5cm (width) × 0.1 cm (thickness).

*6.2 Functional Recovery*

From the average functional AOB scores of each group, we found that rats in the control group of unstimulated but robot supported rats slightly recovered after training on the treadmill for 7 weeks, but the recovery level only reached a score of 4. In AOB scoring this means very occasional right-left alternation of the hind limbs can be observed, and the amplitude is weak. The conventional stimulation group could recover to around 9 in their AOB score, which means they showed consistent right-left alternation of the hind limbs which could be observed, and the amplitude was large. The robot-driven stimulation group recovered to 11 in AOB score, which means not only right-left alternation, but also some planter stepping was observed. The average starting AOB score of the robot-driven stimulation group was also the highest among the three. Based on the information above, the robot-driven stimulation had the best functional recovery scores. The rats were trained daily (5 days per week, 15 minutes per day) in a massed training paradigm.

Results of AOB scoring between conventional stimulation group and robot-driven stimulation group might look similar. However, this may be caused by the design of AOB scoring. AOB scoring assesses hindlimb alternation frequency, hindlimb alternation amplitude, body weight support, foot placement together. Binding parameters to each other may reduce distiguishability. Recently, a new functional scoring method for spinalized rats, HiJK (Hillyerrnalize Kinematics) scale, was developed to distinguish more effectively between groups of spinal rats [129]. Differing from AOB scoring, HiJK scoring separates the assessment of joint extension (of hip, knee, and ankle joints), transition quality of phase changing from one step phase to another, alternation frequency, foot placement, weight support, and stepping consistency. After statistical testing, it was reported that HiJK scoring showed high correlation with the widely used BBB scoring (>0.8), and could distinguish between different groups of spinalized rats (ANOVA, $p<0.05$). Reliability was also tested, and Cronbach's alpha was 0.91, which indicates considerable internal consistency. After applying HiJK scoring, differences in functional recovery in our data could potentially be clearer and this would enhance the effectiveness to distinguish the results of functional recovery between conventional epidural stimulation and robot-driven epidural stimulation.

*6.3 Robot Data Analysis*

The Z-direction force contribution of the robot can be used to assess the recovery of self-body weight support. This measure differed among all treatments but only showed

major trend in the robot driven stimulation. The rats were similarly prepared, yet the Z-force in robot-driven epidural stimulation began higher. The initial AOB scores were similar. We believe these robot force differences indicate the robot driven stimulation likely allowed more initial drops of the pelvis. Statistical tests of the Z-force showed significant differences among the treatments. Based on the Z-force data, self body weight-support level after treatment with the neurorobotic system was not significantly altered over time in either the control group, or in the conventional stimulation group. It was improved by conventional stimulation significantly over control, but was only significantly increased (with a clear and statistically significant trend of downward robot contribution) in the robot-driven stimulation group. The robot-driven stimulation was less effective initially, but likely provided superior improvement long term. It is suggested that specific spinal circuits activated determine the optimal stimulation frequency to elicit motor responses [11]. Comparing it with conventional stimulation, the triggering mechanism of robot-driven stimulation could modulate stimulation frequency based on the extent of self-body weight support recovery and activated specific spinal circuits for specific rat and for specific recovery stage. This optimization of activating spinal circuits could activate motor pools related to hindlimb extensors and contributed to enhancement in self-body weight support recovery. We conclude that rats in the robot-driven stimulation group are likely to ultimately have better recovery of self body weight support.

From the average lateral position of the rats, it was found that rats often show a mean bias and tend to lean on a specific side as they walked on the treadmill, with

most showing a rightward bias. We estimated the mean lateral deviations against the isotropic support field as the rats walked on the treadmill. Both mean bias and lateral variation showed the differences in walking stability and precision in each group. Rats in the control group showed large variances of the left-right movements of the pelvis. The rats in the conventional stimulation group showed reduced bias, but their deviations were increased. The standard deviation of the lateral position of this group was the largest among the three, presumably with greater roll, and less precision. The rats in the robot-driven stimulation group showed least bias and variance, they stayed close to the field center, and the standard deviations were small, indicating more stability and precision in their lateral motion. The hypothesized explanation for this result is that robot-driven epidural stimulation modulated stimulation frequency based on the extent of body weight support recovery and activated optimal spinal circuits for specific rats in specific training stages to trigger hindlimb stepping, which could activate lumbar motor pools and flexors for improving trunk-limb interaction and made the walking mechanism of the rat closer to that of normal animal, finally improved the walking stability and reduced lateral excursion. In Lavrov's study in 2008, it was suggested that specific spinal circuits activated determine the optimal frequency [11]. In Giszter's study in 2008, it was found that normal rats had better walking precision and stability than spinalized rats [117]. Based on information above, as a short conclusion, the robot-driven stimulation rats had better walking stability and support, as expected from [11, 18, 116, 117]. Our method may perhaps aid cortical

integration of trunk control and stepping, since Giszter et al. 2008 showed a cortical dependence of the stability and roll control.

We also found that the way we set up the supporting robot and stimulation may affected the rats' willingness to walk, and that affected the recovery level. Under our settings and design, the rat was connected to the robot arm and walked quadrupedally on the treadmill. In comparison to other researchers, we found that if the stimulation voltage was increased higher than 3V, the activations of the back muscles caused by the stimulation would cause discomfort to the rats and they would not locomote quadrupedally. Thus, the maximum value of the stimulation voltage was here more constrained. In Ichiyama's and Lavrov's experiments, the robot held the rats in a vertical standing position, and the rats haunches walked bipedally on the treadmill. In this latter case, in the bipedal design, the hindlimb motions could still be recorded regardless of volitional behaviors of the rats. In their experiments, the stimulation voltage could be increased up to 10V. This difference in design and stimulation may affect the amplitude of the hindlimb motion being triggered, and cause the differences between the recovery level of the conventional epidural stimulation rats under our neurorobotic system and those under their settings. They found kinematics almost completely resembling normal intact, although the hip angle ranges were extended, while we found kinematics different from the intact. However, neonatal spinalized rats that walk autonomously as adults also frequently vary from the intact normal kinematics. Actually, the mechanism of bipedal walking and quadrupedal walking are different. Under bipedal walking, the angle at the hip joint of a rat is larger than that of

a rat under quadrupedal walking. The thigh muscles are also more extended than their normal condition. In Wada's experiment, they found that bipedal walking rats have significant shorter swing duration than quadrupedal walking rats [130]. Johnson *et al.* built a three-dimension model of the rat hindlimb to study musculoskeletal geometry and muscle moment arms [131]. Under their model, it was found that "muscle function changes with posture, particularly in the transition from quadrupedal to bipedal posture, which eliminates the stabilizing behavior of some muscles while severely altering the moment arms of others." Moreover, Giszter *et al.* found that upper trunk is still under supraspinal control and could activate lumbar motor pools and reflexes below the level of injury, subsequently impacting the lumbar CPG to induce hindlimb locomotion [40, 118]. Therefore, quadrupedal walking model includes trunk and trunk-limb interaction, could achieve better recovery and fit better to natural configuration, whereas trunk and trunk-limb interaction are excluded in bipedal walking model and could lead to mis-assessment and restriction of recovery.

In addition, it might also be possible to overcome the stimulation amplitude limitation in our quadrupedal walking setup by reducing the pulse width to half of the original setting (200 μs → 100 μs). This could limit the range of back muscle vibration and alleviate the discomfort activated by epidural stimulation, so that the strength of the stimulation could be increased and larger hindlimb movement can be facilitated. In spinal cord stimulation, the effective pulse width to trigger motor responses is usually between 100 – 400 μs [132], so reducing pulse width to 100 μs could still be sufficient to trigger hindlimb locomotion. Reducing the pulse width reduces the density of the

stimulus, which reduces the size of area stimulation will cover, and reduces the size of area of back muscle vibration. It may also reduce small fiber recruitment. In this case, back muscle vibration will be constrained to lower lumber level, where the spinalized rats may not feel the vibration, so that quadrupedal locomotion will not be interrupted. As a result, by decreasing the pulse width, the strength of the stimulation could be extended, the scale of the movement produced by epidural stimulation could be increased, and quadrupedal locomotion would not be interrupted.

After comparing the differences between bipedal walking rats and quadrupedal walking rats, we believe our setup is closer to natural condition than their setup, although our rats could not reach the recovery level as intact rats as their rats did. In addition, our rats could also reach a better recovery level after modulating stimulation parameters.

### *6.4 Stimulation Event Analyses*

We found that the frequency of the stimulation events for the robot-driven epidural stimulation decreased during the training. This meant that the rat raised the pelvis higher than the elastic center more often, [from Fig. 26(A)]. The hypothesized explanation for this frequency decreasing is that the rats adapted to the robot-driven epidural stimulation and found the optimal epidural stimulation frequency for themselves, which may vary from rat to rat and from stage to stage in the recovery process. The best frequency to facilitate locomotion is different from species to species and from types to types of stimulation. In human, epidural stimulation triggers

stepping at 30-40 Hz [13]. In decerebrated cats, intraspinal stimulation triggers stepping at 40-60 Hz [133], whereas epidural stimulation triggers stepping at 3-10 Hz [14, 134]. In one of Lavrov's papers, they tested the effects of frequency of epidural stimulation on facilitation of stepping [11]. They found that stimulation frequency lower than optimal frequency (40-60 Hz) is not sufficient to trigger hindlimb motion, when stimulation frequency higher than optimal frequency caused overlapping of the hindlimb movement. They suggested that the specific spinal circuits activated determine the optimal frequency based on their EMG response. Between 40-60 Hz, the late response would not be interrupted by subsequent stimuli. Stimulation larger than 60 Hz causes a middle response to interfere the generation of a subsequent late response. Stimulation lower than 40 Hz was insufficient to trigger hindlimb locomotion. Under continuous stimulation, 40 Hz may be the optimal stimulation frequency for the starting stage, or certain specific stages during the rehabilitation process for some rats, but may not always be the best stimulation frequency for all of the rats and for all of the rehabilitation stages. Both physiological condition and recovery level may affect the function of the spinal cord, and the specific spinal circuits to be activated to trigger hindlimb locomotion may be different, which lead to different optimal epidural stimulation frequency. Better recovery of the robot-driven epidural stimulation rats may be found by optimization of the spinal epidural stimulation frequency following adaptation of robot-driven epidural stimulation. As a short conclusion, robot-driven stimulation may adapt to the condition of the spinal cord and activate the optimal spinal circuits to trigger stepping.

Based on the information collected from stimulation parameters, the pattern of pelvic motion of a rat received robot-driven epidural stimulation is similar as follows:

1. 0-2 s: Epidural stimulation is triggered at 0 s. The pelvis starts lifting, where pelvic height is still lower than the elastic center.
2. 2-2.2 s: The rat's pelvis becomes higher than the elastic center. Epidural stimulation stops.
3. 2.2-4 s: The rat's pelvis drops lower than the elastic center. Epidural stimulation is triggered again.

Based on Fig. 28, the stimulation modulation in the robot driven stimulation framework was phase dependent. Most stimulation of all happened in non-stepping phases, when the rat's pelvis was lower than elastic center. During stepping, comparing stepping phases, most stimulation events were triggered in phase 2 ($\pi/2$-$\pi$), when the rat's hind limb was in the second quarter of swing phase, i.e., when the hind limb was dropping down, whereas least stimulation events were triggered in phase 4 ($3\pi/2$-$2\pi$), when the rat's hind limb was in the second quarter of stance phase, i.e., when the hind limb was lifting. In effect the pauses in stimulation bursts and burst onsets tended to be in specific parts of the step cycle, possible with a handedness also present. In summary, we found there was relation between stimulation event triggering and step phase. The stimulation events were triggered most as the rat's hind limb dropping, and when the rat walked lower than the elastic center, which matched the original design.

From the point of view of long-term potentiation of the spinal cord, robot-driven epidural stimulation may also potentially have better effects on spinal cord plasticity. Although continuous epidural stimulation gives the rat spinal cord stimuli more frequently than robot-driven epidural stimulation does, the plasticity induced may be less specific. As the conclusion in the first paragraph of this section, robot-driven stimulation may adapt to the condition of the spinal cord and activate the optimal spinal circuits to trigger stepping. Therefore, the spinal circuits activated could be more specific and enhanced more appropriate spinal plasticity for locomotor functional recovery.

# 7. Conclusion and Recommendations for Future Work

## *7.1 Conclusion*

Rats recovered better in these experiments on quadrupedal stepping with a combination of our trunk based neurorobotic system, and epidural stimulation, when compared to controls. However, when treated by our novel robot-driven epidural stimulation as well as robot therapy, we found that rats achieved a still higher and significantly improved level of recovery, compared to the conventional stimulation treated rats. Robot-driven epidural stimulation could modulate stimulation frequency to activate optimal spinal circuits to facilitate hindlimb locomotion for particular rat and for particular stage in recovery, and improved the effect of epidural stimulation, subsequently enhanced better hindlimb motor function recovery than conventional epidural stimulation. Our data suggest that some measure of intermittency and/or use of a closed loop epidural stimulation related to stepping and locomotor state may be significant in clinical applications of epidural stimulation for locomotor therapies in the future.

## *7.2 Recommendations for Future Work*

Over the past decade, the exploration of using brain-machine interface (BMI) technology to assist recovery after neuromuscular impairments has become more and more flourishing. BMI provides a new communication option which can bypass

injured nerves and muscles. Song *et al.* developed a hindlimb/trunk-coupled BMI for rats under PHANTOM neurorobotic system [135]. It is found that the rats were capable to utilize the designed BMI to cancel elastic load. Movement-related variables in hindlimb/trunk cortex were also decoded [136]. The mechanism used to trigger cancelation of elastic field with BMI neural activity may be applied to trigger epidural spinal cord stimulation.

Robot-driven epidural spinal cord stimulation can also be integrated with other therapies to improve the recovery after spinal cord injury, such as quipazine administration and neurotrophic factor transplantation. In a clinical case study, Harkema *et al.* found continuous epidural stimulation at 15Hz can help a complete paraplegia person to sustain standing without manual facilitation, and epidural stimulation at 30-40 Hz can trigger locomotor like patterns. Furthermore, after 7 months of implantation, the patient also regained limited lower limb voluntary control [25]. It suggested that epidural stimulation may also enhance plasticity in the spinal circuits. In this study, all of the rats received epidural stimulation less than 8 weeks. Therefore, the effect of long-term robot-driven epidural stimulation to adult spinal rats may also be an interesting aspect to explore.

# List of References


1. Grillner S: **Biological pattern generation: the cellular and computational logic of networks in motion.** *Neuron* 2006, **52:**751-766.

2. Kiehn O: **Locomotor circuits in the mammalian spinal cord.** *Annu Rev Neurosci* 2006, **29:**279-306.

3. Duysens J, Van de Crommert HW: **Neural control of locomotion; The central pattern generator from cats to humans.** *Gait Posture* 1998, **7:**131-141.

4. Antri M, Mouffle C, Orsal D, Barthe JY: **5-HT1A receptors are involved in short- and long-term processes responsible for 5-HT-induced locomotor function recovery in chronic spinal rat.** *Eur J Neurosci* 2003, **18:**1963-1972.

5. Chau C, Barbeau H, Rossignol S: **Early locomotor training with clonidine in spinal cats.** *J Neurophysiol* 1998, **79:**392-409.

6. Landry ES, Lapointe NP, Rouillard C, Levesque D, Hedlund PB, Guertin PA: **Contribution of spinal 5-HT1A and 5-HT7 receptors to locomotor-like movement induced by 8-OH-DPAT in spinal cord-transected mice.** *Eur J Neurosci* 2006, **24:**535-546.

7. Gerasimenko YP, Lavrov IA, Courtine G, Ichiyama RM, Dy CJ, Zhong H, Roy RR, Edgerton VR: **Spinal cord reflexes induced by epidural spinal cord stimulation in normal awake rats.** *J Neurosci Methods* 2006, **157:**253-263.

8. Ichiyama RM, Gerasimenko YP, Zhong H, Roy RR, Edgerton VR: **Hindlimb stepping movements in complete spinal rats induced by epidural spinal cord stimulation.** *Neurosci Lett* 2005, **383:**339-344.

9. Jilge B, Minassian K, Rattay F, Pinter MM, Gerstenbrand F, Binder H, Dimitrijevic MR: **Initiating extension of the lower limbs in subjects with complete spinal cord injury by epidural lumbar cord stimulation.** *Exp Brain Res* 2004, **154:**308-326.

10. Lavrov I, Courtine G, Dy CJ, van den Brand R, Fong AJ, Gerasimenko Y, Zhong H, Roy RR, Edgerton VR: **Facilitation of stepping with epidural stimulation in spinal rats: role of sensory input.** *J Neurosci* 2008, **28:**7774-7780.

11. Lavrov I, Dy CJ, Fong AJ, Gerasimenko Y, Courtine G, Zhong H, Roy RR, Edgerton VR: **Epidural stimulation induced modulation of spinal locomotor networks in adult spinal rats.** *J Neurosci* 2008, **28:**6022-6029.

12. Gerasimenko YP, Ichiyama RM, Lavrov IA, Courtine G, Cai L, Zhong H, Roy RR, Edgerton VR: **Epidural spinal cord stimulation plus quipazine administration enable stepping in complete spinal adult rats.** *J Neurophysiol* 2007, **98:**2525-2536.

13. Dimitrijevic MR, Gerasimenko Y, Pinter MM: **Evidence for a spinal central pattern generator in humans.** *Ann N Y Acad Sci* 1998, **860:**360-376.

14. Gerasimenko YP, Avelev VD, Nikitin OA, Lavrov IA: **Initiation of locomotor activity in spinal cats by epidural stimulation of the spinal cord.** *Neurosci Behav Physiol* 2003, **33:**247-254.

15. Gerasimenko YP, Makarovskii AN, Nikitin OA: **Control of locomotor activity in humans and animals in the absence of supraspinal influences.** *Neurosci Behav Physiol* 2002, **32:**417-423.

16. Barthélemy D, Leblond H, Rossignol S: **Characteristics and Mechanisms of Locomotion Induced by Intraspinal Microstimulation and Dorsal Root Stimulation in Spinal Cats.** *J Neurophysiol* 2007, **97:**1986-2000.

17. Guevremont L, Renzi CG, Norton JA, Kowalczewski J, Saigal R, Mushahwar VK: **Locomotor-Related Networks in the Lumbosacral Enlargement of the Adult Spinal Cat: Activation Through Intraspinal Microstimulation.** *Neural Systems and Rehabilitation Engineering, IEEE Transactions on* 2006, **14:**266-272.

18. Giszter SF, Hockensmith G, Ramakrishnan A, Udoekwere UI: **How spinalized rats can walk: biomechanics, cortex, and hindlimb muscle scaling--implications for rehabilitation.** *Ann N Y Acad Sci* 2010, **1198:**279-293.

19. Udoekwere UI, Ramakrishnan A, Mbi L, Giszter SF: **Robot application of elastic fields to the pelvis of the spinal transected rat: a tool for detailed assessment and rehabilitation.** *Conf Proc IEEE Eng Med Biol Soc* 2006, **1:**3684-3687.

20. Ichiyama RM, Courtine G, Gerasimenko YP, Yang GJ, van den Brand R, Lavrov IA, Zhong H, Roy RR, Edgerton VR: **Step training reinforces specific spinal locomotor circuitry in adult spinal rats.** *J Neurosci* 2008, **28:**7370-7375.

21. De Leon RD, Hodgson JA, Roy RR, Edgerton VR: **Retention of hindlimb stepping ability in adult spinal cats after the cessation of step training.** *J Neurophysiol* 1999, **81:**85-94.

22. Lavrov I, Gerasimenko YP, Ichiyama RM, Courtine G, Zhong H, Roy RR, Edgerton VR: **Plasticity of spinal cord reflexes after a complete transection in adult rats: relationship to stepping ability.** *J Neurophysiol* 2006, **96:**1699-1710.

23. Edgerton VR, Courtine G, Gerasimenko YP, Lavrov I, Ichiyama RM, Fong AJ, Cai LL, Otoshi CK, Tillakaratne NJ, Burdick JW, Roy RR: **Training locomotor networks.** *Brain Res Rev* 2008, **57:**241-254.

24. Courtine G, Gerasimenko Y, van den Brand R, Yew A, Musienko P, Zhong H, Song B, Ao Y, Ichiyama RM, Lavrov I, et al: **Transformation of nonfunctional spinal circuits into functional states after the loss of brain input.** *Nat Neurosci* 2009, **12:**1333-1342.

25. Harkema S, Gerasimenko Y, Hodes J, Burdick J, Angeli C, Chen Y, Ferreira C, Willhite A, Rejc E, Grossman RG, Edgerton VR: **Effect of epidural stimulation of the lumbosacral spinal cord on voluntary movement, standing, and assisted stepping after motor complete paraplegia: a case study.** *Lancet* 2011, **377:**1938-1947.

26. Marchal-Crespo L, Reinkensmeyer DJ: **Review of control strategies for robotic movement training after neurologic injury.** *J Neuroeng Rehabil* 2009, **6:**20.

27. Reinkensmeyer DJ, Emken JL, Cramer SC: **Robotics, motor learning, and neurologic recovery.** *Annu Rev Biomed Eng* 2004, **6:**497-525.

28. Cai LL, Fong AJ, Otoshi CK, Liang Y, Burdick JW, Roy RR, Edgerton VR: **Implications of assist-as-needed robotic step training after a complete spinal cord injury on intrinsic strategies of motor learning.** *J Neurosci* 2006, **26:**10564-10568.

29. Kahn LE, Zygman ML, Rymer WZ, Reinkensmeyer DJ: **Robot-assisted reaching exercise promotes arm movement recovery in chronic hemiparetic stroke: a randomized controlled pilot study.** *J Neuroeng Rehabil* 2006, **3:**12.

30. Nef T, Mihelj M, Riener R: **ARMin: a robot for patient-cooperative arm therapy.** *Med Biol Eng Comput* 2007, **45:**887-900.

31. Frey M, Colombo G, Vaglio M, Bucher R, Jorg M, Riener R: **A novel mechatronic body weight support system.** *IEEE Trans Neural Syst Rehabil Eng* 2006, **14:**311-321.

32. Matjacic Z, Hesse S, Sinkjaer T: **BalanceReTrainer: a new standing-balance training apparatus and methods applied to a chronic hemiparetic subject with a neglect syndrome.** *NeuroRehabilitation* 2003, **18:**251-259.

33. Sukal TM, Ellis MD, Dewald JP: **Source of work area reduction following hemiparetic stroke and preliminary intervention using the ACT3D system.** *Conf Proc IEEE Eng Med Biol Soc* 2006, **1:**177-180.

34. Dipietro L, Ferraro M, Palazzolo JJ, Krebs HI, Volpe BT, Hogan N: **Customized interactive robotic treatment for stroke: EMG-triggered therapy.** *IEEE Trans Neural Syst Rehabil Eng* 2005, **13:**325-334.

35. Kawamoto H, Taal S, Niniss H, Hayashi T, Kamibayashi K, Eguchi K, Sankai Y: **Voluntary motion support control of Robot Suit HAL triggered by bioelectrical signal for hemiplegia.** *Conf Proc IEEE Eng Med Biol Soc* 2010, **2010:**462-466.

36. Song R, Tong KY, Hu X, Li L: **Assistive control system using continuous myoelectric signal in robot-aided arm training for patients after stroke.** *IEEE Trans Neural Syst Rehabil Eng* 2008, **16:**371-379.

37. Aoyagi D, Ichinose WE, Harkema SJ, Reinkensmeyer DJ, Bobrow JE: **A robot and control algorithm that can synchronously assist in naturalistic motion during body-weight-supported gait training following neurologic injury.** *IEEE Trans Neural Syst Rehabil Eng* 2007, **15:**387-400.

38. Marchal Crespo L, Reinkensmeyer DJ: **Haptic guidance can enhance motor learning of a steering task.** *J Mot Behav* 2008, **40:**545-556.

39. Riener R, Lunenburger L, Jezernik S, Anderschitz M, Colombo G, Dietz V: **Patient-cooperative strategies for robot-aided treadmill training: first experimental results.** *IEEE Trans Neural Syst Rehabil Eng* 2005, **13:**380-394.

40. Giszter SF, Kargo WJ, Davies M, Shibayama M: **Fetal transplants rescue axial muscle representations in M1 cortex of neonatally transected rats that develop weight support.** *J Neurophysiol* 1998, **80:**3021-3030.

41. Darling D: **spinal cord, The Encyclopedia of Science.** *http://wwwdaviddarlinginfo/encyclopedia/S/spinal_cordhtml*.

42. LasieWorks: **Spinal cord information.** *http://wwwlaesieworkscom/spinal/SCIinfo01html*.

43. Silverthron DU: **Human Physiology : An Integrated Approach, 4th edition.** *Benjamin Cummings* 2007**:**436.

44. Wilson DM: **Central nervous mechanisms for the generation of rhythmic behaviour in arthropods.** *Symp Soc Exp Biol* 1966, **20:**199-228.

45. Wilson DM: **The flight-control system of the locust.** *Sci Am* 1968, **218:**83-90.

46. Wilson DM, Wyman RJ: **Motor Output Patterns during Random and Rhythmic Stimulation of Locust Thoracic Ganglia.** *Biophys J* 1965, **5:**121-143.

47. Brown TG: **The Intrinsic Factors in the Act of Progression in the Mammal.** *Proceedings of the Royal Society of London* 1911, **B84:**308-319.

48. Brown TG: **The Factors in Rhythmic Activity of the Nervous System.** *Proceedings of the Royal Society of London* 1912, **B85:**278-289.

49. Barbeau H, Rossignol S: **Recovery of locomotion after chronic spinalization in the adult cat.** *Brain Res* 1987, **412:**84-95.

50. Pearson KG, Rossignol S: **Fictive motor patterns in chronic spinal cats.** *J Neurophysiol* 1991, **66:**1874-1887.

51. Marder E, Bucher D: **Central pattern generators and the control of rhythmic movements.** *Curr Biol* 2001, **11:**R986-996.

52. Kandel ER, Schwartz JH, Jessell TM: **Principles of Neural Science, 4th edition.** *McGraw-Hill* 2000**:**740.

53. DTIC: **Step cycle for walking and running.** *http://wwwdticmil/dticasd/edc/EDCSec09/e09-0306f1html*.

54. Kriellaars DJ, Brownstone RM, Noga BR, Jordan LM: **Mechanical entrainment of fictive locomotion in the decerebrate cat.** *J Neurophysiol* 1994, **71:**2074-2086.

55. Ollivier-Lanvin K, Krupka AJ, AuYong N, Miller K, Prilutsky BI, Lemay MA: **Electrical stimulation of the sural cutaneous afferent nerve controls the amplitude and onset of the swing phase of locomotion in the spinal cat.** *J Neurophysiol* 2011, **105:**2297-2308.

56. Sherrington CS: **Flexion-reflex of the limb, crossed extension-reflex, and reflex stepping and standing.** *J Physiol* 1910, **40:**28-121.

57. Hiebert GW, Whelan PJ, Prochazka A, Pearson KG: **Contribution of hind limb flexor muscle afferents to the timing of phase transitions in the cat step cycle.** *J Neurophysiol* 1996, **75:**1126-1137.

58. Whelan PJ, Hiebert GW, Pearson KG: **Stimulation of the group I extensor afferents prolongs the stance phase in walking cats.** *Exp Brain Res* 1995, **103:**20-30.

59. Forssberg H: **Stumbling corrective reaction: a phase-dependent compensatory reaction during locomotion.** *J Neurophysiol* 1979, **42:**936-953.

60. Shik ML, Severin FV, Orlovskii GN: **[Control of walking and running by means of electric stimulation of the midbrain].** *Biofizika* 1966, **11:**659-666.

61. Mori S, Matsuyama K, Kohyama J, Kobayashi Y, Takakusaki K: **Neuronal constituents of postural and locomotor control systems and their interactions in cats.** *Brain Dev* 1992, **14 Suppl:**S109-120.

62. Bonner JF, Connors TM, Silverman WF, Kowalski DP, Lemay MA, Fischer I: **Grafted neural progenitors integrate and restore synaptic connectivity across the injured spinal cord.** *J Neurosci* 2011, **31:**4675-4686.

63. Boyce VS, Tumolo M, Fischer I, Murray M, Lemay MA: **Neurotrophic factors promote and enhance locomotor recovery in untrained spinalized cats.** *J Neurophysiol* 2007, **98:**1988-1996.

64. Campos L, Ambron RT, Martin JH: **Bridge over troubled waters.** *Neuroreport* 2004, **15:**2691-2694.

65. Rossignol S, Frigon A: **Recovery of locomotion after spinal cord injury: some facts and mechanisms.** *Annu Rev Neurosci* 2011, **34:**413-440.

66. Perreault MC, Rossignol S, Drew T: **Microstimulation of the medullary reticular formation during fictive locomotion.** *J Neurophysiol* 1994, **71:**229-245.

67. Gossard JP, Floeter MK, Degtyarenko AM, Simon ES, Burke RE: **Disynaptic vestibulospinal and reticulospinal excitation in cat lumbosacral motoneurons: modulation during fictive locomotion.** *Exp Brain Res* 1996, **109:**277-288.

68. Russel DF, Zajac FE: **Effects of stimulating Deiter's sucleus and medial longitudinal fasciculus on the timing of the fictive locomotor rhythm induced in cats by DOPA.** *Bran Res* 1979, **177:**588-592.

69. Afelt Z: **Functional significance of ventral descending tracts of the spinal cord in the cat.** *Acta Neurobiol Exp (Wars)* 1974, **34:**393-407.

70. Eidelberg E, Story JL, Walden JG, Meyer BL: **Anatomical correlates of return of locomotor function after partial spinal cord lesions in cats.** *Exp Brain Res* 1981, **42:**81-88.

71. Eidelberg E, Walden JG, Nguyen LH: **Locomotor control in macaque monkeys.** *Brain* 1981, **104:**647-663.

72. Bem T, Gorska T, Majczynski H, Zmyslowski W: **Different patterns of fore-hindlimb coordination during overground locomotion in cats with ventral and lateral spinal lesions.** *Exp Brain Res* 1995, **104:**70-80.

73. Brustein E, Rossignol S: **Recovery of locomotion after ventral and ventrolateral spinal lesions in the cat. II. Effects of noradrenergic and serotoninergic drugs.** *J Neurophysiol* 1999, **81:**1513-1530.

74. Gorska T, Bem T, Majczynski H: **Locomotion in cats with ventral spinal lesions: support patterns and duration of support phases during unrestrained walking.** *Acta Neurobiol Exp (Wars)* 1990, **50:**191-199.

75. Gorska T, Bem T, Majczynski H, Zmyslowski W: **Unrestrained walking in cats with partial spinal lesions.** *Brain Res Bull* 1993, **32:**241-249.

76. Gorska T, Majczynski H, Bem T, Zmyslowski W: **Hindlimb swing, stance and step relationships during unrestrained walking in cats with lateral funicular lesion.** *Acta Neurobiol Exp (Wars)* 1993, **53:**133-142.

77. Rossignol S, Drew T, Brustein E, Jiang W: **Locomotor performance and adaptation after partial or complete spinal cord lesions in the cat.** *Prog Brain Res* 1999, **123:**349-365.

78. Zmyslowski W, Gorska T, Majczynski H, Bem T: **Hindlimb muscle activity during unrestrained walking in cats with lesions of the lateral funiculi.** *Acta Neurobiol Exp (Wars)* 1993, **53:**143-153.

79. Vilensky JA, Moore AM, Eidelberg E, Walden JG: **Recovery of Locomotion in Monkeys With Spinal Cord Lesions.** *J Mot Behav* 1992, **24:**288-296.

80. Nathan PW: **Effects on movement of surgical incisions into the human spinal cord.** *Brain* 1994, **117 ( Pt 2):**337-346.

81. Drew T, Prentice S, Schepens B: **Cortical and brainstem control of locomotion.** *Prog Brain Res* 2004, **143:**251-261.

82. Leblond H, Menard A, Gossard JP: **Corticospinal control of locomotor pathways generating extensor activities in the cat.** *Exp Brain Res* 2001, **138:**173-184.

83. Rho MJ, Lavoie S, Drew T: **Effects of red nucleus microstimulation on the locomotor pattern and timing in the intact cat: a comparison with the motor cortex.** *J Neurophysiol* 1999, **81:**2297-2315.

84. Eidelberg E, Yu J: **Effects of corticospinal lesions upon treadmill locomotion by cats.** *Exp Brain Res* 1981, **43:**101-103.

85. Bareyre FM, Kerschensteiner M, Raineteau O, Mettenleiter TC, Weinmann O, Schwab ME: **The injured spinal cord spontaneously forms a new intraspinal circuit in adult rats.** *Nat Neurosci* 2004, **7:**269-277.

86. Rossignol S: **Plasticity of connections underlying locomotor recovery after central and/or peripheral lesions in the adult mammals.** *Philos Trans R Soc Lond B Biol Sci* 2006, **361:**1647-1671.

87. Rossignol S, Dubuc R, Gossard JP: **Dynamic sensorimotor interactions in locomotion.** *Physiol Rev* 2006, **86:**89-154.

88. Rossignol S, Giroux N, Chau C, Marcoux J, Brustein E, Reader TA: **Pharmacological aids to locomotor training after spinal injury in the cat.** *J Physiol* 2001, **533:**65-74.

89. Li Y, Oskouian RJ, Day YJ, Kern JA, Linden J: **Optimization of a mouse locomotor rating system to evaluate compression-induced spinal cord injury: correlation of locomotor and morphological injury indices.** *J Neurosurg Spine* 2006, **4:**165-173.

90. Majczynski H, Maleszak K, Gorska T, Slawinska U: **Comparison of two methods for quantitative assessment of unrestrained locomotion in the rat.** *J Neurosci Methods* 2007, **163:**197-207.

91. Poon PC, Gupta D, Shoichet MS, Tator CH: **Clip compression model is useful for thoracic spinal cord injuries: histologic and functional correlates.** *Spine (Phila Pa 1976)* 2007, **32:**2853-2859.

92. Shields CB, Zhang YP, Shields LB, Han Y, Burke DA, Mayer NW: **The therapeutic window for spinal cord decompression in a rat spinal cord injury model.** *J Neurosurg Spine* 2005, **3:**302-307.

93. Singh A, Balasubramanian S, Murray M, Lemay M, Houle J: **Role of Spared Pathways in Locomotor Recovery after Body-Weight-Supported Treadmill Training in Contused Rats.** *J Neurotrauma* 2011.

94. Magnuson DS, Lovett R, Coffee C, Gray R, Han Y, Zhang YP, Burke DA: **Functional consequences of lumbar spinal cord contusion injuries in the adult rat.** *J Neurotrauma* 2005, **22:**529-543.

95. Barriere G, Leblond H, Provencher J, Rossignol S: **Prominent role of the spinal central pattern generator in the recovery of locomotion after partial spinal cord injuries.** *J Neurosci* 2008, **28:**3976-3987.

96. Helgren ME, Goldberger ME: **The recovery of postural reflexes and locomotion following low thoracic hemisection in adult cats involves compensation by undamaged primary afferent pathways.** *Exp Neurol* 1993, **123:**17-34.

97. Barriere G, Frigon A, Leblond H, Provencher J, Rossignol S: **Dual spinal lesion paradigm in the cat: evolution of the kinematic locomotor pattern.** *J Neurophysiol* 2010, **104:**1119-1133.

98. Brustein E, Rossignol S: **Recovery of locomotion after ventral and ventrolateral spinal lesions in the cat. I. Deficits and adaptive mechanisms.** *J Neurophysiol* 1998, **80:**1245-1267.

99. Suresh Babu R, Muthusamy R, Namasivayam A: **Behavioural assessment of functional recovery after spinal cord hemisection in the bonnet monkey (Macaca radiata).** *J Neurol Sci* 2000, **178:**136-152.

100. Gulino R, Dimartino M, Casabona A, Lombardo SA, Perciavalle V: **Synaptic plasticity modulates the spontaneous recovery of locomotion after spinal cord hemisection.** *Neurosci Res* 2007, **57:**148-156.

101. Robblee LS RT: ***Electrochemical guidelines for selection of protocols and electrode materials for neural stimulation.*** 1990**:**25-66.

102. Emken JL, Reinkensmeyer DJ: **Robot-enhanced motor learning: accelerating internal model formation during locomotion by transient dynamic amplification.** *IEEE Trans Neural Syst Rehabil Eng* 2005, **13:**33-39.

103. Lam T, Wirz M, Lunenburger L, Dietz V: **Swing phase resistance enhances flexor muscle activity during treadmill locomotion in incomplete spinal cord injury.** *Neurorehabil Neural Repair* 2008, **22:**438-446.

104. Lum PS, Burgar CG, Shor PC: **Evidence for improved muscle activation patterns after retraining of reaching movements with the MIME robotic system in subjects with post-stroke hemiparesis.** *IEEE Trans Neural Syst Rehabil Eng* 2004, **12:**186-194.

105. Lum PS, Burgar CG, Shor PC, Majmundar M, Van der Loos M: **Robot-assisted movement training compared with conventional therapy techniques for the rehabilitation of upper-limb motor function after stroke.** *Arch Phys Med Rehabil* 2002, **83:**952-959.

106. Mercier C, Bourbonnais D, Bilodeau S, Lemay JF, Cross P: **Description of a new motor re-education programme for the paretic lower limb aimed at improving the mobility of stroke patients.** *Clin Rehabil* 1999, **13:**199-206.

107. Patterson LA, Spivey WE: **Validity and Reliability of the LIDO Active Isokinetic System.** *J Orthop Sports Phys Ther* 1992, **15:**32-36.

108. Patton JL, Stoykov ME, Kovic M, Mussa-Ivaldi FA: **Evaluation of robotic training forces that either enhance or reduce error in chronic hemiparetic stroke survivors.** *Exp Brain Res* 2006, **168:**368-383.

109. Lambercy O, Dovat L, Gassert R, Burdet E, Teo CL, Milner T: **A haptic knob for rehabilitation of hand function.** *IEEE Trans Neural Syst Rehabil Eng* 2007, **15:**356-366.

110. Lum PS, Uswatte G, Taub E, Hardin P, Mark VW: **A telerehabilitation approach to delivery of constraint-induced movement therapy.** *J Rehabil Res Dev* 2006, **43:**391-400.

111. Mataric MJ, Eriksson J, Feil-Seifer DJ, Winstein CJ: **Socially assistive robotics for post-stroke rehabilitation.** *J Neuroeng Rehabil* 2007, **4:**5.

112. Krebs H, Palazzolo J, Dipietro L, Ferraro M, Krol J, Rannelkleiv K, Volpe B, Hogan N: **Rehabilitation robotics: Performance-based Progressive Robot-assisted Therapy.** *Autonomous Robots* 2003, **15:**7-20.

113. de Leon RD, Acosta CN: **Effect of robotic-assisted treadmill training and chronic quipazine treatment on hindlimb stepping in spinally transected rats.** *J Neurotrauma* 2006, **23:**1147-1163.

114. de Leon RD, Kubasak MD, Phelps PE, Timoszyk WK, Reinkensmeyer DJ, Roy RR, Edgerton VR: **Using robotics to teach the spinal cord to walk.** *Brain Research Reviews* 2002, **40:**267-273.

115. de Leon RD, Reinkensmeyer DJ, Timoszyk WK, London NJ, Roy RR, Edgerton VR: **Use of robotics in assessing the adaptive capacity of the rat lumbar spinal cord.** *Prog Brain Res* 2002, **137:**141-149.

116. Giszter S, Davies MR, Ramakrishnan A, Udoekwere UI, Kargo WJ: **Trunk sensorimotor cortex is essential for autonomous weight-supported locomotion in adult rats spinalized as P1/P2 neonates.** *J Neurophysiol* 2008, **100:**839-851.

117. Giszter SF, Davies MR, Graziani V: **Coordination strategies for limb forces during weight-bearing locomotion in normal rats, and in rats spinalized as neonates.** *Exp Brain Res* 2008, **190:**53-69.

118. Miya D, Giszter S, Mori F, Adipudi V, Tessler A, Murray M: **Fetal transplants alter the development of function after spinal cord transection in newborn rats.** *J Neurosci* 1997, **17:**4856-4872.

119. Giszter SF, Davies MR, Graziani V: **Motor strategies used by rats spinalized at birth to maintain stance in response to imposed perturbations.** *J Neurophysiol* 2007, **97:**2663-2675.

120. Antri M, Orsal D, Barthe JY: **Locomotor recovery in the chronic spinal rat: effects of long-term treatment with a 5-HT2 agonist.** *Eur J Neurosci* 2002, **16:**467-476.

121. Olds J: **Pleasure centers in the brain.** *Scientific American* 1956, **195:**105-116.

122. Wise RA: **Forebrain substrates of reward and motivation.** *J Comp Neurol* 2005, **493:**115-121.

123. Bao S, Chan VT, Merzenich MM: **Cortical remodelling induced by activity of ventral tegmental dopamine neurons.** *Nature* 2001, **412:**79-83.

124. Giszter S, Graziani V, Kargo W, Hockensmith G, Davies MR, Smeraski CS, Murray M: **Pattern generators and cortical maps in locomotion of spinal injured rats.** *Ann N Y Acad Sci* 1998, **860:**554-555.

125. Matsuishi M, Endo T: **Fatigue of metals subjected to varying stress.** *Japan Soc Mech Engineering* 1968.

126. Downing SD, Socie DF: **Simple rainflow counting algorithms.** *International Journal of Fatigue* 1982, **4:**31-40.

127. 1049-85 AE: **Standard practices for cycle counting in fatigue analysis.** *ASTM International* Reapproved 2005.

128. Jacobs CR, E. Yellowley C, Nelson DV, Donahue HJ: **Analysis of Time-Varying Biological Data Using Rainflow Cycle Counting.** *Computer Methods in Biomechanics and Biomedical Engineering* 2000, **3:**31-40.

129. Hillyer JE, Joynes RL: **A new measure of hindlimb stepping ability in neonatally spinalized rats.** *Behav Brain Res* 2009, **202:**291-302.

130. Wada N, Toba Y, Iwamoto W, Goto M, Miyata H, Mori F, Morita F: **Investigation and characterization of rat bipedal walking models established by a training program.** *Brain Res* 2008, **1243:**70-77.

131. Johnson WL, Jindrich DL, Roy RR, Reggie Edgerton V: **A three-dimensional model of the rat hindlimb: musculoskeletal geometry and muscle moment arms.** *J Biomech* 2008, **41:**610-619.

132. Kunnumpurath S, Srinivasagopalan R, Vadivelu N: **Spinal cord stimulation: principles of past, present and future practice: a review.** *J Clin Monit Comput* 2009, **23:**333-339.

133. Kazennikov OV, Shik ML: **[Propagation of the activity along the "stepping strip" of the spinal cord in the cat].** *Neirofiziologiia* 1988, **20:**763-769.

134. Iwahara T, Atsuta Y, Garcia-Rill E, Skinner RD: **Spinal cord stimulation-induced locomotion in the adult cat.** *Brain Research Bulletin* 1992, **28:**99-105.

135. Song W, Giszter SF: **Adaptation to a cortex-controlled robot attached at the pelvis and engaged during locomotion in rats.** *J Neurosci* 2011, **31:**3110-3128.

136. Song W, Ramakrishnan A, Udoekwere UI, Giszter SF: **Multiple types of movement-related information encoded in hindlimb/trunk cortex in rats and potentially available for brain-machine interface controls.** *IEEE Trans Biomed Eng* 2009, **56:**2712-2716.

# Appendix

## Visual C code for robot-driven stimulation control for PHANTOM robot (rcp_epi_stimulus.dll)

```
#include "..\code\rcpdll.h"
#include "..\code\etsmacro.hpp"
#include <math.h>
#include <stdio.h>
#include <tchar.h>

// add an isotropic sphere constraint RCP with a polynomial stiffness up to square terms

class RcpDll_epi_stimulus : public RcpDll {
	public:

		RcpDll_epi_stimulus(void); // Constructor
		~RcpDll_epi_stimulus(void); //Destructor
		RcpDll_epi_stimulus* Clone(void); // Copy
		int getEpoch(void); // check DLL compatibility
		string getName(void) { return "Rcp_epidural_stimulus"; }; // Name of DLL for robot

		string getDescription(void) { return "Sphere: center, radius, stiffness"; };
		void getConsoleRef( ConsoleIO *MainConsole){console=MainConsole;};

		bool Validate(VarPool* vp); // tests values of control from main program are correct
		bool Reset(VarPool* vp); // resets variable pool
		bool isOk(void); // check all values

		// control step for robot
		point3D* Step( long timer, const point3D* x, const point3D* xp , const point3D**
interactforces, const BYTE* cerebusdata );

	private:
		static int def_on_off;
		static int def_counter;
		static int def_offSet;

		// parameter passing strings
		static const char *SphereCtrStr;
		static const char *OnOffCounterStr;
		static const char *CounterStr;
		static const char *offSetStr;

		// variables themselves
		int on_off;
		int stimulus;
		int counter;
		int on_off_counter;
		int on_off_counter_limit;
```

```
		int counterLimit;
		int offSet;
		point3D *ctr;
		point3D center;

int RcpDll_epi_stimulus::def_on_off = 25;// how frequent the program check the position of the robot arm (/ms)
int RcpDll_epi_stimulus::def_counter = 3;
int RcpDll_epi_stimulus::def_offSet = 0;// how far away from the sphere center;for z: (+:lower, -:heigher) than the center

// define constant strings for passed variables
const char *RcpDll_epi_stimulus::SphereCtrStr = "Point of Reference\0";
const char *RcpDll_epi_stimulus::OnOffCounterStr = "Refraction Length(ms)\0";
const char *RcpDll_epi_stimulus::CounterStr = "Stimulus Length(ms)\0";
const char *RcpDll_epi_stimulus::offSetStr = "Offset Distance\0";

RcpDll_epi_stimulus::RcpDll_epi_stimulus(void) : RcpDll()
{

	vars.push_back(VarDef(SphereCtrStr, VarDef::VAR_REFPOINT));
	vars.push_back(VarDef(OnOffCounterStr, VarDef::VAR_INT, &RcpDll_epi_stimulus::def_on_off));
	vars.push_back(VarDef(CounterStr, VarDef::VAR_INT, &RcpDll_epi_stimulus::def_counter));
	vars.push_back(VarDef(offSetStr, VarDef::VAR_INT, &RcpDll_epi_stimulus::def_offSet));
}

RcpDll_epi_stimulus::~RcpDll_epi_stimulus(void)
{
}

RcpDll_epi_stimulus* RcpDll_epi_stimulus::Clone()
{
	return new RcpDll_epi_stimulus();
}

int RcpDll_epi_stimulus::getEpoch(void)
{
	return RCPDLL_EPOCH;
}

bool RcpDll_epi_stimulus::Validate(VarPool* vp)
{

	int *p3, *p2,*p5;

	double *pd2;
	p3 = getIntRef(vp, OnOffCounterStr);
	if ((*p3<1)||(*p3>20000)) {
		LastError = "Length of Refraction must be between 1 and 20000 ms)";
		return false;
```

```
	}

		p2 = getIntRef(vp, CounterStr);
	if ((*p2<1)||(*p2>1000)) {
		LastError = "Length of Stimulus must be between 1 and 1000 ms)";
		return false;
	}

		p5 = getIntRef(vp, offSetStr);
		if((*p5 > 1000) || (*p5<-1000)){
		LastError = "Offset must be greater than -1000 or less than 1000.";
		return false;
		}

	point3D* p1 = getRefPointRef(vp, SphereCtrStr);
	if (p1 == NULL) {
		LastError = "Sphere_center must be defined.";
		return false;
	}

	return true;
}

bool RcpDll_epi_stimulus::Reset(VarPool* vp)
{

	//get variable values
	ctr = getRefPointRef(vp, SphereCtrStr);
	on_off_counter_limit= *getIntRef(vp, OnOffCounterStr);
	counterLimit= *getIntRef(vp, CounterStr);
	offSet= *getIntRef(vp, offSetStr);
	on_off_counter=0;
	int counter=0;
	int i=0;
	double height=0;
	double avg_height=0;
	return true;
}

bool RcpDll_epi_stimulus::isOk(void)
{
	if(ctr)center= *ctr;
	else return false;
	int on_off = 1;
	int stimulus = 0;
	return true;
}

point3D* RcpDll_epi_stimulus::Step( long timer, const point3D* x, const point3D* xp, const
point3D** interactforces, const BYTE * cerebusdata )

{
```

```
		double ctr_timer= (double)timer;
		point3D v = (*x) - (center); //vector from center to position point

		//get vertical distance from center
		double p = (v.Z);

		// configuration of epidural stimulation
		if(((p+offSet)<=0) && (on_off==1)){
			stimulus=1;
			on_off=0;
		}

		if(stimulus==1){
			counter++;
			outpw(0x378, 0x01);
		}

		if(counter==counterLimit) {
			counter=0;
			stimulus=0;
			outpw(0x378, 0x00);
		}

		if(on_off==0)
			on_off_counter++;

		if(on_off_counter==(on_off_counter_limit+counterLimit)) {
			on_off=1;
			on_off_counter=0;
		}

		Force = nill;

		return &Force;
}

RCPDLL_DECL RcpDll* GetInstance(void)
{
		return new RcpDll_epi_stimulus();
}
```

# Vita

## Fu-Han Hsieh

## Education

Ph.D. in Biomedical Engineering – Drexel University, Philadelphia, PA, USA
M.S. in Electronic Engineering – Chang Gang University, Taiwan, 2002
B.S. in Physics – National Chung Cheng University, Taiwan, 2000

## Experience

Research Assistant – Drexel University, Philadelphia, PA, USA, 2006 - 2011
Teaching Assistant – Soochow University, Taiwan, 2004 - 2005
Electronic Officer (Military Service) – Air Force, Taiwan, 2002 - 2004
Teaching Assistant – Chang Gang University, Taiwan, 2000-2002

## Publications and Presentations

FH Hsieh, SF Giszter, "Robot-driven spinal epidural stimulation compared with conventional stimulation in adult spinalized rats," Conf Proc IEEE Eng Med Biol Soc., 2011, Boston, MA

FH Hsieh, M Smeltzer, SF Giszter, "Robot driven epidural stimulation tested and compared with conventional epidural stimulation in adult spinalized rats," Neuroscience 2009.

## Membership

Student member, IEEE